UZHHOROD NATIONAL UNIVERSITY

Mikla V. I., Shpenik A. O., Troshki V. B., Turovtsi-Shiutev Y. M.

Introduction to Raman Measurements and Spectra: From Fundamentals to Applications in Materials, Sensing and Medicine

Monograph

Uzhhorod-2019

UDC 539.2
BBK B37
M-59

Recommended for publication by the Academic Council of Ukrainian-Hungarian educational institute of Uzhhorod National University
(*Protocol number 1 of September 24 , 2019*)

Reviewers: Safa Kasap, Professor of Department of Electrical Engineering, University of Saskatchewan, Canada
Alexei Sokolov, Professor of Department of Chemistry/Physics, University of Tennessee, USA

Mikla V. I., Shpenik A. O., Troshki V. B., Turovtsi-Shiutev Y. M.
M-59 Introduction to Raman Measurements and Spectra: From Fundamentals to Applications in Materials, Sensing and Medicine: Monograph - Uzhhorod: «AUTDOR-Shark», 2019. -p. 135.

Domus intézményi konferencia- és kiadvány-támogatási pályázat 2019

ISBN 978-617-7796-04-5

Content

PREFACE

Raman Measurements and Spectra: Fundamentals and Applications in Materials, Sensing, and Medicine examines the most common uses of Raman spectroscopic techniques and their related challenges in a concise yet practical reference. Specific chapters address a range of topics including Raman scattering, low frequency light scattering, the effects of light and temperature on Raman spectra, boson peak, and Raman spectroscopy of glasses and amorphous films. Clinical applications that aid in the determination of heart disease and cancer broaden the content's multi-disciplinary focus and reach. This book is ideal for junior scientists who need deeper exposure to Raman spectroscopy as well as more seasoned professionals who simply want a quick refresher on Raman spectroscopic techniques and interpretations.

Includes input from a scientist with more than 30 years of experience in Raman spectroscopy research and applications Features more than 70 figures and illustrations to aid in the retention of key concepts. Arms readers with a versatile stable of optical techniques with specific research applications. Covers a range of topics including Raman scattering, low frequency light scattering, the effects of light and temperature on Raman spectra, boson peak, and Raman spectroscopy of glasses and amorphous films.

CHAPTER 1. Introduction to Raman Spectroscopy: Basic theory and measurement of light scattering

1.1. Raman Effect as a phenomenon.

Raman scattering is an inelastic scattering of visible (or ultraviolet) light from matter. Starting from the early 1960s, due to development of lasers, Raman scattering has become a powerful and informative tool for the studies of elementary excitations in gases, liquids and solids.

A phenomenon observed in the scattering of light as it passes through a material medium, whereby the light suffers a change in frequency and a random alteration in phase. Raman scattering differs in both these respects from Rayleigh and Tyndall scattering, in which the scattered light has the same frequency as the un-scattered and bears a definite phase relation to it. The intensity of normal Raman scattering is roughly one-thousandth that of Rayleigh scattering in liquids and smaller still in gases. In other words, it is the scattering of light by matter, accompanied by a noticeable change in the frequency of the scattered light. If a source emits a line spectrum, the Raman Effect produces additional lines, whose number and location are closely related to the molecular structure of the substance, in the spectrum of the scattered light.

1.2. From the history of Raman Effect

The Raman Effect was discovered by Chandrasekhara Venkata Raman (Fig. 1). He was a brilliant student; but higher education was considered below his caste. So in 1907 he went to Calcutta to join the Indian Financial Civil Service as Assistant Accountant General. Raman, a “self-made scientist”, with intense drive, worked early mornings and evenings in the underutilized facilities of the Indian Association for the Cultivation of Science, in Calcutta, to study problems in

acoustics. He conducted research independently, for nearly 10 years, and established his reputation. In 1917, Raman was appointed professor at the University of Calcutta.

Fig.1.1. Professor Sir C V Raman.

Somewhat latter, in 1921, on his first voyage outside India, to Oxford, he performed some experiments and published a note entitled “The color of the sea” in Nature. He showed that the color of the ocean is independent of sky reflection or absorption, and is instead due to scattering. It is a beginning of his scientific research into the scattering of light. The work led to his discovery of the Raman Effect in 1928, and he was awarded the Nobel Prize just two years later (a record time) "for his work on the scattering of light and for the discovery of the effect named after him". [1-3]. He was the first Asian, and the only Indian, to receive this award.

Among scientists, Raman is best known for his strikingly ingenious yet simple experimental design, the lucidity of his ideas, and the depth of his observations.

The Raman Effect is a fundamental process in which energy is exchanged between light and matter. When light impinges on a substance it can be scattered or absorbed. Most of the scattered light will have the same frequency as that of the incident light. However, a small fraction of the incident light can go into setting molecules in the material into vibration. The energy for this must come from the incident light. Since light energy is proportional to frequency, the frequency change of this scattered light must equal the vibrational frequency of the scattering

molecules. This process - energy exchange between scattering molecules and incident light - is known as the Raman Effect.

According to Hindu tradition, Raman was originally named Venkataraman after a Hindu deity, preceded by the initial of his father's first name, Chandrasekhara. In school his name was split to C. Venkata Raman, which later became C.V. Raman. With a father who was a professor of physics and mathematics and a mother who came from a family of Sanskrit scholars, Raman exhibited a precocious nature at an early age. He received a B.A. degree from Presidency College in Madras at the age of 16, placing first in his class and receiving a gold medal in physics.

While studying for his M.A. degree, he published his first research paper in Philosophical Magazine at the age of 18. It was the first research paper ever published from Presidency College.

Because of poor health, he was unable to go to England for further education. With nothing else available in India, in 1907 he passed the Financial Civil Service exam, married, and was posted to Calcutta as assistant accountant general.

Shortly after arriving in Calcutta, Raman began after-hours research at the Indian Association for the Cultivation of Science (IACS). In the first 10 years, working almost alone, he published 27 research papers and led the way for the IACS to become recognized as a vibrant research institute. Much of this early work was on the theory of vibrations as it related to musical instruments. After brief postings in Rangoon and Nagpur, he returned to Calcutta, took up residence next door to the IACS, and constructed a door that led directly into the institute, giving him access at any time. He received research prizes in 1912 and 1913.

Other investigations carried out by Raman were: his experimental and theoretical studies on the diffraction of light by acoustic waves of ultrasonic and hypersonic frequencies (published 1934-1942), and those on the effects produced by X-rays on infrared vibrations in crystals exposed to ordinary light. In 1948 Raman, through studying the spectroscopic behavior of crystals, approached in a new manner fundamental problems of crystal dynamics. His laboratory has been

dealing with the structure and properties of diamond, the structure and optical behavior of numerous iridescent substances (labradorite, pearly felspar, agate, opal, and pearls).

Among his other interests has been the optics of colloids, electrical and magnetic anisotropy, and the physiology of human vision.

Raman has been honored with a large number of honorary doctorates and memberships of scientific societies. He was elected a Fellow of the Royal Society early in his career (1924), and was knighted in 1929.

Somewhat latter, in 1921, on his first voyage outside India, to Oxford, he performed some experiments and published a note entitled “The color of the sea” in Nature. He showed that the color of the ocean is independent of sky reflection or absorption, and is instead due to scattering. It is a beginning of his scientific research into the scattering of light. The work led to his discovery of the Raman effect in 1928, and he was awarded the Nobel prize just two years later (a record time).. He was the first Asian, and the only Indian, to receive this award.

Among scientists, Raman is best known for his strikingly ingenious yet simple experimental design, the lucidity of his ideas, and the depth of his observations.

1.3. Phenomenon of Raman scattering

The process of Raman scattering, from the energy level point of view, can be considered as the transition of a molecule from its ground state to an excited vibrational state, accompanied by the simultaneous absorption of an incident photon and emission of a Raman scattered photon (Fig. 1.2).

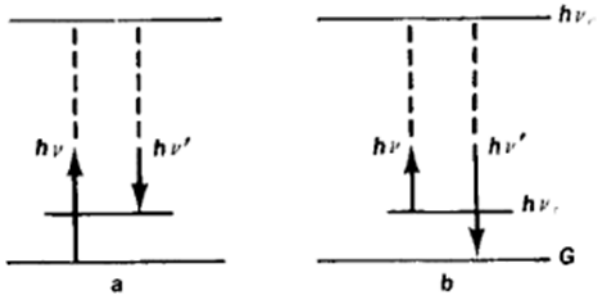

Fig. 1.2. Raman Effect.

The horizontal lines indicate vibrational energy levels. Ground electronic state and excited electronic states are shown. The diagrams show how a molecule in the ground state can make a transition from the lowest vibrational level to the first excited vibrational level by means of Raman scattering. Black up-arrows indicate the frequency of the laser excitation light; black down-arrows indicate frequency of the Raman scattered light. The difference in length between black up- and down-arrows indicates molecular vibration frequency [4].

It should be noted here that Raman scattering at different excitation wavelengths, UV, visible and near-IR, produces the same change in vibrational energy. Therefore the excitation wavelength can be chosen to avoid spectral interference by fluorescence. For visible excitation, the fluorescence light frequency and Raman scattered light frequency are similar. This leads to intense fluorescence background in visible excitation Raman spectra. Near-IR light has too low a frequency to excite fluorescence, while for UV excitation, the fluorescence light frequency is much lower than the Raman scattered light frequency. Hence, fluorescence background in the Raman spectrum can be reduced by using UV or near-IR excitation.

Because of its low intensity, the Raman Effect was not discovered until 1928, although the scattering of light by transparent solids, liquids, and gases had been investigated for many years before. Adolf Smekal, an Austrian physicist, predicted in 1923 the existence of sidebands in the spectrum of the scattered light. The development of the laser has led to a resurgence of interest in the Raman Effect and to the discovery of a number of related phenomena. When the exciting radiation falls within the frequency range of a molecule's absorption band in the visible or ultraviolet spectrum, the radiation may be scattered by two different processes, resonance fluorescence or the resonance Raman Effect. Both these processes give much more intense scattering than the normal non-resonant Raman Effect. The absolute frequencies of the resonance Raman Effect shift by exactly the amount of any shift in the exciting frequency, just as do those of the normal Raman Effect. Thus the main characteristic of the resonance as compared to the

normal Raman Effect is its intensity, which may be greater by two or three orders of magnitude.

Raman scattering is analyzed by spectroscopic means. The collection of new frequencies in the spectrum of monochromatic radiation scattered by a substance is characteristic of the substance and is called its Raman spectrum. Although the Raman Effect can be made to occur in the scattering of radiation by atoms, it is of greatest interest in the spectroscopy of molecules and crystals. In a typical experiment monochromatic radiation from a laser impinges on the sample in an appropriate transparent cell. Raman scattering is approximately uniform in all directions and is usually studied at right angles. In this way the intense radiation of the laser beam interferes least with the observation of the weak scattered light.

Raman spectroscopy is of considerable value in determining molecular structure and in chemical analysis. Molecular rotational and vibrational frequencies can be determined directly, and from these frequencies it is sometimes possible to evaluate the molecular geometry, or at least to find the molecular symmetry. Even when a precise determination of structure is not possible, much can often be said about the arrangement of atoms in a molecule from empirical information about the characteristic Raman frequencies of groups of atoms. This kind of information is closely similar to that provided by infrared spectroscopy; in fact, Raman and infrared spectra often provide complementary data about molecular structure. Raman spectra also provide information for solid-state physicists, particularly with respect to lattice dynamics but also concerning the electronic structures of solids [5].

To observe Raman-effect spectra, an intense light beam must be concentrated on the object under study. A mercury lamp— or, since the 1960's, a laser beam—is most often used as the source of the exciting light. The scattered light is focused and strikes a spectograph, where the Raman-effect spectrum is recorded by photographic or photoelectric methods.

The Raman Effect is most often associated with a change in the oscillatory states of molecules. Such a Raman-effect spectrum consists of a system of companions that lie symmetrically about an exciting line with frequency v

(Fig. 1.2). A companion with frequency v+ v, (a violet, or anti-Stokes, companion) corresponds to every companion with frequency v — v_i (a red, or Stokes, companion). Here v_i is one of the natural oscillation frequencies of the molecule. Thus the frequencies of the natural (or normal) oscillations of a molecule, which are manifested in the Raman-effect spectrum, may be determined by measuring the frequency of Raman-effect lines. Similar mechanisms also exist for a rotational Raman-effect spectrum. In this case the frequencies of the lines are determined by the rotational transitions of the molecules. In the simplest case a rotational Raman-effect spectrum is a sequence of nearly equidistant, symmetrically situated lines whose frequencies are combinations of the rotational frequencies of the molecules and the frequency of the exciting light.

According to quantum theory, the process of the Raman effect consists of two interconnected events, the absorption of a primary photon with energy hv (where h is Planck's constant) and the emission of a photon with energy hv' (where $v' = v \pm v_i$), which take place as a result of the interaction of the molecule's electrons with the field of the incident light wave. Under the action of a quantum with energy hv through the compound state, a molecule in an unexcited state passes into a state with oscillatory energy hv_i, emitting a quantum $h(v — v_i)$. This process leads to the appearance of a Stokes line with frequency v — v_i in the scattered light (Figure 1.2,a). If the photon is absorbed by a system in which oscillations already have been excited, then after scattering it may pass into a zero state; here the energy of the scattered photon exceeds the energy of the absorbed photon. This process leads to the appearance of an anti-Stokes line with frequency $v + v_i$.

The probability w of the Raman effect (and consequently the intensity of the Raman-effect lines) depends on the intensity of the exciting radiation and the scattered radiation I:w =aI0(b + I), where a and b are some constants; when the Raman effect is excited by ordinary light sources (such as a mercury lamp), the second term is small and may be disregarded. The intensity of the Raman-effect lines is extremely low in most cases, and at ordinary temperatures the intensity of anti-Stokes lines Ia generally is much less than the intensity of the Stokes lines Is.

Since the probability of scattering is proportional to the number of scattering molecules, the ratio Ia/Is is defined by the ratio of the populations of the ground and excited levels.

At ordinary temperatures the population of the excited levels is not great, and consequently the intensity of the anti-Stokes component is low. The population rises with increasing temperature, leading to an increase in the intensity of the anti-Stokes lines. The intensity of Raman-effect lines / depends on the frequency v of the exciting light: at great distances (on the frequency scale) from the molecules' region of electron absorption, $I \sim v^4$; as the electron absorption band is approached, a more rapid increase in their intensity is observed. In some cases, when the concentration of matter is low, it is possible to observe a resonance Raman Effect, in which the frequency of the exciting light enters the region of the substance's absorption band. When the Raman Effect is excited by high-powered lasers, its probability increases and a stimulated Raman Effect, whose intensity is of the same order as that of the exciting light, arises.

Raman-effect lines are polarized to a greater or lesser extent. Here various companions of a given exciting line have different degrees of polarization, but the nature of the polarization of Stokes and anti-Stokes companions is always identical.

The Raman Effect, like infrared spectroscopy, is an effective method for studying the structure of molecules and their interaction with the surrounding medium. It is significant that the Raman-effect spectrum and the infrared absorption spectrum do not duplicate each other, since they are defined by ratio of the populations of the ground and excited levels. At ordinary temperatures the population of the excited levels is not great, and consequently the intensity of the anti-Stokes component is low. The population rises with increasing temperature, leading to an increase in the intensity of the anti-Stokes lines. The intensity of Raman-effect lines / depends on the frequency v of the exciting light: at great distances (on the frequency scale) from the molecules' region of electron absorption, $I \sim v^4$; as the electron absorption band is approached, a more rapid increase in their intensity is observed. In some cases, when the concentration of

matter is low, it is possible to observe a resonance Raman effect, in which the frequency of the exciting light enters the region of the substance's absorption band. When the Raman effect is excited by high-powered lasers, its probability increases and a stimulated Raman effect, whose intensity is of the same order as that of the exciting light, arises.

Raman-effect lines are polarized to a greater or lesser extent. Here various companions of a given exciting line have different degrees of polarization, but the nature of the polarization of Stokes and anti-Stokes companions is always identical.

The Raman Effect, like infrared spectroscopy, is an effective method for studying the structure of molecules and their interaction with the surrounding medium. It is significant that the Raman-effect spectrum and the infrared absorption spectrum do not duplicate each other, since they are defined by different selection rules. The symmetry of normal oscillations—and, consequently, the symmetry of the molecule as a whole—may be assessed by comparing the frequencies of the lines in the Raman-effect spectrum and the infrared spectrum of a given chemical compound. In this manner, a real model corresponding to the mechanisms in the observed spectra may be chosen from among several proposed models of a molecule. In many cases the frequencies and other parameters of Raman-effect lines are retained upon transition from one compound to another that has the same structural element. This so-called characteristic nature of the parameters of Raman-effect lines underlies the structural analysis of molecules of unknown structure.

In crystals the Raman Effect has certain distinctive features. The oscillations of atoms in a crystal may be identified with a phonon gas, whereas the Raman Effect in crystals may be viewed as scattering by phonons. Other quasiparticles of a crystal (such as polarons and magnons) are also studied using methods involving the Raman Effect.

The Raman-effect spectra of every compound are so specific that they may serve to identify the compound and to detect it in mixtures.

1.3.1. A brief look at Raman scattering theory.

1.3.1(a) The Raman Effect and Normal Raman Scattering.

When light is scattered from a molecule most photons are elastically scattered. The scattered photons have the same energy (frequency) and, therefore, wavelength, as the incident photons. However, a small fraction of light (approximately 1 in 10^7photons) is scattered at optical frequencies different from, and usually lower than, the frequency of the incident photons. The process leading to this inelastic scatter is the termed the Raman effect. Raman scattering can occur with a change in vibrational, rotational or electronic energy of a molecule. Chemists are concerned primarily with the vibrational Raman effect and thus in this tutorial we use the term Raman effect to mean vibrational Raman effect only.

The difference in energy between the incident photon and the Raman scattered photon is equal to the energy of a vibration of the scattering molecule. A plot of intensity of scattered light versus energy difference is a Raman spectrum.

1.3.1(b) The Scattering Process.

When a beam of light is impinged upon a molecule, photons are absorbed by the material and scattered. The vast majority of these scattered photons have exactly the same wavelength as the incident photons and are known as Rayleigh scatter. In the scattering process, the incident photon excites an electron into a higher “virtual” energy level (or virtual state) and then the electron decays back to a lower level, emitting a scattered photon. In Rayleigh scattering the electron decays back to the same level from which it started and thus Rayleigh scattering is often referred to as a form of elastic scatter.

The Raman Effect arises when a photon is incident on a molecule and interacts with the electric dipole of the molecule. It is a form of electronic (more accurately, vibronic) spectroscopy, although the spectrum contains vibrational frequencies. In classical terms, the interaction can be viewed as a perturbation of the molecule's electric field. In quantum mechanical terms the scattering can be described as an excitation to a virtual state lower in energy than a real electronic

transition with nearly coincident de-excitation and a change in vibrational energy. The virtual state description of scattering is shown in Fig. 1.3.

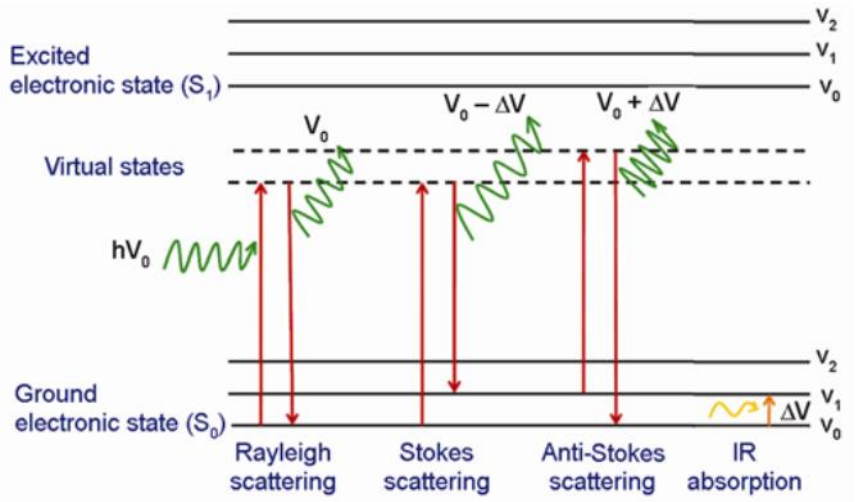

Fig. 1.3. Physical processes at various types of light scattering [6].

The energy difference between the incident and scattered photons is represented by the arrows of different lengths (Fig. 1.3). Numerically, the energy difference between the initial (v_0) and final ($v_{1,2}$) vibrational levels, or Raman shift in wave numbers (cm^{-1}), can be calculated.

The vibrational energy is ultimately dissipated as heat. Because of the low intensity of Raman scattering, the heat dissipation does not cause a measurable temperature rise in a material.

At room temperature the thermal population of vibrational excited states is low, although not zero. Therefore, the initial state is the ground state, and the scattered photon will have lower energy (longer wavelength) than the exciting photon. This Stokes shifted scatter is what is usually observed in Raman spectroscopy.

A small fraction of the molecules are in vibrationally excited states. Raman scattering from vibrationally excited molecules leaves the molecule in the ground state. The scattered photon appears at higher energy. At room temperature the anti-Stokes-shifted Raman spectrum is always weaker than the Stokes-shifted spectrum

and since the Stokes and anti-Stokes spectra contain the same frequency information most Raman experiments look at Stokes-shifted scatter only.

1.3.1 (c) Vibrational Energies.

The energy of a vibrational mode depends on molecular structure and environment. Atomic mass, bond order, molecular substituents, molecular geometry and hydrogen bonding all effect the vibrational force constant which, in turn dictates the vibrational energy. For example, the stretching frequency of a phosphorus-phosphorus bond ranges from 460 to 610 to 775 cm^{-1} for the single, double and triple bonded moieties, respectively. Much effort has been devoted to estimation or measurement of force constants. For small molecules, and even for some extended structures such as peptides, reasonably accurate calculations of vibrational frequencies are possible with commercially available software.

Vibrational Raman spectroscopy is not limited to intramolecular vibrations. Crystal lattice vibrations and other motions of extended solids are Raman-active. Their spectra are important in such fields as polymers and semiconductors. In the gas phase, rotational structure is resolvable on vibrational transitions. The resulting vibration/rotation spectra are widely used to study combustion and gas phase reactions generally. Vibrational Raman spectroscopy in this broad sense is an extraordinarily versatile probe into a wide range of phenomena ranging across disciplines from physical biochemistry to materials science.

1.3.1(d).Raman Selection Rules and Intensities.

A simple classical electromagnetic field description of Raman spectroscopy can be used to explain many of the important features of Raman band intensities. The dipole moment, P, induced in a molecule by an external electric field, E, is proportional to the field.

The proportionality constant is the polarizability of the molecule. The polarizability measures the ease with which the electron cloud around a molecule can be distorted. The induced dipole emits or scatters light at the optical frequency of the incident light wave.

Raman scattering occurs because a molecular vibration can change the polarizability.

The change is described by the polarizability derivative. The selection rule for a Raman-active vibration, that there be a change in polarizability during the vibration.

The Raman selection rule is analogous to the more familiar selection rule for an infrared-active vibration, which states that there must be a net change in permanent dipole moment during the vibration. From group theory it is straightforward to show that if a molecule has a center of symmetry, vibrations which are Raman-active will be silent in the infrared, and vice versa.

Scattering intensity is proportional to the square of the induced dipole moment that is to the square of the polarizability derivative.

If a vibration does not greatly change the polarizability, then the polarizability derivative will be near zero, and the intensity of the Raman band will be low. The vibrations of a highly polar moiety, such as the O-H bond, are usually weak. An external electric field can not induce a large change in the dipole moment and stretching or bending the bond does not change this.

Typical strong Raman scatterers are moieties with distributed electron clouds, such as carbon-carbon double bonds. The pi-electron cloud of the double bond is easily distorted in an external electric field. Bending or stretching the bond changes the distribution of electron density substantially, and causes a large change in induced dipole moment.

Chemists generally prefer a quantum-mechanical approach to Raman scattering theory, which relates scattering frequencies and intensities to vibrational and electronic energy states of the molecule. The standard perturbation theory treatment assumes that the frequency of the incident light is low compared to the frequency of the first electronic excited state. The small changes in the ground state wave function are described in terms of the sum of all possible excited vibronic states of the molecule.

1.4. Polarization Effects.

Raman scatter is partially polarized, even for molecules in a gas or liquid, where the individual molecules are randomly oriented. The effect is most easily seen with an exciting source which is plane polarized. In isotropic media polarization arises because the induced electric dipole has components which vary spatially with respect to the coordinates of the molecule. Polarized Raman experiments can be a power tool in studying the mechanism of orientation and the final structure of polymeric films and fibers as well as in the characterization of single crystals.

1.4.1. Resonance-Enhanced Raman Scattering.

If the wavelength of the exciting laser is within the electronic spectrum of a molecule then the intensity of some Raman-active vibrations increases by a factor of 10^2-10^4. This resonance enhancement or resonance Raman (RR) effect may be useful. Resonance enhancement does not begin at a sharply defined wavelength. In fact, enhancement is commonly observed if the exciting laser is even within a few hundred wavenumbers below the electronic transition of a molecule. This pre-resonance enhancement may also be experimentally useful.

RR, however, is only observed in molecules possessing vibrations that can be resonantly enhanced and as such this approach is limited to certain chemistries. This limits the generalized applicability of RR for analytical applications. An in-depth review of resonance enhancement is beyond the scope of this tutorial and the interested reader is referred to specific publications on the theory and application of RR.

1.4.2. Surface-Enhanced Raman Scattering.

The Raman scattering from a compound (or ion) adsorbed on or even within a few Angstroms of a structured metal surface can be 10^3 - 10^6 greater than in solution. This surface-enhanced Raman scattering is strongest on silver, but is

observable on gold and copper as well for common excitation sources. At practical excitation wavelengths, enhancement on other metals is unimportant. Surface-enhanced Raman scattering (SERS) arises from two mechanisms.

Although SERS allows observation of Raman spectra from solution concentrations in the micro molar (1 - 10^{-6}) range, slow adsorption kinetics, competitive adsorption, and the fact that only certain chemistries and states exhibit enhancements limits the general applicability of SERS outside the R&D laboratory.

1.4.3. The Raman Spectrum

A Raman spectrum is a plot of the intensity of Raman scattered radiation as a function of its frequency difference from the incident radiation (usually in units of wavenumbers, cm^{-1}). This difference is called the Raman shift. Note that, because it is a difference value, the Raman shift is independent of the frequency of the incident radiation.

1.5. Qualitative *versus* Quantitative Raman

Historically, due to the complexity and inefficiency of the optical components used, the challenge for Raman instruments has been to simply measure a useable Raman spectrum. A spectrum is used to chemical fingerprint the sample, provide a qualitative assessment of the chemical composition of the sample. Kaiser, have revolutionized Raman spectroscopy, by pioneering the holographic technology that has allowed high-throughput, compact analyzers to be developed. Kaiser's technology has enabled Kaiser and its users to move beyond qualitative Raman spectroscopy to quantitative analysis. Quantitative Raman spectroscopy provides for species' chemical concentrations to be measured, monitored, and controlled. Real-time ‘in situ‘ qualitative Raman spectroscopy has allowed Kaiser's Raman analyzers to be deployed beyond the laboratory and provide over 20 years of successful 24/7 process control installations.

1.6. Advantages of Raman Spectroscopy

Raman spectroscopy is useful for chemical analysis for several reasons:

Specificity: Because Raman detects fundamental vibrations, Raman bands have a good signal-to-noise ratio and are non-overlapping. This allows a Raman spectrum to be used for everything from "fingerprinting" of samples to constructing complex chemical models of reaction processes.

Analysis of aqueous systems: The IR spectrum of water is strong and relatively complex, making IR inadequate for analysis of aqueous solutions due to heavy interference by the water bands. However, the Raman spectrum of water is weak and unobtrusive, allowing good spectra to be acquired of species in aqueous solution.

Analysis of organic and inorganic chemistries: If a covalent chemical bond exists between chemical species then a unique Raman signature may be produced.

Wide Concentration Range: The measured intensity of a Raman species is directly proportional to the concentration. This allows a Raman analysis to measure a species concentration from a fraction of 1% to 100% without sample dilution.

No sample preparation: Unlike most other chemical analysis techniques, Raman requires any special preparation of the sample. In fact, no contact with the sample is needed at all because Raman involves only illuminating a sample with a laser and collecting the scattered photons.

Non-destructive Analysis: Because Raman involves only illuminating a sample, often through a window, with a laser and collecting the scattered photons this makes Raman spectroscopy non-destructive.

Compatible with Common Windows: Can utilize standard sampling containers and windows manufactured of glass, sapphire, transparent polymers, and diamond to measure samples in situ.

Quantitative Raman: Because the intensity of a Raman band is directly proportional to the number of molecules giving rise to the band,

then the Raman band can be used to provide a measure of the concentration of a molecule.

Short measurement times: A Raman spectrum can, typically, be acquired on a timescale from a fraction of a seconds to several minutes, thus Raman can be used to monitor chemical reactions in "real time."

1.7. Basic Components of a Raman System

A Raman system is conceptually simple and includes the following main components (see Chapter 2):

Excitation source.

A sample.

A detector and associated electronics.

A recording device.

In practice because the Raman Effect is weak, the efficiency of and optimization of each of the instrumental components into an integrated system is critically important. Only an optimized system can be capable of producing the greatest measurement potential, over the widest range of same types, and able to measure the lowest concentration of species in the shortest amount of time possible.

Raman scattering is perhaps most easily understandable if the incident light is considered as consisting of particles, or photons (with energy proportional to frequency), that strike the molecules of the sample. Most of the encounters are elastic, and the photons are scattered with unchanged energy and frequency. On some occasions, however, the molecule takes up energy from or gives up energy to the photons, which are thereby scattered with diminished or increased energy, hence with lower or higher frequency. The frequency shifts are thus measures of the amounts of energy involved in the transition between initial and final states of the scattering molecule.

The Raman Effect is feeble; for a liquid compound the intensity of the affected light may be only 1/100,000 of that incident beam. The pattern of the Raman lines is characteristic of the particular molecular species, and its intensity is proportional to the number of scattering molecules in the path.

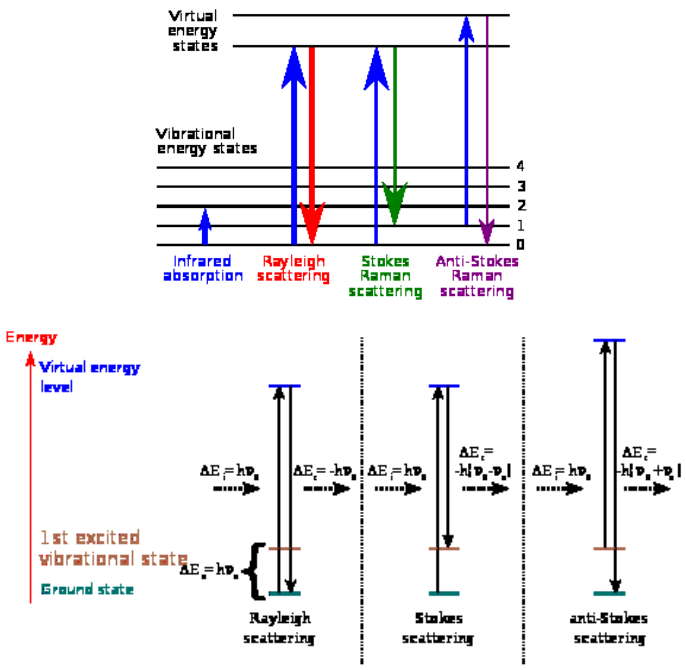

Fig. 1.4. Raman Effect.

The horizontal lines indicate vibrational energy levels. Ground electronic state, and excited electronic states are shown. The diagrams show how a molecule in the ground state can make a transition from the lowest vibrational level to the first excited vibrational level by means of Raman scattering. Black up-arrows indicate the frequency of the laser excitation light; black down-arrows indicate frequency of the Raman scattered light. The difference in length between black up- and down-arrows indicates molecular vibration frequency [8].

It should be noted here that Raman scattering at different excitation wavelengths, UV, visible and near-IR, produces the same change in vibrational energy. Therefore the excitation wavelength can be chosen to avoid spectral interference by fluorescence. For visible excitation, the fluorescence light frequency and Raman scattered light frequency are similar. This leads to intense

fluorescence background in visible excitation Raman spectra. Near-IR light has too low a frequency to excite fluorescence, while for UV excitation, the fluorescence light frequency is much lower than the Raman scattered light frequency. Hence, fluorescence background in the Raman spectrum can be reduced by using UV or near-IR excitation.

The Raman scattered light can be collected by a spectrometer and displayed as a "spectrum", i.e. intensity versus frequency change. Since each molecular species has its own unique set of molecular vibrations, the Raman spectrum of a particular species will consist of a series of peaks or "bands", each shifted by one of the vibrational frequencies characteristic of that molecule.

References

1. C.V.Raman, K.S.Krishnan. Nature,121 (1928) p.501.
2. C.V.Raman, K.S.Krishnan. Naturwissenshaften 16 (1928) p.557.
3. C.V.Raman. "The molecular scattering of light". Nobel Lecture, December 11, 1930 (nobelprize.org,1930).
4. encyclopedia 2. Thefreedictionary.com.
5. McGraw-Hill. Concise Encyclopedia of Physics, 2002 by The McGraw-Hill Companies, Inc.
6. Bhawana Singh, et all. Application of vibrational microspectroscopy in biology and medicine. Current Science, vol. 102, iss. 2 (2012)
7. From Nobel Lectures, Physics 1922-1941, Elsevier Publishing Company, Amsterdam, 1965.
8. https://en.wikipedia.org

CHAPTER 2.Raman Spectroscopy

2.1. Milestones in development of Raman spectroscopy

*Discovered in 1928 by Sir Chandrasekhara Venkata Raman, using sunlight as a source, telescope as a collector, his eyes as a detector;

*Subsequent mercury sources replaced by lasers in 1962;

*Photographic plates replaced by photomultiplier tubes by 1953;

*Double and triple monochromators introduced in 1960s;

*Holographic gratings in 1968;

*FT-Raman, array detectors, Raman microscopes.

Raman spectroscopy has been applied in numerous scientific fields, from chemistry and biochemistry to arts and archaeology, as a powerful spectroscopic technique which allows a spectral fingerprint capable of identifying the structure and function of molecules, cells, tissues, or materials [1]. In particular, its application to medical diagnostics has been of increasing interest in the past few decades [1-3].

2.2. Instrumentation for Conventional Raman Spectroscopy

Raman spectroscopy provides an invaluable analytical tool for molecular finger printing as well as monitoring changes in molecular bond structure (e.g. state changes/modification and stresses, strains).

In comparison to other vibrational spectroscopy methods such as FT/IR and NIR, Raman has several major advantages. These advantages stem from the fact that the Raman Effect manifests itself in the light scattered off of a sample as opposed to the light absorbed by a sample. As a result, Raman spectroscopy requires little to no sample preparation as is insensitive to aqueous absorption bands. The property mentioned facilitates the measurement of solids, liquids, and gases not only directly, but also through transparent containers such as glasses, quartz, and plastic.

For many years the instruments were large, complicated, and the experiments could be quite complex. With advances in modern technology, Raman spectrometers have become small, portable. As a rule, these devices are exploited by people who are neither specialists in spectroscopy nor analysts.

Typical Raman spectrometer consists of:

- Excitation source (generally a CW laser);
- Sample illumination and scattered light collection system;
- Sample holder;
- Monochromator or spectrograph;
- Detection system (detector, amplifier, output device).

Scattering efficiency for Raman is 1 in 1000 photons. Reasonably, spectroscopists/researchers need extremely high intensity source, spectrometer with high degree of discrimination against stray light, extremely sensitive detection system able to detect small numbers of photons over dark background.

2.3. Excitation Sources

Chronology of the excitation sources used in Raman Spectroscopy:

1928 - Sun, Hg lamp;

1960 - Townes suggests the use of lasers;

1963 – First laser use;

1964 – He-Ne;

1969 – Ar^+, Kr^+;

2000 – Nd-Yag;

2005 – Layer diodes.

Commercially Available Laser Sources for Raman Spectroscopy

Laser Type	Wavelength, nm
Argon ion	488.0 or 514.5
Krypton ion	530.9 or 647.1
Helium-Neon	632.8
Diode	785 or 830
Nd-YAG	1064

Table 2.1

In addition to Table 2.1:

•CW gas lasers (Ar^+, Kr^+, Ne, N_2 (337.1 nm UV, pulsed), CO_2 (9-11 μm, IR, CW/pulsed), excimer XeCl, 308 nm UV, pulsed);

•Dye lasers;

•Solid-state lasers: Ruby (694.3 nm, pulsed), Nd:YAG (1064 nm near-IR,CW/pulsed), Diode (3500-380 cm^{-1} IR, CW/pulsed);

•Pulsed Nd: YAG.

Also used are laser harmonics (532 nm, 355 nm, 266 nm) for time-resolved and UV-resonance Raman applications.

To detect very weak Raman scattering, proper focusing of laser and efficient collection of scattered radiation is required: 90^o for scattering, $180^o$for back-scattering.

Laser focuses to ~ 1mm; F-number (F=f/D) of collection lens should be small for large light-gathering power and should be matched to F-number of monochromator (usually two lenses are used, a short focal length, low F-number to collect the largest solid angle, and the second to F-match the monochromator.

2.4. Detectors

2.4.1. Single-Channel Detectors

Historically, Photon Multiplier Tubes (PMTs) were first used in Raman Spectroscopy in the 1960s.

The instruments that were used between the mid-1960s and the mid-1980s were double scanning monochromators with laser sources and low-noise photomultipliers.

Practically immediately following the invention of optical lasers in the early 1960s all instruments use lasers as the light source. It should be noted here that the physics on which both laser and photomultiplier operation are based is derived from Albert Einstein's work.

Photomultipliers operate by using photoelectric effect for which Einstein received the Nobel Prize for work performed in 1905.

Laser action was a demonstration of stimulated emission predicted by Einstein in 1905.

Raman's instrument was a small spectrograph with a photographic plate. Similar instruments used in the early years typically required more than 12 hours to acquire spectra.

The continuous-wave (CW) He-Ne laser was implemented in the next two years, 1962-1964.

In photomultiplier tube, photocathode emits electrons when struck by photon; series of dynodes each emit a number of secondary electrons when struck by electron; anode collects electrons as output signal.

The advantage of this approach is their relatively high sensitivity compared to the earlier measurement geometries. The disadvantage of these tubes is their rather high background signal (typically $10e^-/s$) and their sensitivity to permit heat damage: if the detectors are exposed to extremely high light intensities (e.g. laser beam, light in the room) this could result in permanent damage. Even more, this approach has the disadvantage that you can only measure at a single wavelength and said that analysis of a complete wavelength sequentially, which is time-consuming.

The attractiveness of PMTs, as mentioned, arose from their high sensitivity, very wide dynamic range, and linearity of response. The basic reason for superiority of the photomultipliers is the secondary-emission amplification that makes it possible for the tube to approach "ideal" device performance limited only by the statistics of photoemission. In other words, this means that with amplifications between 10^3 and 10^8 signals are not swamped by electronic noise. In addition, extremely fast response times (10^{-10} s) can be achieved.

The linearity of the response and the wide range of gain made these detectors particularly useful for recording line spectra. Therefore, including them in Raman systems seemed natural.

Whereas the earliest Raman measurements were recorded with low-pressure mercury sources and photographic plates, scanning multistage monochromators with lasers and PMTs became the standard instruments during 1960s and 1970s. These systems provided high stray light performance, allowing examination of all types of samples including highly "scattering" solids. Raman bands at shifts as low as 5-10 $cm^{-1}$from the line were observed.

2.4.2. Multi-Channel Detectors

In practice researchers want to record multiple wavelengths simultaneously. Therefore, usually a multi-channel detector is used. Basically, a multi-channel detector is a linear array of single-channel detectors. A particular part of the spectrum is projected along the linear axis of the detector and thus, each channel of the detector corresponds with a different wavelength. Linear detectors are often used in small, handhold Raman instruments.

2.4.3. Detection: Photodiode array

Multichannel detector, 2.5 cm long with 1024 silicon photodiodes, each 25μm wide, 2.5 mm high.

Dispersed radiation striking detector causes charge pattern to develop that is related to intensity of radiation in focal plane.

Intensifier (multichannel plate) in front of detector increases sensitivity by ~10^4

2.4.4. CCD detectors

Charge-Coupled-Device (CCD) was invented in 1969 at Bell Telephone Laboratories by Willard S. Boyle and George E. Smith [4]. On that fateful day in 1969 Smith and Boyle not only described the basic structure and principles of operation, they also predicted its applications in imaging as well as memory.

The inventors received Nobel Prize of Physics in 2009 "for the invention of an imaging semiconductor circuit - the CCD sensor". CCD is 2D Array of individual “detectors” – pixels (1024×256 pixels).

CCD is electronic device which work by converting light into electric charge in a silicon chip (integrated circuit). This charge is digitalized and stored as image file on a computer. Charge-coupled-devices appeared as reliable, commercial products for spectroscopic applications in the early 1990s. The fundamental element of every CCD is the metal oxide semiconductor (MOS) [5-6] capacitor. The heart of a CCD imager is a large number of MOS capacitors densely packed in a two-dimensional array.

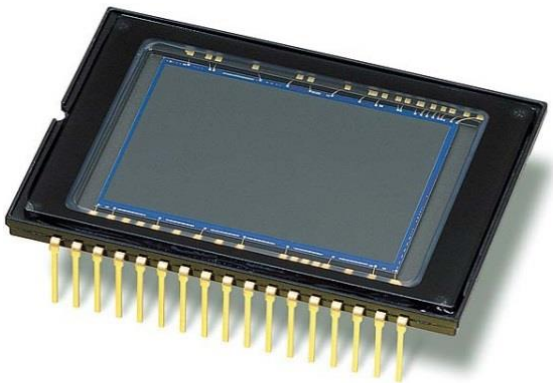

Fig. 2.1. A charge-couple device.

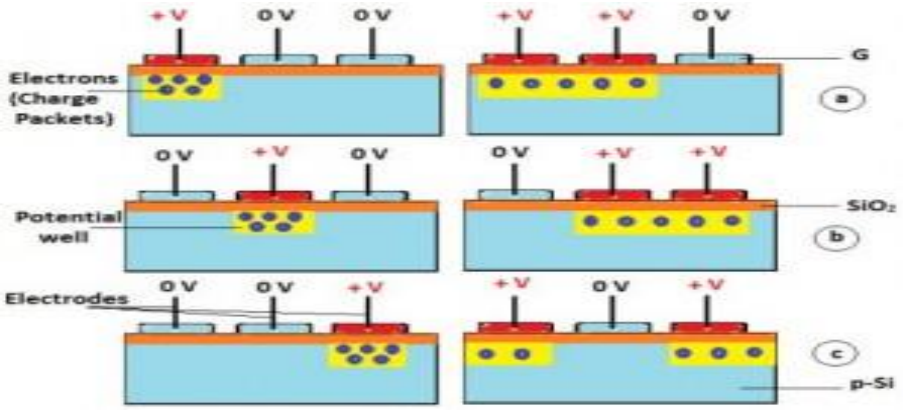

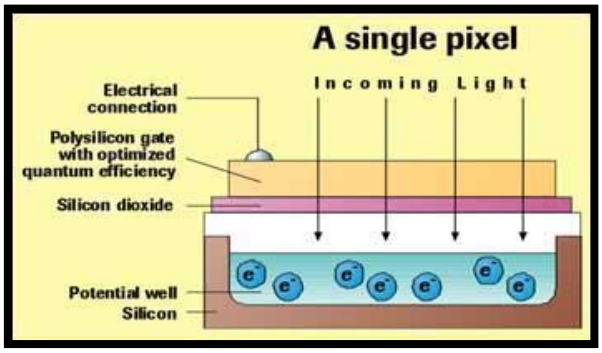

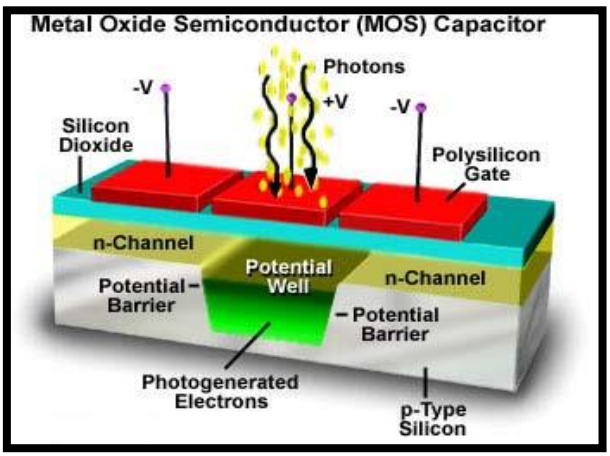

Fig. 2.2. A single pixel cross section and architecture of metal oxide semiconductor capacitor.

The charge-coupled device is truly one of the great developments of our time. It is conceptually quite simple. It uses a quantity of electrical charge to represent an analog quantity, such as light intensity, sampled at discrete times. The

memory function comes from shifting these charges, simultaneously, down a row of cells, also in discrete time. The CCD is, therefore, a discrete-time device, i.e., a continuous, or analog, signal sampled at discrete times.

The CCD (charge-coupled device) is an optical array detector consisting of a two-dimensional array of silicon diodes. CCDs have low readout noise, high quantum efficiency and sensitivity over wide wavelength range (100-1000 nm).

CCD was invented in 1969at AT&T Labs by Willard Boyle and George Smith. Charge-coupled-devices appeared as reliable, commercial products for spectroscopic applications in the early 1990s.

Important events in the development of CCD:

1974, Buried Channel CCD – Smiths & Boyle;

1970 -1975 – Early Video Camera Development;

1983 - CCD Replace Photographic Plates in Telescopes;

1995 – Digital Cameras Invade the Consumer Market.

A charge-coupled device (CCD) is a light-sensitive integrated circuit that stores and displays the data for an image in such a way that each pixel (picture element) in the image is converted into an electrical charge the intensity of which is related to a color in the color spectrum.

Fundamentally, a charge coupled device (CCD) is an integrated circuit etched onto a silicon surface forming light sensitive elements - pixels. Each cell of a CCD contains a metal oxide semiconductor (MOS), the same device that forms the gate of a MOS field effect transistor (FET). Although both surface channel and buried channel MOS capacitors have been utilized in CCD construction, virtually all CCDs manufactured today are of the buried channel type [8]. The buried channel structure was developed to alleviate the problems caused by surface irregularities at the interface of the oxide and semiconductor.

Solid-state electronics has always had its two sides: electrons and holes, n-type and p-type, and so on. Although the duality continues with charge-coupled devices, we find that CCDs are typically fabricated on a p-type substrate. In order to implement the “buried” channel a thin n-type region is formed on its surface. An insulator, in the form of a silicon dioxide layer is grown on top of the n-region.

The capacitor is finished off by placing one or more electrodes, also called gates, on top of the insulating silicon dioxide. These electrodes could be metal, but more likely a heavily doped polycrystalline silicon conducting layer would be used.

Photons incident on this surface generate charge that can be read by electronics and turned into a digital copy of the light patterns falling on the device. CCDs come in a wide variety of sizes and types and are used in many applications from cell phone cameras to high-end scientific applications.

The function of a CCD can be visualized as an array of buckets (pixels) collecting rainwater (photons). Each bucket in the array is exposed for the same amount of time to the rain. The buckets fill up with a varying amount of water, and the CCD is then read one bucket at a time. This process is initiated by pouring water into the adjacent empty column. The buckets in this column transfer their 'water' down to a final pixel where the electronics of the camera read-out this pixel (the computer measuring the bucket) and turn it into a number that can be understood and stored by a computer.

There is no doubt that this is an oversimplification. All the pixels in a CCD are actually shifted simultaneously, not one column at a time. We'll start the explanation process by explaining how a simple pixel works.

A CCD (Charge Coupled Device) is a silicon based multichannel array detector of UV, visible and near-infra light. They are used for Raman spectroscopy because they are extremely sensitive to light (and thus suitable for analysis of the inherently weak Raman signal), and allow multichannel operation (which means that the entire Raman spectrum can be detected in a single acquisition). CCDs are widely used, not least as the sensors in digital cameras, but versions for scientific spectroscopy are of a considerably higher grade to give the best possible sensitivity, uniformity and noise characteristics.

CCD detectors are typically one dimensional (linear) or two dimensional (area) arrays of thousands or millions of individual detector elements (also known as pixels, picture elements). Each element interacts with light to build up a charge

– the brighter the light, and/or the longer the interaction, the more charge is registered. At the end of the measurement read out electronics pull the charge from the elements, at which point each individual charge reading is measured.

The acronym MOS stands for metal–oxide–semiconductor. An MOS capacitor (Fig. 2.2) is made of a semiconductor body or substrate, an insulator film, such as SiO_2, and a metal electrode called a gate. The oxide film can be as thin as 1.5 nm. One nanometer is equal to 10 Å, or the size of a few oxide molecules.

Before 1970, the gates withstand high temperature without reacting with SiO_2. But the MOS name stuck.

Unless specified otherwise, you may assume that the gate is made of heavily doped, highly conductive, polycrystalline silicon, or poly-Si for short. After 2008, the trend is to reintroduce metal gate and replace SiO_2 with more advanced dielectrics for the most advanced transistors.

The MOS capacitor is not a widely used device in itself. However, it is part of the MOS transistor. The MOS transistor is by far the most widely used semiconductor device. An MOS transistor (Fig. 2.2) is an MOS capacitor with two PN junctions flanking the capacitor. This transistor structure is often a better structure for studying the MOS capacitor properties than the MOS capacitor itself was typically made of metals such as Al (hence the M in MOS). After 1970, heavily doped polycrystalline silicon has been the standard gate material because of its ability to withstand high temperature without reacting with SiO_2. But the MOS name stuck.

Unless specified otherwise, you may assume that the gate is made of heavily doped, highly conductive, polycrystalline silicon, or poly-Si for short. After 2008, the trend is to reintroduce metal gate and replace SiO2 with more advanced dielectrics for the most advanced transistors.

The principals of forming MOS structure are similar to the metal-semiconductor (MS) contact structures, but the MOS structure is like a sandwich structure which has a thin layer of silicon oxides in the middle between metal and

semiconductor (Si) layer. Figure 1 below shows a schematic of an ideal MOS-C device. For an ideal MOS-C structure, some properties should follow below.

(1) The metallic gate should thick enough to be equipotential region, where every point has the same potential in the space, under a.c and d.c biasing conditions.

(2) The oxides layer in the middle should be a perfect insulator with zero current flowing through under all static biasing conditions.

(3) There should be no charge centers located on the oxide-semiconductor interface.

(4) The semiconductor should be uniformly doped with donors or acceptors as p-type or n-type semiconductors.

(5) The semiconductor (Si) should be thick enough for charges to encounter a field free region (Si bulk) before reaching the back contact.

(6) The Ohmic contacts should be established on the backside of the MOS device.

(7) MOS-C is a one-dimensional structure with variables only related to the x-coordinate (distance) as the Figure 1 below.

(8) The metal work function (ΦM) should equal to the semiconductor work function (ΦS) as well as the electron affinity (X) with the difference of conduction band (Ec) and Fermi energy (EF) in forward flat band, $\Phi M=\Phi S=\chi+(Ec-EF)FB$. This property can be omitted, but it is easier to help with the initial understanding of the static behavior in MOS devices.

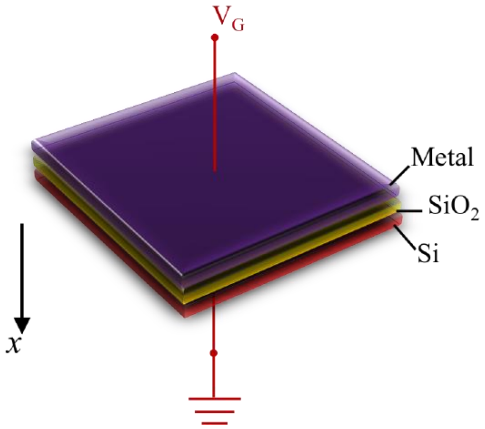

Fig. 2.3 The structure of an ideal MOS-C device.

In a typical Raman spectrometer, the Raman scattered light is dispersed using the diffraction grating, and this dispersed light is then projected onto the long axis of the CCD array. The first element will detect light from the low cm^{-1} edge of the spectrum; the second element will detect light from the next spectral position, and so on. The last element will detect light from the high cm^{-1} edge of the spectrum.

CCDs require some degree of cooling to make them suitable for high grade spectroscopy. Typically this is done using either Peltier cooling (suitable for temperatures down to -90^{o}C), and liquid nitrogen cryogenic cooling. Most Raman systems use Peltier cooled detectors, but for certain specialized applications liquid nitrogen cooled detectors still have advantages.

Methods to avoid local heating from absorption of laser beam: line focus with cylindrical lens, focuses beam on sample, over 10 to 25 mm instead of a few microns.

Rotating cylindrical cell: centrifugal force drives liquid to outer part of cell. Laser is focused near the wall to minimize self-absorption of Raman scattered light.

2.5. Fluorescence elimination

Some residual fluorescence is detected and, despite all of experimental attempts, fluorescence signal cannot be avoided. It should be noted here that the fluorescence and Raman signals lie at the same spectral interval. As a result, fluorescence signal cannot be subtracted fully.

There exist several experimental tools (methods) to separate the fluorescence contribution.

A simple approach requires a quencher that is not Raman active.

The wavelength of the excitation light can also be modulated to reject fluorescence.

Using multiple dispersion stages is another way of stray light reduction. Double and triple spectrometers allow taking Raman spectra without use of notch filters. In such systems Raman-active modes with frequencies as low as 3-5 cm-1 can be efficiently detected.

In earlier times, single-point detectors such as photon-counting Photomultiplier Tubes (PMT) were used. However, a single Raman spectrum obtained with a PMT detector in wavenumber scanning mode was taking substantial period of time, slowing down any research or industrial activity based on Raman analytical technique. Nowadays, more and more often researchers use multi-channel detectors like Photodiode Arrays (PDA) or, more commonly, a Charge-Coupled Devices (CCD) to detect the Raman scattered light. Sensitivity and performance of modern CCD detectors are rapidly improving. In many cases CCD is becoming the detector of choice for Raman spectroscopy.

FT-Raman spectroscopy solves problems of fluorescence and sample degradation by excitation in the near-IR. Interferometric optics achieves multiplex measurement. Avoidance of fluorescence by long-wavelength excitation is not without a cost in sensitivity, however, Normal Raman scattering intensity decreases with l/λ^4, leading to a factor of 18 less scattering at 1064 nm than at 514.5 nm. Silicon CCD detectors have a lower quantum efficiency in the 800-1000 nm region than in the visible and cannot detect light above 1.1 pm at all. The available detectors for FT-Raman have good quantum efficiency(-0.7), but high dark signal and accompanying noise. Finally, resonance Raman enhancement depends on the same electronic transitions as fluorescence, so avoiding fluorescence by using a longer excitation wavelength will generally negate resonance enhancement.

2.6. Advantages & disadvantages of Raman spectroscopy

Advantages

(a) Essential that it a non-destructive technique (probe);

(b) Raman spectroscopy is powerful and very informative;

(c) No or minimal sample preparation needed. Provides for easy and practical sampling;

(d) Provides a full set of vibrational and rotational spectral information;

(e) Avoids the sampling difficulties entailed in MIR and FIR (middle-infrared, far-infrared);

(f) Quenching does not cause any problem for quantitative measurements;

(g) High pressure facilitates the use of Raman scattering;

(h) Raman experiments do not require any tunable laser source; any laser with high average power can be used, but since the signal is proportional λ^{-4}, short wavelengths are preferred.

In addition to the advantages listed above, it should be mentioned also:

- Samples to be examined in a whole range of physical states, for example, as solids, liquids or vaporsю;

- Because Raman spectroscopy is a scattering process, samples of any size or shape can be used;

- Very small amounts of material can be studied down to microscopic levels in the range of 10 microns. The region from 80-500 cm^{-1} can be studied with no changes on the same instrument. Raman spectroscopy can be used with solids, liquids or gasses. As mentioned above no sample preparation is needed and it is a non-destructive technique. There is no concern with sample thickness, size or shape. Furthermore samples can be analyzed directly in bottles, bags or blisters;

- Also no vacuum is needed which saves on various expensive pieces of vacuum equipment. In terms of time, the spectra are produced relatively quickly. Further advantages include use of aqueous solutions, use of glass and the use of down fiber optic cables for remote sampling;

- Several species can be measured simultaneously;

- Atoms, radicals as well as molecules that absorb well down in the UV region can be measured;

- The signal is linear in intensity, no saturation effects;

- For fiber-optic sampling, the spectral transmission of the fiber materials is even more suitable for Raman than for NIR spectroscopy.

Disadvantages

(1)The Raman signal is very weak, ~ 1000 times lower than Rayleigh scattering. For solids, this difference can be more than 10^6. Typically,

$$I_{Raman} \approx 10^{-3} I_{Rayleigh} \approx 10^{-6} I_{incident};$$

(2) It is very hard to make 2D-visualisation;

(3)The technique is sensitive to background fluorescence and stray light;

(4) It is an incoherent technique. This means, in other words, that background emission can be a problem;

(5) It requires a laser with high average power;

(6) Trade-off between having a sufficient signal ant bot damaging the windows;

(7) Disadvantages include that metals or alloys cannot be used. The Raman Effect is very weak, which leads to low sensitivity, making it difficult to measure low concentrations of a substance;

(8) Sample heating through the intense laser radiation can destroy the sample or mask the Raman spectrum;

(9) Serious problems in Raman occur when large background signals from fluorescence from impurities or the sample itself arise;

(10) Other disadvantages of Raman spectroscopy include equipment cost and the sensitivity of the technique. Raman spectrophotometers can be quite costly, depending on their applications, and the technique generally cannot compete with chromatography for analytical sensitivity in quantitative analyses.

Also should be noted here the following:

Unfortunately, the measured Raman spectrum is typically masked by a strong fluorescence background in most applications. This is due to the fact that the probability of Raman scattering (cross-section) is much lower that of fluorescence gives, A strong fluorescence background gives rise to two problems.

Firstly, it becomes the dominant element in the photon shot noise and thus detracts from signal-to-noise ratio (SNR) even if the Raman bands are narrow and fluorescence has a quite smooth and featureless spectrum.

In spite of the obvious advantages of Raman spectroscopy, the strong fluorescence background has so far restricted its use in otherwise potential applications.

Fluorescence has been effectively suppressed up to now by using near-infrared laser excitation, e.g. Nd:YAG 1004 nm, instead of the traditional shorter laser excitation wavelengths (400-830 nm) but this requires the use of InGaAs or Ge detectors, which produce dark current and read noise levels that are several orders of magnitude higher than the Si CCD, which is predominantly used with traditional shorter wavelength excitation (400 nm, 830 nm).

This results in an increased noise level and a need for high excitation power (> 1000 mW versus typically a few tens to a few hundred mW with CCD-based systems) and a long integration times (30 minutes to several hours vs. from a few seconds to a few minutes with CCD-based systems).

Fortunately, since Raman scattering has a lifetime of much less than a picosecond whereas fluorescence lifetimes are typically in the range of few thousand picoseconds or even tens of nanoseconds, it is possible to suppress the fluorescence background to a great extent if short, intensive laser pulses are used to illuminate the sample rather than CW radiation and the sample response is recorded only during short pulses. Thus, by "time-gating" the measurement to the period of the laser pulse, the total intensity of the fluorescence in the recorded spectrum can be substantially reduced.

Ways to improve Raman signal intensity

Before the advent of laser, an ideal excitation source for light scattering, Raman spectroscopy suffered from the low intensity of the inelastic scattering and the much larger intensity of the Rayleigh scattering.

Raman signal is normally quite weak and people are constantly improving Raman spectroscopy techniques. Many different ways of sample preparation, sample illumination or scattered light detection were invented to enhance intensity of Raman signal. Here we will examine some of them.

Interpretation of Raman spectrum

In Raman spectra, the intensity of measured Raman scattering is plotted versus the Raman shift. The Raman shift is defined as difference between the measured frequency of scattered light and incident light beam. Hence Raman spectra are independent of the wavelength of the light source. However, instead of using the wavelength, the Raman shift is given as change of the wavenumber n (cm^{-1}) which is inversely proportional to the wavelength. In other words, Raman spectra depict the intensity of scattered light for each frequency of scattered light. The frequency is traditionally measured in unit termed the wavenumber, number of waves per cm^{-1}. The *x*-axis frequencies are plotted relative to that of the laser.

A Raman spectrum consists of a range of features, each associated with a vibrational mode. It should be stressed on that the spectrum is unique to the material and enables researchers to identify it.

The information we get from Raman spectrum:

- One can identify the material by the Raman shifts and relative intensities of all of the Raman bands of the material;
- Individual Raman band may shift, narrow or broaden, or vary in intensity;
- These changes reveal information about stresses in the sample, variations in crystallinity, and the amount of material;
- Variations in spectra with position on the sample reveal changes in the homogeneity of the material;
- One can identify unknown materials from their unique Raman spectral fingerprints using database of known spectra.

In addition, we can determine if materials are the same or different by comparing their Raman spectra.

From the height, width and position of Raman lines information about the relative amount of the material, layer thickness, crystallinity, whether it is under compression or tension, temperature can be obtained.

References

1. Ruchta S. Das, Y.K.Agarval. Vibrational Spectroscopy, **67**, 2 (2011)163-176.
2. Y.Ozaki. Appl. Spectr. Rev. **45,** 3-4(1988) 259-213.
3. I.Pence, A.Mohadevan-Jansen. Chem.Soc.Rev. **45,** 7 (2016) 1958-1979.
4. W.S.Boyle, G.E.Smith. Bell.Syst.Tech. J. (apr.1970) 587-593.
5. W.E.Engeler, J.J.Tieman, R.D.Baertsh. SSCC Digest Tech. Papers 1971(Solid State Circuits Conf., 17-19 February).
6. Muller R.S., T.Kanins, and M.Chen. Devise Electronics for Integrated Circuits, 3rd.ed. New York. John Wiley & Sons, 2003.

CHAPTER 3. Raman spectra of glasses & amorphous films.

Structural changes induced by light and heat treatment in vacuum deposited amorphous chalcogenide films prepared by thermal evaporation methods with different rates have been investigated using Raman scattering. The changes in the Raman spectra of thermally evaporated amorphous As_2S_3 films after light treatment are interpreted in terms of rearrangement of bonding configurations of molecular species that exist just after deposition. As the evaporation temperature or deposition rate is increased, irradiation with band-gap light and even more annealing of the films induces arsenic-enrichment and the formation of micro crystallites. The reversible photo-induced changes in annealed films involve negligible small change in bonding statistics. Discernable change occurs in the medium-range order.

3.1. Amorphous chalcogenides – general information

During the last decades the increasing use of amorphous chalcogenides and V1b group elements of the periodic table – namely selenium, sulfur, and tellurium – in semiconductor films has been very impressive.

In the follow we try to consider their physical properties.

It seems quite logical to start with amorphous selenium (a-Se). This material can be considered as the most representative among this class of materials. The properties of a-Se are well documented. In addition, it can serve as an ideal test material for the comparison of various mobility-lifetimes ($\mu\tau$) measurement techniques.

The nature of deep traps in a-Se and its technologically important chemically modified forms such as Cl-doped and halogenated a-Se-Te have not been satisfactory identified. The capture radius of the deep traps, for example, is not known.

Additional reason for using a-Se is that it can be readily prepared by using conventional vacuum deposition techniques with reproducible properties so that the results presented will be typical for aby photoreceptor grade a-Se or Cl-doped As-Se film.

Undoubtedly, a-Se not only offers advantages of reduced cost, but it can also be readily produced as large area elements of the type required im applications.

The successful use of non-crystalline chalcogenide semiconductors in various applications, especially in various imaging applications depends on our understanding of their origin and unique physical properties. These properties can be compared to the standard that presently exists in the case of their crystalline counterparts.

For many years, during and after development of modern band theory of electronic conduction in crystalline solids, amorphous materials were not considered for use as semiconductors. The occurrence of bands of allowed electronic energy states, separated by forbidden ranges of energy, had become firmly identified with the interaction of electronic waveforms with a periodic lattice. This is proved difficult for physicists to contemplate the existence of similar features in materials lacking such long-range order.

3.2. The influence of preparation conditions

The structural, optical and photo-physical properties of chalcogenide glasses have been permanently the subjects of systematic interest more than 40 years [1-4]. The interest have been stimulated both by unresolved fundamental scientific problems of non-crystalline materials (e.g. the structure, electronic properties, to say about few) and the need to assess their potential as optical memory elements, for image formation and other useful applications.

The structural and physical properties of amorphous chalcogenides depend on preparation conditions and subsequent sample treatments, although in less sensitive manner as their crystalline counterparts. In many cases the initial

structures of amorphous films differs from those of well-annealed films or their bulk-glass counterparts and undergo significant irreversible structural changes in response to band-gap illumination or annealing (so-called photo- and thermo-induced changes). Although the induced effects mentioned above have been reviewed many times, their origin still remains disputable.

In the following we take an attempt only to give our experience on examining the influence of preparation conditions (e. rates) and of various treatments (irradiation or annealing) on the structure of fresh (as-deposited) AsxS1-x amorphous films. The latter are particularly suitable objects for such a study because the irreversible changes in the optical properties of these materials, especially in As_2S_3, are much more pronounced than those in other chalcogenide glasses, e.g. As_xSe_{1-x}.

3.3. Samples and technique to probe local structure

Usually the samples used in these studies were amorphous films, typically 5-20 μm thick. The films were prepared in conventional manner, by thermal vacuum evaporation of glassy As_xS_{1-x} alloys (high-purity elements were alloyed by melting in evacuated and sealed quartz ampoules) from a molybdenum boat onto glass and quartz substrates. The evaporation was performed under two different conditions: evaporation onto a substrate with deposition rate ~20 Å s^{-1} (conventional mode) and evaporation onto a substrate with deposition rate ~1000 Å s^{-1} (flash evaporation). The deposition rate was varied by changing the source (evaporation boat) temperature while the substrate temperature was held constant at T=300 K. Chemical compositions of the films, e.g. As_2S_3, were found to be $As_{39.7}S_{40.3}$ on the basis of electron microprobe analysis. The lack of crystallinity in the film samples was systematically verified by X-ray diffraction measurements.

Raman spectra were measured by conventional and Fourier Transform IR Raman spectrometry (Bruker, model IFS 55). Laser irradiation of the wavelength of 647.1 and 1064 nm from Kr-ion and Nd:YAG lasers were used for the excitation of the Raman spectra. Such a low energy, especially for the latter case,

is well below the values of the optical band gaps for the glassy alloys under study. Thus, no detectable photo structural transformation took place under data collection. It is quite naturally that the amplitudes of some Raman lines from As_xS_{1-x} films were often low (respectively to that in bulk glass), the spectra usually were "noisy" and not smooth. Back-scattering method was exploited with the resolution of 1 cm^{-1}. Raman spectra of the amorphous films were recorded at sufficiently low incident laser-beam power density (3-5 mW) to avoid possible photo structural changes in a case of 647 nm excitation line. A Kr+-ion laser was used as an exposure source and the films were exposed at an intensity of 30 mW × cm^{-2}. Although structural transformations in As_xS_{1-x} films were the subject of numerous articles [5-17], some important aspects are still not fully understood.

3.4. Local structure of As_2S_3 amorphous films

First of all we consider the results obtained for conventionally prepared amorphous films. Fig. 1 shows the Raman spectra for the as-deposited (1), exposed (2), annealed film (3), and bulk-glass (4) forms of As_2S_3.

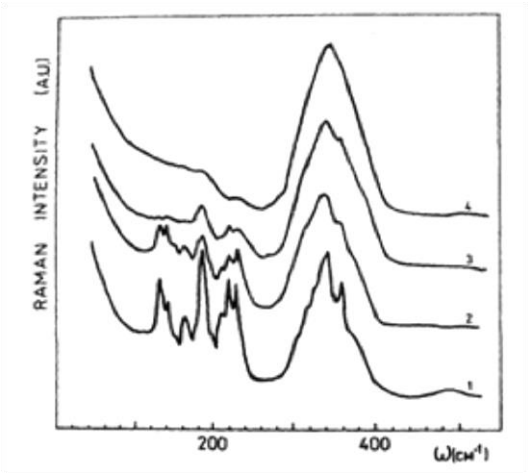

Fig. 3.1. Raman spectra of as-deposited (1), photo darkened (2), and annealed (3) As_2S_3 amorphous films. For comparison, the spectrum (4) of bulk glass is also shown.

Qualitatively similar results for irreversible thermostructural transformation have been firstly reported by Solin and Papatheodorou [5], Nemanich et al. [6], Frumar [8,9] and the present authors [e.g., 7]. The spectrum of the as-deposited

film consists of relatively sharp peaks on the background, typical of bulk As2S3 glass. These sharp features, characteristic to the as-deposited film, broaden, decrease in the intensity or even disappear irreversibly after annealing or on illumination. Such a behavior indicates that significant (in the sense of amorphous semiconductors) structural modification has take place. Note that in bulk glass and amorphous film with As content exceeding 40 at % all the relatively sharp features mentioned above are also observed. The data analysis [7-11] indicates that all the sharp spectral features (except of the 490 cm^{-1} band) originate from "wrong" (like-atom or homopolar) As-As bonds in As_4S_4 molecular units. The presence of A_s4S_4 molecules in the as-deposited As2S3 films is strongly supported by IR [12], EXAFS [13] and recent Raman scattering [7-9] measurements. Taking this into account, as-deposited films of As_2S_3 possess AsS_3 pyramidal units, which form glassy matrix of As_2S_3 and, in addition, a partially polymerized mixture of As_4S_4 (realgar-type) and Sn molecular species.

After annealing, the spectrum of the as-deposited film becomes very similar to that of bulk glass. However, some broad features, namely maxima at 187 and 230 cm^{-1}, remain. This indicates that some "wrong" bonds of the As-As, S-S -type exist even in well-annealed As_2S_3 films. During this treatment the bond breaking and switching due to an increased mobility of atoms is accompanied (to a considerable extent) by structure polymerization. This is manifested in the S-As-S stretching mode (120-170 cm^{-1}) frequency spreading and vibration band broadening typical of the bulk glass. Similar behavior in the valence-mode region of As-S and As-As vibration bands takes place if the as-deposited film were initially pre-illuminated by band-gap light. Consequently, one can suggests that the structure of illuminated films remains closer to that of as-deposited films then the structure of annealed ones.

In most studies on arsenic-based chalcogenide films including those examined in the present section the experimentalists deposit amorphous layers at fairly low deposition rates in 10 to 100 Å s^{-1} range. Illumination of these samples with band-gap light shifts the absorption edge to lower energies (so-called "red" shift or photo darkening). In contrast, setting the evaporator temperature

T_{evap}=800-900 ^{o}C and deposition rate of $\geq$ 300 Å s^{-1} leads to a structural modification which in turn results in a decrease in the optical band-gap. The exposed samples behave like "positive" (in contrast to materials with negative image formation) photosensitive layers, i.e. they exhibit a "blue" shift of absorption edge.

In Fig. 3.2, a typical Raman spectrum of a film deposited at a higher rate is shown.

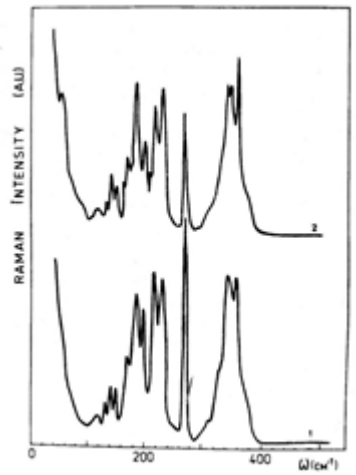

Fig. 3.2. The Raman spectrum of As_2S_3 film prepared with high deposition rate (see the text for details). (1) - un-annealed sample , (2) – annealed sample.

In general, it is clear that raising the evaporation temperature and deposition rate leads to significant sharpening of spectral bands. Synchronously, both the smooth background and the high-frequency component at 490 cm-1, which represent S-S bonds polymerized in the glass network, disappear. At the same time, additional spectral features at 120, 150, 200, 233 and 273 cm^{-1} appeared. Note that the peak at 273 cm^{-1} which dominate the Raman spectrum of the film deposited at high deposition rate is not resolved in As_2S_3 crystals and α,β-As_4S_4 polymorphs. This feature was observed in the Raman spectrum of crystalline As4S3 sample obtained by vacuum sublimation of As_4S_3 melt [14].

As the deposition rate increased, the films were found to become sulfur-deficient. This is the case even for sulfur-rich compositions (see Fig. 3.3).

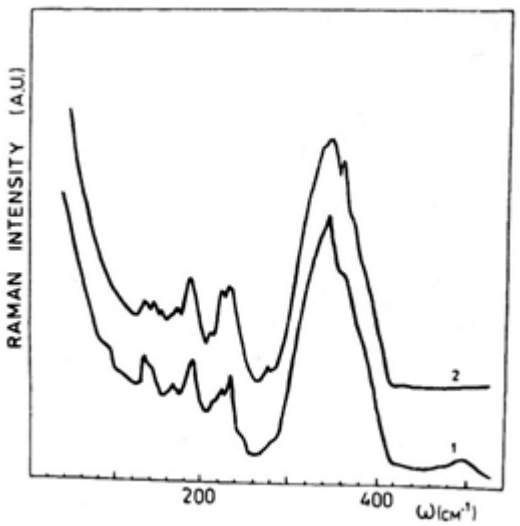

Fig. 3.3. Typical Raman spectra observed for $As_{0.30}S_{0.70}$ films. Curve (1) is the spectrum of the film prepared in conventional manner (slow-deposited), curve (2) corresponds to the fast-deposited film.

One of the reasons for such As-enriching of the samples may be the partial fragmentation of As_2S_3 into As_2S_2 and sulfur species during the deposition. Note that an increase in temperature from which the melt was quenched has a similar effect on the structure of melt-quenched As_2S_3, as was demonstrated by Yang et al. [13], Mikla et al. [7] and Zitkovsky and Bolchand [15].

Only a slight change in the Raman spectrum was observed after irradiation of such films. In contrast, annealing leads to further narrowing of the bands, splitting, and intensity redistribution. A distinct shoulder at 60 cm^{-1} appeared in the low-frequency region of annealed films. Probably, this shoulder corresponds to the lattice (intermolecular) vibrations of the α,β-As_4S_4 crystals [11].

It is important to point out here that the transformation of the Raman spectrum with As content increasing above stoichiometric $As_{0.4}S_{0.6}$ composition is similar to that observed with an increase in deposition rate for As_2S_3 as-deposited films (see Figs. 3.2 and 3.4 for comparison). Results suggest that high deposition rate induce microcrystallites formation. Annealing further enhances the crystallization processes and the films become polycrystalline. The above structural transformations, observed for the films deposited at high rates, are irreversible in the sense that the initial structure (and structure-related properties)

cannot be eliminated by annealing at the temperatures close to the glass transition temperature, T_g. Moreover, the films deposited at higher rates always appeared smooth, but took on a "dusty" appearance after light- and, especially, heat-treatment.

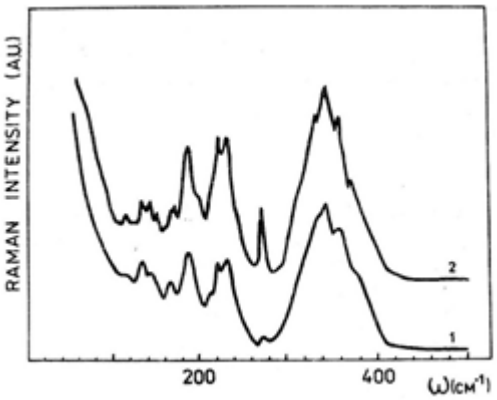

Fig. 3.4. Raman spectra of $As_{0.44}S_{0.56}$ films prepared by slow (1) and fast (2) evaporation.

Regarding the films prepared in conventional mode (slow-deposited films), we have examined how photo darkening of well-annealed films and bulk samples (i.e. reversible photo induced changes) influences their structure. Undoubtedly, the magnitude of reversible photo induced changes is small compared to irreversible ones. Structural changes detected by means of direct structural probes (e.g. X-ray diffraction [16]) were subtle. Indirect probes of local structure by means FT Raman spectroscopy (which is believed more sensitive than conventional Raman spectroscopy) indicate only negligibly small changes. At the same time, it should be noted that low-frequency light scattering which is sensitive to mediate-range order can provide some structural information in terms of correlation length. In Ref. [8] authors observed an increase in the intensity of the 231 cm^{-1} Raman band characteristic of As-As vibrations in a-As2S3 with photo darkening. In contrast, the present authors cannot detect even slight changes in Raman spectrum in the frequency range 100-500 cm^{-1}. Only low-frequency Raman spectra show discernible changes caused by band-gap illumination.

Fig. 3.5 is the summary of the low-frequency Raman data measured at room temperature. As_2S_3 glassy samples were illuminated for different times ranged

from 1 to 240 min. One can observe gradual shift of the above peak to higher frequencies with the illumination time. In addition, the intensity of the low-frequency peak also changes. The intensity of so-called Boson peak seemed to decrease at reversible photo darkening.

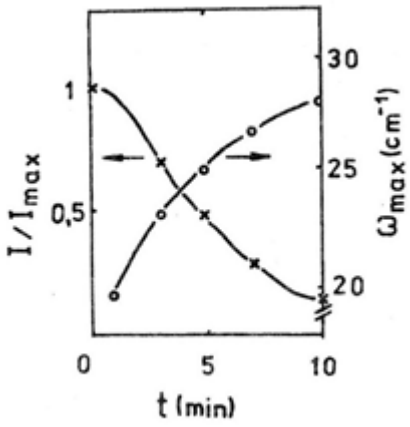

Fig. 3.5. Changes in the low-frequency peak position and relative intensity with exposure time. $I_{max,}$ is the peak intensity for virgin sample.

Irreversible structural changes that occur in thin films prepared in conventional regime upon optical illumination can be understood in terms of the mechanism described in Refs. [5-12,17]. These changes are associated with a photo polymerization of As_4S_4 and S_n molecular species. The resultant structure is layer-like two-dimensional with restored chemical ordering.

Flash evaporation enhances significantly compositional as well as structural disorder in amorphous samples compared to stoichiometric composition. An increase in As concentration leads to a condensation of As_4S_3 and some other As-rich molecular species; chemically disordered molecular solid is obtained. These compositions are unstable; phase separation occurs upon thermal annealing and light irradiation. Irreversible photo induced changes observed in fast-deposited films differs from irreversible changes in conventionally prepared amorphous films from a phenomenological point of view and also with respect to their origin.

On the basis of present Raman results we can suggest that, in contrast to the irreversible structural changes, changes in local structure do not accompany the reversible photo-induced changes observed in well-annealed amorphous films.

This means that covalent (intra-molecular) bond breaking is unlikely to be the dominant mechanism responsible for reversible light-induced effects in amorphous chalcogenides.

The most significant changes are observed in the low-frequency region ($\omega_{max}\approx25$ cm^{-1} for As_2S_3) of light scattering spectra. The presence of the Boson peak signifies certain medium-range order in the amorphous structure [18-20]. The position and the intensity of the peak can be used to estimate the structural correlation length $R_c\sim(\omega_{max}/V)^{-1}$, where ω is the frequency of the peak maximum and V is a sound velocity, and to characterize the degree of structural ordering. The structural correlation length is generally associated with the dimensions of some cluster-like structure. For a-As_2S_3, the R_c value is ~7.6 Å. The clusters may exist in the form of linked pyramids. Although the origin of low-energy excitations in disordered solids is still disputable, differences in the parameters of Boson peak observed for annealed and photo darkened states are presently attributed to changes in medium-range order. A decrease in the peak height and a shift to higher ω values may be related to an increase in structural randomness. This is consistent with an increase in structural disorder under illumination detected by EXAFS spectra [13,21]. In spite of experimental results presented on Raman scattering, photo darkening is accompanied by certain structural change on the scale of medium-range order: weakly linked AsS_3 pyramids move with respect to each other, as proposed in Ref. [22]. The advantage of this mechanism is that it does not require covalent bonds breaking. There exists another possible explanation - modification of short-range order (see e.g. Refs. [22-26]). It seemed that unconventional (diffraction-like) experiments are the only that can give unambiguous evidences on the origin of structural changes at reversible photo darkening.

3.5. Concluding remarks

In this section the influence of thermal evaporation conditions and subsequent light and heat treatments on the atomic structure was studied. The major experimental findings of these studies may be summarized as follows.

The pronounced irreversible change observed in the Raman spectra of slowly deposited films with illumination is direct evidence for gross structural changes caused by optical irradiation occur. Such behavior has been interpreted in terms of a photo polymerization mechanism.

The films were found to become sulfur-deficient as the deposition (evaporation) rate increased, because of partial fragmentation of As_2S_3 into As_3S_2 and sulfur during the deposition. Fast-deposited films are unstable and phase separation occurs upon light irradiation.

The reversible photo induced effects in well-annealed amorphous films involve structural modifications in the medium-range order.

References

1. A. Madan, M. P. Shaw, The Physics and Applications of Amorphous Semiconductors, Academic Press, Boston, MA, 1988. 2. A. Feltz, Amorphous Inorganic Materials and Glasses, VCH,

Weinheim, Germany 1993.

3. S. O. Kasap, in Handbook of Imaging Materials, edited by A. S. Diamond and D. S. Weiss, Marcel Dekker, Inc., New York, p. 329, 2002, and references therein.

4. K. Tanaka, in Encyclopedia of Materials, Elsevier Science Ltd., p. 1123, 2001.

5. S. A. Solin, G. N. Papatheodorou, Phys. Rev. B 15, 2084 (1977).

6. R. J. Nemanich, G. A. N. Connell, T. N. Hayes, R. A. Street, Phys. Rev. B 12, 6900 (1978).

7. V. I. Mikla, Yu. M. Vysochanskij, A. A. Kikineshi, Soviet Physics Journal 11, 73 (1983);

8. M. Frumar, A. P. Firth, P. J. S. Owen, Philos. Mag. B 50, 453 (1984).

9. M. Frumar, Z. Polak, Z. Cernosek, J. Non-Crystall. Solids 256-257, 105 (1999).
10. M. L. Slade, R. Zallen, Solid State Commun. 30, 387 (1975).
11. P. J. S.Even, M. L. Sik, A. E. Owen, Solid State Commun. 33, 1067 (1980).
12. U. Strom, T. P.Martin, Solid State Commun. 29, 527 (1979).
13. S. Y. Young, D. E.Sayers, M. A. Paesler, Phys. Rev. B 36, 8122 (1987).
14. A. Bertoluzza, C. Fagnano, P. Monti, A. Semerano, J. Non-Crystall. Solids 29, 49 (1978).
15. I. Zitkovsky, P. Bolchand, J. Non-Crystall. Solids 114, 70 (1989).
16. K. Tanaka, Appl. Phys. Lett. 26, 243 (1975).
17. A. E. Owen, A. P. Firth, P. J.S. Ewen, Philos. Mag. B 52, 347 (1985).
18. A. J. Martin, W. Brenig, Phys. Stat. Solidi b 63, 163 (1974).
19. R. J. Nemanich, Phys. Rev. B 16, 1655 (1977).
20. V. K. Malinovsky, A. P. Sokolov, Solid State Commun. 57, 757 (1986).
21. L. Gladen, S. R. Elliott, G. N. Greaves, J. Non-Crystall. Solids 106, 189 (1988).
22. G. Pfeiffer, M. A. Paesler, S. C. Agarwal, J. Non-Crystall. Solids 130, 111 (1991).
23. Non-Crystalline Materials for Optoelectronics, edited by G. Lucovsky, M. Popescu, INOE Publishers, Bucharest, 2004.
24. K. Tanaka, in Handbook on Advanced Electronic and Photonic Materials and Devices, Nalwa, San Diego, 2001.
25. V. M. Lyubin, M. L. Klebanov, Photo-Induced Metastability in Amorphous Semiconductors, Wiley-VCH, Wenheim, Ch. 6, 2003.
26. M. A. Popescu, Non-Crystalline Chalcogenides, Kluwer Academic, Dordrecht, 2000.
27. V. I. Mikla, V. I. Fedelesh, V. A. Stefanovich, V. Yu. Slivka, Mater. Sci. & Eng. B 38, 122 (1996);
28. V. I. Mikla, J. of Physics: Condensed Matter 8, 429 (1996).

CHAPTER 4. Molecular structure of Se-rich amorphous films

Structure and its transformation are examined for amorphous Se-rich As_xSe_{1-x} ($0 \leq x \leq 0.2$) alloys by employment of diffraction and non-diffraction structural probes. It is shown that the molecular structure of amorphous Se (a-Se) on the scale of short-range order is close to that of crystalline phase, while medium-range order differs from the structure of most inorganic glasses and may be placed between three-dimensional network glasses and polymeric ones. Further experiments show the existence of successive phases in laser-induced glass-crystalline transition with pronounced threshold behavior. Below the energy density threshold, E_{th}, only small changes in the local structure of the system can be detected. Above Eth, the changes were attributed to crystallization transformation. The corresponding Raman spectra reveal transformation of the system from amorphous into the crystalline phase under laser irradiation. In the binary As_xSe_{1-x} glass system, a change of structural regime takes place near the composition $x \approx 0.04$. The presence of this topological threshold is established by direct and indirect evidence, such as peculiarities in the composition dependence of the basic parameters for electron diffraction and Raman vibration modes. The peculiarities are caused by the transition from a chain-ring-like structure to preferentially a chain-like structure. Experiments described in this section have shown that Raman technique is a particularly sensitive method to determine the presence of microcrystal's in the glassy matrix. Room-temperature polarized Raman scattering spectra of model glass have been collected. Low-frequency peaks were observed in the spectra. A model is proposed for explanation of their appearance. It is shown clearly that the low-frequency Raman spectra allow determining the conditions at the boundaries, sizes as well as concentration of micro-heterogeneities in non-crystalline materials. It was established earlier that for all amorphous (glassy) materials a low-frequency peak, observed in the corresponding spectral region of Raman scattering and called boson peak, is inherent. This peak is absent in crystals of the same chemical composition and is

associated with space correlations on the scale of medium-range order $R_c \approx 10$Å. On the contrary, less known is that a boson peak can give important information about the presence of microcrystalline inclusions and heterogeneities in the low-frequency Raman spectra of glasses irrespective to their chemical composition.

4.1. Introduction

Amorphous selenium has been extensively studied over the past 70 years, but its molecular structure is still disputable. For a long time it was believed that the amorphous phase consisted of selenium chain, Se_n, and 8- ring, Se_8, structures mixed together. This model arose from the fact that in the crystalline phase, selenium can exist in two forms, α-monoclinic Se (α-Se) and trigonal Se (γ-Se). The former consisted of Se_8 rings and the latter of Se_n chains. Reasonably, one can consider a structure for the amorphous phase based on a mixture of ring and chain members. However, the length of the selenium chains is uncertain. In addition, it is unclear whether a-Se contains cyclic structure or rings. In recent years there has been enhanced interest in structural studies of chalcogenide glasses owing to their imaging applications. As-containing chalcogenides, especially Se-rich alloys, usually have been studied in thin film form. Since change in the structure can have an influence on photo generation, charge carriers transport, trapping and other important fundamental properties, knowledge of the molecular structure of such materials is needed for further improvement of their characteristics [1-11]. Undoubtedly, elemental semiconductors are useful and suitable testing objects for studying the influence of structure on physical properties [5-7, 12-19]. This is particularly true in respect of selenium. In the past, the latter was successfully used in photocells, rectifier diodes and solar cells. In its amorphous form, selenium has a good application as photoreceptor in copying machines and X-ray imaging plates [1,8,11]. Despite the increasing commercial using of a-Se in various applications (see [8] and references therein), e.g. as promising X-ray flat panel detectors for medical purposes [1], its structure is not fully understood. On the other hand,

binary non-crystalline semiconductors of As-Se system are also of continued scientific and practical interest because of real opportunity of their technological uses (e.g. as functional elements of multi-layer photoreceptors in xerography). Among them the stoichiometric composition, As_2Se_3, and compositions from the range 30-50 at % As are perhaps the most studied ones [12-19]. As for a most of stable binary glasses in As-Se system atomic ratios can be varied in a wide range. Although the information about various physical properties of Se-rich alloys is not so extensive and numerous [5-8,15-20], their compositional dependence manifests extrema or thresholds also in the range 6-12 at % As. It is necessary to accentuate that the As-Se amorphous alloy system display main extrema of various properties at the composition where the valence requirements appear to be satisfied that is at the stoichiometric composition. It seems to be reasonable to connect the mentioned non-monotonic behavior with a specific character of local structure changes. Another prominent feature of the materials studied consists in the following. Certain type of glasses, whose common feature is the presence of chalcogen atoms, sulfur, selenium, and tellurium, exhibit various photo induced phenomena (the reader may refer to K.Shimakawa [10] and Ke.Tanaka [21]). Among these are photo structural transformations and photo crystallization phenomena: a change in optical, electrical and other physical properties is observed. The phase transformation of selenium and its alloys can also be induced relatively simply by laser illumination [22-26]. Reasonably, this unique property makes them attractive for optical data storage and holographic recording. Many experimental results using selenium and its alloys have been reported [27], but few cases of phase transformation properties were mentioned.

In the present chapter electron diffraction and Raman scattering in pure amorphous selenium (a-Se) and Se-rich As-Se amorphous films are reviewed. Below we attempt to clarify the structural transformations induced by light treatment and compositional changes. We focus our attention mainly on photo crystallization transformations. The Chapter also deals with the composition induced structural modifications in amorphous As_xSe_{1-x}. As shows the analysis of

electron diffraction and Raman scattering data, some discontinuity of atomic arrangement with rising As content exists.

4.2. Techniques exploited in structural studies

Methods used for structural study of solids may be classified into two groups.

4.2.1 Direct methods

Direct methods include diffraction of X-Rays, electrons and neutrons.

4.2.2 Indirect methods

Among indirect methods Raman scattering, infrared absorption, extended X-Ray absorption fine spectroscopy and nuclear magnetic resonance can be considered.

The first ones are the methods of determining the arrangement of atoms within a solid, in which a beam of X-rays strikes a crystal and diffracts into many specific directions (Fig. 4.1).

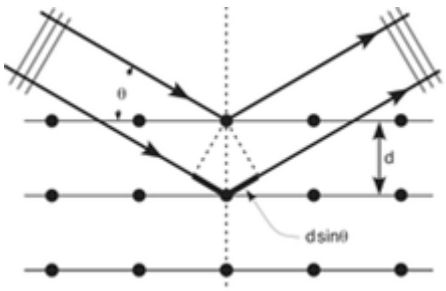

Fig. 4.1. Illustration of X-Ray diffraction from solids.

The incoming beam causes each atom to re-radiate a small portion of its intensity as a spherical wave. If atoms are arranged symmetrically with a separation d, these spherical waves will be only in directions where their path-length difference 2d sin θ equals an integer multiple of the wavelength λ. In that case, part of the incoming beam is deflected by an angle 2θ, producing a reflection spot in the diffraction pattern.

From the angles and intensities of these diffracted beams, a crystallographer can extract information about the mean positions of the atoms in the solid, as well as their chemical bonds, their disorder. Since many materials are solids - such as semiconductors, as well as various inorganic, organic and biological molecules - X-ray crystallography has been fundamental in the development of many scientific fields.

In its first decades of use, this method determined the size of atoms, the lengths and types of chemical bonds, and the atomic scale differences among various materials, especially alloys. X-ray crystallography is still the chief method for characterizing the atomic structure of new materials.

It should be noted here that while diffraction of X-rays, electrons or neutrons gives definite information about the structure of crystalline solids, such measurements give much less information about the structure of amorphous solids [28,29]. The diffraction patterns of amorphous solid consists of diffuse rings whose radial variation of intensity provides a merely one-dimensional representation of the three-dimensional glass structure. Some information about the structure is "averaged out" in the experiments and the structure is surely not 1-to-1 with the diffraction data. In practice one imagines a likely amorphous structure, predicts experiment and compares with the observation. This illustrates the need for the use of many different experimental probes. Diffraction, vibrational spectroscopy and other techniques emphasize different aspects of structure, such as interatomic distance, or angles, or local symmetry, or range of order. Each technique provides an alternative view of the structure and generally averages the structure differently, thus revealing aspects that may be de-emphasized or obscured by another technique. Although each probe gives limited information, the results of several different probes leading to a conviction of truth.

Raman spectroscopy (named after C. V. Raman) is a spectroscopic technique used to study vibrational, rotational, and other low-frequency modes in a system. It relies on inelastic scattering of monochromatic light, usually from a laser in the visible, near infrared, or near ultraviolet range. The laser light interacts

with phonons or other excitations in the system, resulting in the energy of the laser photons being shifted up or down (Fig. 4.2).

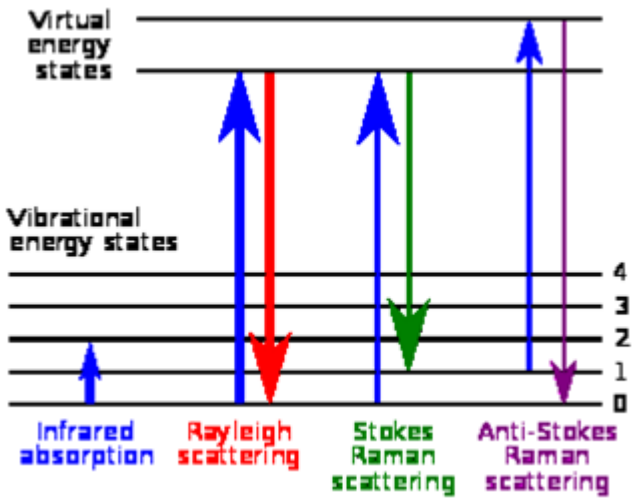

Fig. 4.2. Visible light scattering from molecules.

The shift in energy gives information about the phonon modes in the system. Raman scattering is known to be a powerful technique which give information about local structure of amorphous chalcogenides [30,31].

4.3. Effect of composition on structure of As_xSe_{1-x} amorphous films – electron diffraction study

In the following experimental results of electron diffraction and electron microscopic measurements of the structure of As_xSe_{1-x} amorphous films are considered [27,32]. The results of structural investigations of films with low As content have been compared with the literature data.

The samples used in these studies were amorphous films, about 10 μm thick, prepared by vacuum thermal evaporation of the powdered As_xSe_{1-x} melt-quenched material at the rate of 1 μm/min. Freshly cleaved KCl single crystals on the (001) plane were used as substrates. The As_xSe_{1-x} bulk glasses were prepared according to the conventional melt-quenching method with agitating the ampoules content for homogenization. Annealing of the films was carried out in air at ambient pressure and at temperatures 40, 45, 50, 60, and 70 degrees (in Celsius

scale) for 0, 2, 5, 10, and 20 at% As, respectively. The composition of the films was determined by electron probe microanalysis, and the composition quoted are accurate to within ± 0.5 at.%. Thin film samples were kept in complete darkness until measured to minimize exposure to light sources, which could lead to changes in the properties and structure of the films. Thermal evaporation method was used due to necessity of reproducing films with chemical composition of glasses. Moreover, the evaporation of As-Se glasses is not of a dissociate character, but it proceeds with fractionation [4]. The temperature T_{ev} of an open-type tantalum evaporator, measured with Pt/Pt-Rh thermocouple, was within $670 \leq T \leq 770$ K depending on glass composition.

The chemical composition of amorphous films was checked by X-Ray spectral microprobe method using the EMMA-4 instrument with a relative error ± 1 %. The atomic structure of a film and its changes with thermal annealing were investigated by the electron diffraction method using the EMP-100 instrument and the microstructure was investigated in the EMB-100B transmission electron microscope. It is necessary to note here that the film thickness for structural investigations did not exceed ~ 600-700 Å.

The short-range order parameters of the atomic film structure were obtained by calculating the radial distribution function (RDF). The dependence I = f (s), where $s = 4\pi \sin\theta / \lambda_e$, θ is the diffraction angle and λ_e is the wavelength of electrons, was plotted in a direct electron current recording mode.

The data about the character and changes in the medium-range order of the atomic film structure were measured by the analysis of positions and intensity of the first sharp diffraction peak (FSDP). The thermal annealing of films was carried out in situ, in the electron diffractometer column.

X-ray spectral microprobe data of the film composition was the same as that of the As_xSe_{1-x} initial glasses (within the measurement error). This similarity showed that quazi-equlibrium evaporation conditions were maintained.

The electron diffraction patterns for As_xSe_{100-x} as-deposited amorphous films at x = 0, 2, 4, 6, 8, 10 and 40 are given in Fig. 4.3. For comparative analysis

we plotted I / I_2 intensity curves, where I_2 is the intensity of the second peak of I (s) curve which is less affected by the natural ageing of films [32].

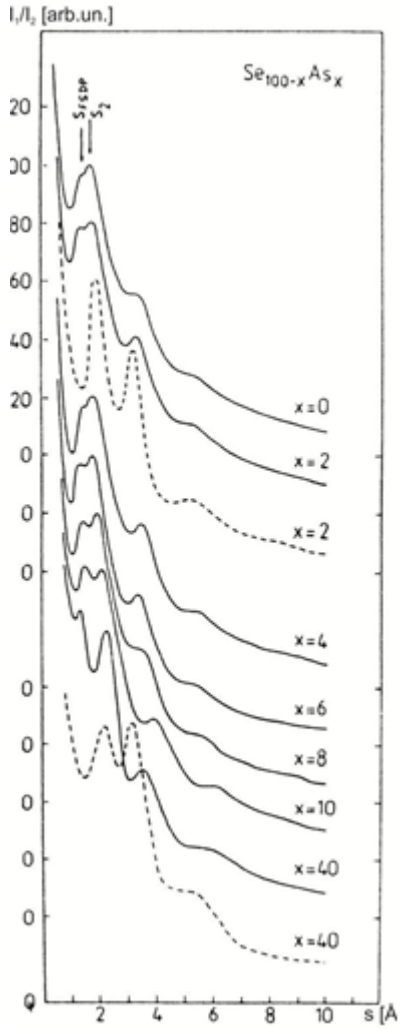

Fig. 4.3. Electron diffraction patterns of As_xSe_{100-x} as-deposited amorphous thin films (solid line) and films after structural transformation (dashed line) stimulated by thermal annealing.

As clearly seen from Fig. 3, the presence of FSDP in the region $S_{FSDP} \approx 1-1.5$ Å is characteristic of diffraction patterns for as-deposited films, and is associated [33-35] with medium-range order of the structure.

The data on the analysis of the first sharp diffraction peak position, S_{FSDP}, and the second peak, S_2, and their intensities, I_{FSDP} and I_2, for different compositions of As_xSe_{100-x} amorphous films are given in Fig. 4.4.

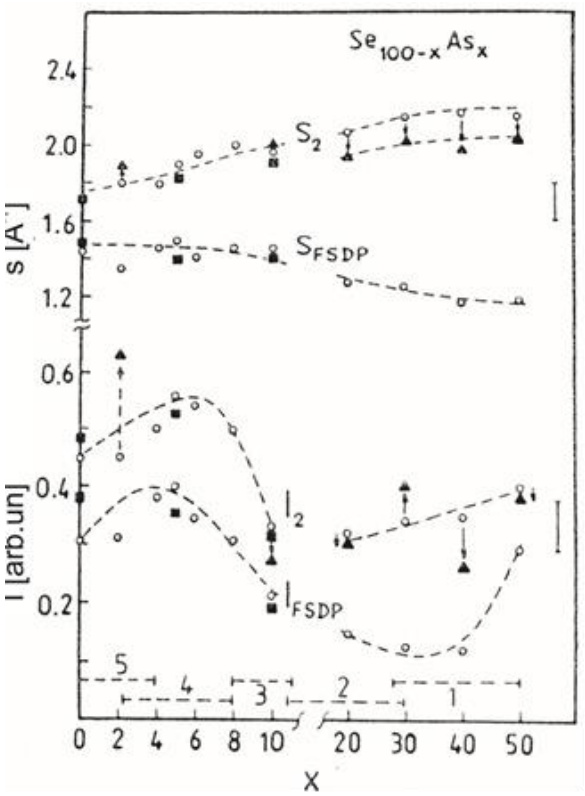

Fig. 4.4. Dependence of S_{FSDP}, S_2, I_{FSDP} and I_2 on composition for amorphous As_xSe_{100-x} amorphous films. Solid circles and squares are referred to different deposition conditions; solid triangles and open symbols referred to S_2 and I_2 after A1→A2 structural transformation. Lines are guide for eyes.

Here circles and square symbols represent the distribution in values of data (for measurements on films prepared with the same evaporation parameters) for compositions with x = 0, 5 and 10. As seen from Fig. 4.4, the reproducibility of the parameters, S_{FSDP}, S_2, I_{FSDP} and I_2 for different evaporation conditions for films of the same composition is comparatively good.

After thermal annealing of films in situ (in the electron diffraction column), we observed a structural transformation, A1→A2, with retention of the amorphous state, where A1 and A2 were the phase state before and after transformation, respectively. Upon further heating, the films crystallized.

The A1→A2 structural transformation in amorphous chalcogenide films is accompanied by a drastic change in the absorption contrast of the electron microscopic image.

The main difference of diffraction patterns between films in the A2 and in A1 state lies in a complete disappearance of T0 transition for the first sharp diffraction peak, I_{FSDP}, at a certain temperature. In Fig. 4.3, typical diffraction patterns of $As_{40}Se_{60}$ and As_2Se_{98} amorphous films after A1→A2 structural transformation are shown by dashed lines. New values of S_2 and I_2 for diffraction patterns of As_xSe_{100-x} amorphous films of different compositions after A1→A2 transformation are shown in Fig. 4.4 by triangular symbols.

It should be noted that diffraction patterns of As_xSe_{100-x} films with low As content after annealing are very similar to those of Se-based bulk glassy samples. This fact is in agreement with the results of Refs. [31,36] in which authors show that the structure of As_xSe_{100-x} deposited films after annealing approaches that of corresponding glasses.

After thermal annealing of As_xSe_{100-x} ($x \leq 10$) amorphous films, the A1→A2 structural transformation occurs even with slight heating caused by electron beam: the films tends to crystallize. It should be noted here that the recording of diffraction patterns for such films in the amorphous state after A1→A2 transformation is difficult.

In Fig. 4.5 the RDFs of AsxSe100-x amorphous films for $x \leq 10$ are given. The data on the values of the first RDF maximum position, r1, and area under it, z1, are presented in Fig. 4.6. The values of r_1 and z_1 for films with x=30, 40 and 50 are given for comparison. The corresponding symbols of Fig. 6 are defined in Fig. 4.4.

The medium-range order of the structure of amorphous films may be characterized to a certain extent by values of S_{FSDP} and I_{FSDP}. From the analysis of Fig. 4.4, it follows that As_xSe_{100-x} as-deposited films in the composition range $0 \leq x \leq 10$ and $20 \leq x \leq 50$ differ in a correlation length, $L = 2\pi / S_{FSDP}$, of the medium-range order and in the degree of medium-range ordering.

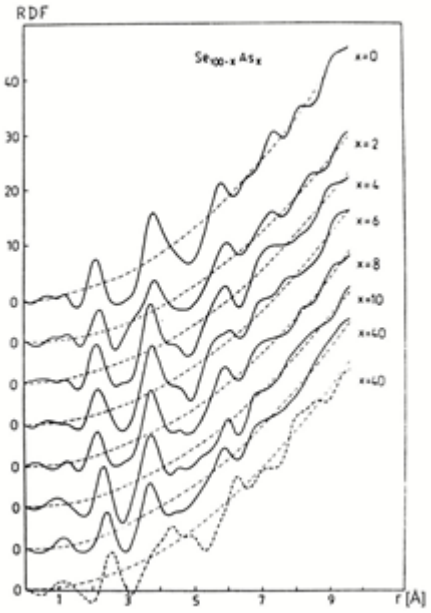

Fig. 4.5. Radial distribution functions (RDF) of As_xSe_{100-x} as-deposited amorphous films (solid lines) and films after structural transformation (dashed lines) stimulated by thermal annealing.

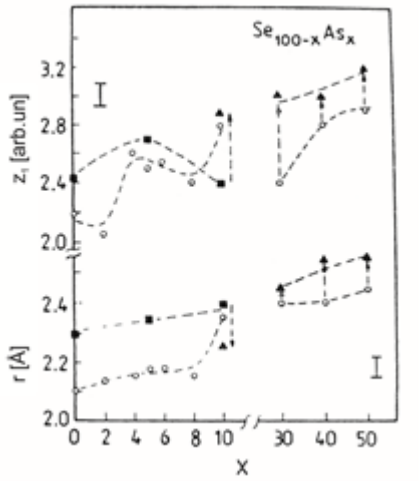

Fig. 4.6. Compositional dependence of the first RDF maximum position, r_1, and area under it, z_1, for As_xSe_{100-x} amorphous films.

The FSDPs for amorphous films of composition close to $As_{40}Se_{60}$ are explained in the approximation of the cluster model. According to this model the correlation length, L, is associated with the size of quasi-molecular (cluster) species in the structure of as-deposited films [37].

In the region of low As content, the calculated values of correlation length are $0.42 \leq L \leq 0.46$ nm, whereas for the region of compositions $30 \leq x \leq 50$ one obtain $0.50 \leq L \leq 0.55$ nm. The latter is fairly well fitted [38] with the distance between the "furthest" Se atoms in As_nSe_m quasi-molecular species (n=4, m=6). The average value of L in the composition range $0 \leq x \leq 10$ correlates with the sizes of Se_6 molecules and with the average distance between Se_n chains in the structure of amorphous selenium [4].

We suppose that the peculiarities observed in composition dependence of structural characteristics for As_xSe_{100-x} films with low As content are conditioned by a topological structure of the disordered network to appear in those local regions where linking, branching of chains and formation of closed rings occur. Generally, this results in an increase in the intensity of the main diffraction peak I_2 and peak IFSDP. The latter is assumed to be responsible for the medium-range order, and in a mutual change in the position of these peaks.

4.4. Raman scattering in pure and alloyed amorphous selenium: high-frequency spectral region

Raman scattering is a very powerful experimental technique for providing information on the constituent structural units in a given material [30]. In the present section the Raman scattering in pure amorphous selenium (a-Se) and Se-rich As-Se amorphous films are studied. Below we attempt to clarify the structural transformations induced by light treatment and compositional changes. We focus our attention mainly on photo crystallization transformations. In addition, the composition-induced structural modifications in amorphous As_xSe_{1-x} are also analyzed. As shows the detailed analysis of Raman data, some discontinuity of atomic arrangement with rising As content exists.

The samples used in these studies were amorphous films, about 10 μm thick, prepared by vacuum thermal evaporation of the powdered As_xSe_{1-x} melt-quenched material at the deposition rate of 1 μm/min onto quartz substrates held at

room temperature as well as polished mirror-like parallelepipeds of vitreous As_xSe_{1-x}. The As_xSe_{1-x} bulk glasses were prepared according to the conventional melt-quenching method. Annealing of the films was carried out in air at ambient pressure and at temperatures below the glass-transition temperature. Thin film samples were kept in complete darkness until measured to minimize exposure to light sources, which could lead to changes in the properties and structure of the films. It is important accentuate that after annealing procedure their Raman spectra become indistinguishable from the corresponding spectra of melt-quenched glassy samples. It should be noted that for Se-rich compositions studied only slight difference in the spectra of melt-quenched and as-deposited samples is observed.

Right-angle Raman spectra were measured using RAMANOR U-1000 spectrometer. The spectral slit width was ~1 cm^{-1} and the excitation wavelength 676 nm. Laser beam of sufficiently low incident power P=3 to 5 mW is focused into 100 μm spot. In other words, Raman spectra of the amorphous films were recorded with sufficiently low incident laser-beam intensity $I=1.3\times102$ W/cm^2 to avoid photo structural changes. The latter is known to transform the Raman spectra. The identity of the experimental spectra obtained from different points of the sample and the good reproducibility of the spectra in repeated scans (the time required to scanning one spectrum in the spectral range 100-300 cm^{-1} is about 5 min) show that photo darkening did not play a role in the subsequent Raman measurements.

The structure of photo-crystallized films was investigated using X-ray diffraction.

In Fig. 4.7, a typical Raman spectrum of a-Se measured at low incident radiation power density, ~3 mW, is shown. The stable level of the scattered light intensity and the good reproducibility of the spectrum in the repetitive cycles clearly indicate the absence of any structural changes in a-Se induced by laser irradiation of such power density. On the high-frequency side (ω=100 to 300 cm^{-1}) the spectrum contains an intensive peak at 255 cm^{-1} and some peculiarity (shoulder) at 237 cm^{-1}.

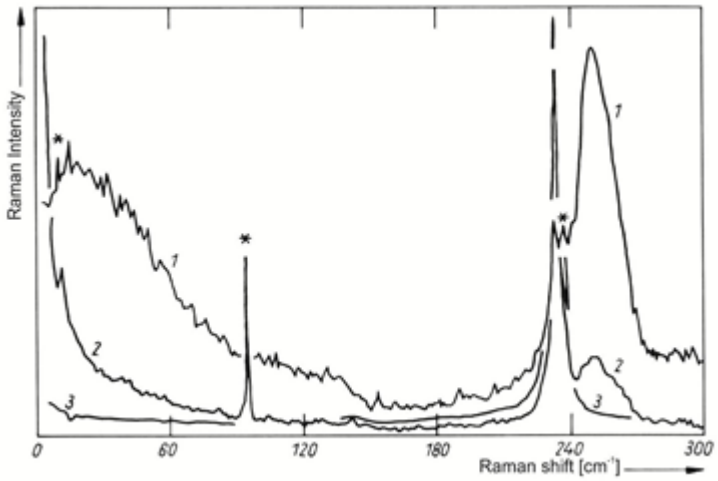

Fig. 4.7. Raman spectra of (1) amorphous and (2), (3) photo crystallized sele- nium. Experimental details for (2) and (3) are: (2) after 5 min exposure of the sample to 10 mW, (3) after 30 min exposure to 10 mW. Asterisks indicate laser plasma lines.

The above features are in good agreement with previously reported data [39-43]. In the low-frequency region one can observe the broad peak with ω_{max}=16 to 20 cm^{-1}. This so-called boson peak occurs in the low-frequency region of the Raman spectra of all amorphous and vitreous solids. We considered this spectral region in separate paragraph.

When we try to identify certain vibration bands observed in the Raman spectrum of a-Se, some difficulties arise. Initially it was proposed to interpret the a-Se Raman spectrum by analogy with sulfur – on the basis of a molecular approach. That is, the main vibration band was considered to be the superposition of the peaks at 237 and 255 cm^{-1} characteristic of chains and rings, respectively [41]. However, further experimental data have caused some doubts to be cast. In such a case one would expect to observe a discernible difference in the contributions of 237 and 255 cm^{-1} mode to the main vibration band in the samples prepared at different conditions (e.g. substrate temperature during deposition for amorphous films or quenching rate for glassy samples). This may be caused by changes in rings to chains ratio. Therefore, it is clear that the spectral region 200 to 300 cm^{-1} is unsuitable for ring diagnostics. This is consistent with the conclusions of [42]

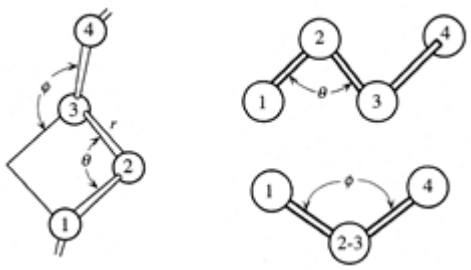

Fig. 4.8. Se chain molecule and definition of the dihedral angle ψ. The definition involves an angle between planes and thus four atoms labeled 1, 2, 3 and 4. It is observed looking down the bond joining atoms 2 and 3.

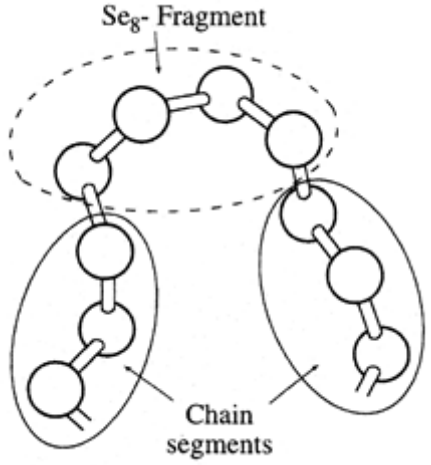

Fig. 4.9. Local molecular order in a selenium chain in which there are segments characterized by repetition of the same dihedral angle ("chainlike" in the sense of trigonal Se) and segments characterized by alternating dihedral angle ("ringlike" in the sense of Se_8 molecule).

The Se_8 peak (112 cm^{-1}) could not be detected in the present experiment. Probably, this is connected with its weakness. This fact indicates evidently the low concentration of rings. Consequently, one can associate the spectral features in the main vibration band, the 255 cm^{-1} peak and the shoulder at 237 cm^{-1}, mainly with the chain vibrations.

In the present section experimental results on Raman scattering spectra for Se-rich amorphous semiconductors As_xSe_{1-x} are also discussed. In Fig. 4.10 typical Raman spectra of amorphous Se and As-Se alloys with As content up to 5 at % are shown. The major spectral feature in the high-frequency region is the 255 cm^{-1} band. Another prominent spectral feature which is not shown in this Figure is the

broad peak at ωmax=16-20 cm^{-1}. As mentioned, the latter is characteristic for Raman scattering of all amorphous solids and glasses.

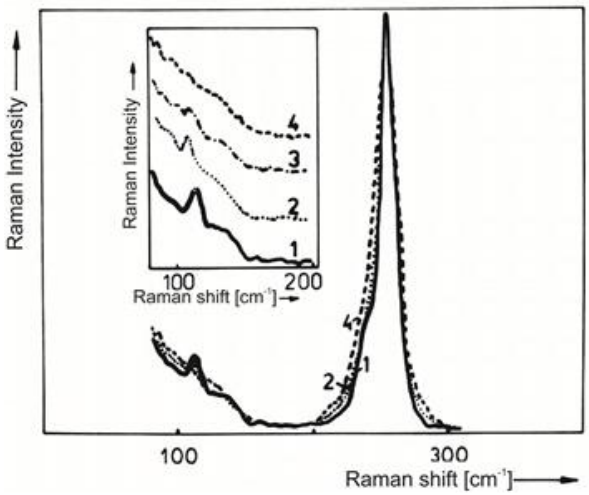

Fig. 4.10. Comparison of the Raman spectra of (1) amorphous Se and As_xSe_{1-x}: (2) x=0.02, (3) 0.04, and (4) 0.05 at %. Each trace has been normalized to the same peak (255 cm^{-1}) intensity.The inset shows the bending mode region.

In the following we consider only the high-frequency region. The weak feature observed at 112 cm^{-1} in the a-Se spectrum diminishes with As addition and at 5 at % completely disappears (see inset Fig. 4.10). At the same time the difference in the spectra in the region of the main vibration band is obvious. Thus, with increase of As content the transformation of the Raman spectrum in this region is retraced (Fig. 4.11).

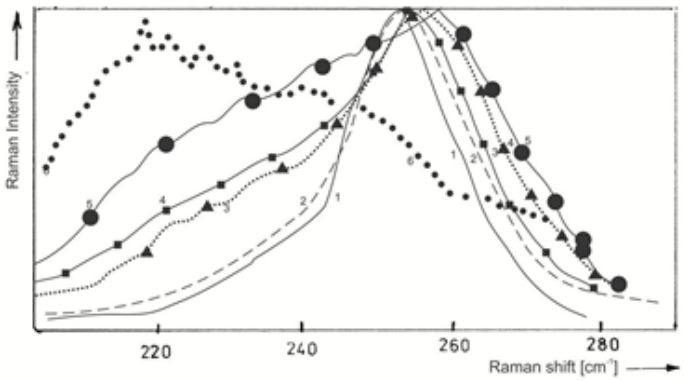

Fig. 4.11. Raman spectra of amorphous AsxSe1-x films annealed at $T=T_g$. (1) x=0 (solid line), (2) 0.05 (dashed line), (3) 0.10 (dashed-doted line), (4) 0.12 (dasheddouble-doted), (5) 0.20 (solid circles), and (6) 0.40 (points). We have used these unconventional denotations for Raman spectra to be distinguishable.

The most important points are the following:

1. Spectrum broadening with increasing As addition;

2. Growth of scattered light intensity from the low-frequency side of the main maximum (255 cm^{-1});

3. Appearance of a broadened band at 220-230 cm^{-1} (this band is the most intense in the Raman spectrum of $As_{0.4}Se_{0.6}$). It should be noted also that the main maximum is slightly shifted to higher frequency for amorphous As_xSe_{1-x} respectively to Se (255cm^{-1}).

The intensity of the 220-230 cm^{-1} band in the As concentration interval 0-5 at % remains practically unchanged. Then, at 6 at % As, an increase of the band intensity occurs. A gradual intensity rise is observed for the band at 220 cm^{-1} as the As content is further increased. For As content exceeding 35 at % the band dominates in the Raman spectrum.

The corresponding calculations have been performed (the scattered intensity was determined as $I(As_xSe_{1-x})=I(Se)+K\times I(As_{0.4}Se_{0.6})$, where the normalization coefficient K was appropriately estimated or each composition) for amorphous materials under investigation.. These calculations yield that a systematic discrepancy between approximated and experimental spectra is observed. As for the latter, the greater values of the main peak width are typical.

Fig. 4.12 shows difference spectra obtained by subtracting the $As_{0.4}Se_{0.6}$ spectrum from experimental Raman spectra. The relative contribution of the $As_{0.4}Se_{0.6}$ spectrum was fitted to the ~230 cm^{-1} region where the contribution from pure Se was negligibly small. It is obvious that after such a procedure some peak remains, width and position of which differs from that for a-Se.

Based on the data given in Fig. 4.12, values of the parameter A were estimated. This parameter represents the ratio of the integrated Raman intensity in the interval limited by the typical frequencies $AsSe_{3/2}$ unit vibrations (205 and 230 cm^{-1}) to the integrated intensity of the whole spectrum of valence vibrations:

$$\frac{\int_{205CM^{-1}}^{230CM^{-1}} i}{\int_{205CM^{-1}}^{290CM^{-1}} i} .$$

Note that this is done after normalizing each spectrum.

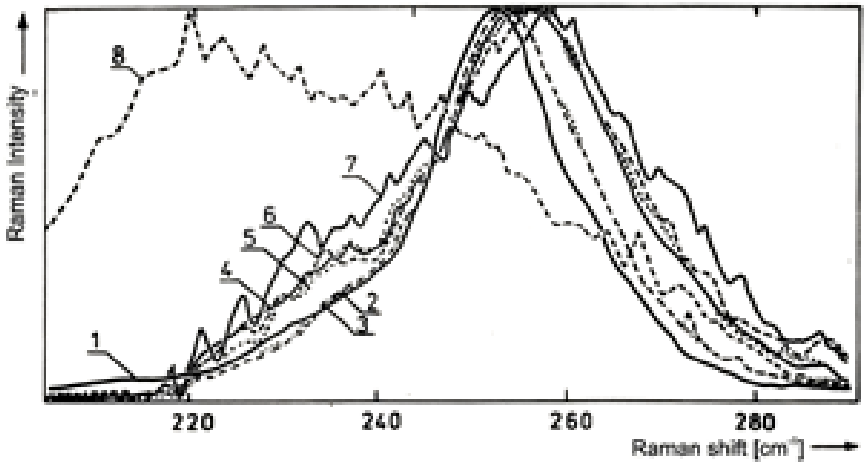

Fig. 4.12. The difference spectra (for details see the text) for a-As_xSe_{1-x}. x=4, 5, 6, 8, 10, and 20 at %, curves 2 to 7, respectively. For the sake of comparison Raman spectra (1) a-Se and (8) $As_{40}Se_{60}$ are also shown.

Fig. 4.13 shows that the dependence A ~ f(x) is non-monotonous – parameter A increases around ~ 6 at % As. For the frequency range 240 to 270 cm^{-1}, the change of scattered intensity with composition has a smoother character. On the same figure, the dependence of the peak frequency, ωmax, and its width, $\Delta\omega_{max}$, on As content for the corresponding spectra is displayed. It is important to note the similarity of the composition dependence of A, ω_{max}, and $\Delta\omega_{max}$.

An attempt to simulate As_xSe_{1-x} Raman spectra by a superposition of two constant spectral forms one of which belongs to a-Se, the other to $As_{0.4}Se_{0.6}$ failed. Onari et al. [44,45] was first who used a similar approach. On the contrary, the experimental spectra could be approximated assuming a considerable broadening of chain vibrations and their frequency displacements. We consider that such an approach is correct and that the difference spectra themselves are convincing arguments in favor of it: the change of the Raman spectra with composition

together with parameters A, ω_{max}, and $\Delta\omega_{max}$ (see the corresponding figures) support this suggestion.

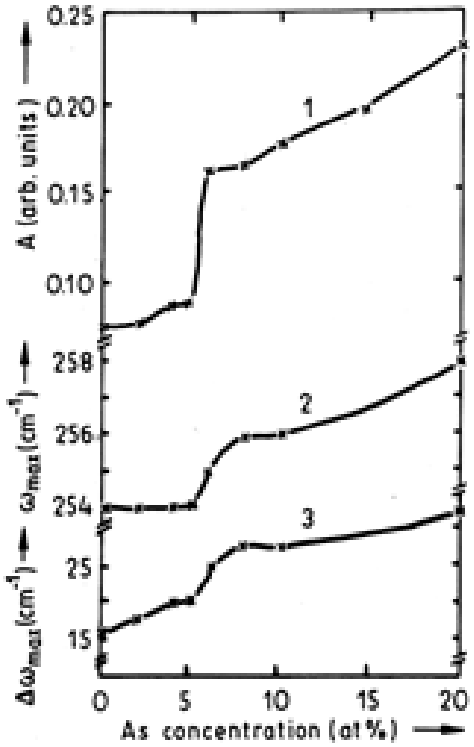

Fig. 4.13. Compositional dependence of the parameters A (1), ω_{max} (2), and $\Delta\omega_{max}$ (3). (1) On the basis of experimental data, (2), (3) from calculated curves of difference spectra.

Composition-dependent studies on the physical properties of binary and ternary chalcogenide glasses give evidence for the existence of mechanical and chemical thresholds at certain compositions of these materials [46-48]. The As-Se system displays main extrema of various properties at the stoichiometric composition (the mechanical and chemical thresholds coincides at x = 0.40).

There seem to exist (see experimental results published by Kasap [49] and present data) an additional threshold at $0.06 \leq x \leq 0.12$. It can be argued that the non-monotonic behavior observed in the concentration dependence of glass transition temperature, density, etc. [50] in this range originates from changes in bond topology [46,49]. We assume that in Se-rich glasses the network is dominated by Se atom chains (quasi-one-dimensional network) and addition of As atoms lead to branching owing to threefold coordination of As atoms. Recent publications [49,51,52], as we believe, give a new approach to the problem of local

bonding in amorphous chalcogenides. The anomalous behavior near $x \approx 0.06$ is ascribed to the disappearance of Se_8-like segments. From the point of view of configuration, it is suggested that the number of cis-configurations in rings starts to decrease, so that the mediate-range correlation is modified. The considerable reduction in the vibration mode at ~112 cm^{-1} associated with cis-segments in ring component strongly supports this suggestion.

Changes in the Raman spectrum with composition allow us to conclude that incorporation of As leads to cross-links between chain-like or ring-like segments of amorphous Se.

There are strong indications that the compositional dependence of physical and chemical properties has no connection with chemical ordering. In fact, the binary As_xSe_{1-x} alloys exhibit extrema in compositional dependence of the density not only at the $As_{0.4}Se_{0.6}$ composition, but also for the non-stoichiometric chalcogen-rich $As_{0.06}Se_{0.94}$ and also for pnictogen-rich $As_{0.6}Se_{0.4}$ samples. This means that the x dependence of the density originates from changes in bonding topolog.

There seem to exist (see experimental results published by Kasap [49] and present data) an additional threshold at $0.06 \leq x \leq 0.12$. It can be argued that the non-monotonic behavior observed in the concentration dependence of glass transition temperature, density, etc. [50] in this range originates from changes in bond topology [46,49]. We assume that in Se-rich glasses the network is dominated by Se atom chains (quasi-one-dimensional network) and addition of As atoms lead to branching owing to threefold coordination of As atoms. Recent publications [49,51,52], as we believe, give a new approach to the problem of local bonding in amorphous chalcogenides. The anomalous behavior near $x \approx 0.06$ is ascribed to the disappearance of Se_8-like segments. From the point of view of configuration, it is suggested that the number of cis-configurations in rings starts to decrease, so that the mediate-range correlation is modified. The considerable reduction in the vibration mode at ~112 cm^{-1} associated with cis-segments in ring component strongly supports this suggestion.

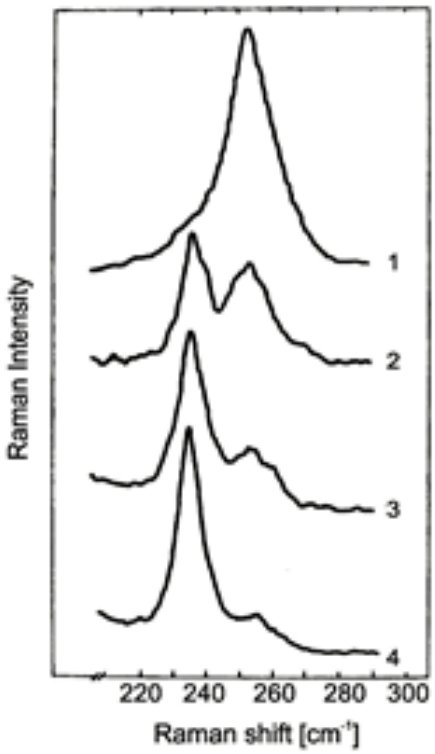

Fig. 4.14. Laser-induced transformation of Raman spectra of amorphous Se. Experimental details f or (1)-(4) are: (1) reference spectrum of amorphous state, (2)-(4) after exposure to E = 3.8, 11,4 and 19×103 J/cm^2, respectively. I = 1.3×102 W/cm^2.

Changes in the Raman spectrum with composition allow us to conclude that incorporation of As leads to cross-links between chain-like or ring-like segments of amorphous Se.

There are strong indications that the compositional dependence of physical and chemical properties has no connection with chemical ordering. In fact, the binary As_xSe_{1-x} alloys exhibit extrema in compositional dependence of the density not only at the $As_{0.4}Se_{0.6}$ composition, but also for the non-stoichiometric chalcogen-rich $As_{0.06}Se_{0.94}$ and also for pnictogen-rich $As_{0.6}Se_{0.4}$ samples. This means that the x dependence of the density originates from changes in bonding topology.

We may summarize the general features of the observed transformation of Raman spectra in the range of bond bands for amorphous selenium. 1) There is (Fig. 4.14) certain threshold energy, E_{th}, of the incident radiation. 2) Below E_{th}, no changes of Raman spectrum are observed. Here we note that the only exception is the so-called boson peak detected at around 17 cm^{-1} which is weakened by illumination. 3) Above E_{th}, an increase of the incident energy density modifies the spectra.

The present experimental results permit to distinguish three successive stages of photocrystallization in a-Se with regard to irradiation energy density. First of all it is necessary to point out the absence of any significant structural transformations in films and bulk samples at Eth $\leq$ 4 J/cm^2. This is strongly supported by the identity of the Raman spectra recorded in repetitive cycles. At the first stage, which is induced by irradiation with incident energy density $\geq$ 3.8 J/cm^2, micro crystallite formation probably takes place. In such a case the 255 cm^{-1} peak dominates the Raman spectra. The second stage of photo crystallization (~ 11 J/cm^2) is characterized by an enlargement of microcrystalline units. This is demonstrated by the growth of the 237 cm^{-1} peak. Finally, at ~ 20 J/cm^2, photo crystallization practically takes place. This stage is marked by a dramatic increase and narrowing of the peak at 237 cm^{-1} with irradiation time. At the same time, the 255 cm^{-1} peak becomes more and more suppressed with respect to other

Raman active modes and, finally, it completely disappears. At this last stage of photo crystallization the absence of the low frequency (17 cm^{-1}) peak is also characteristic.

It seems to be reasonable to assume a thermal, caused by laser heating of the sample, mechanism for the observed structural transformation. This suggestion is strongly confirmed by the clearly manifested threshold behavior. Additional support comes from the fact that at low temperature the threshold power (e.g. 20 J/cm^2 at T=100 K for a-Se) which is necessary for changes in Raman spectra to be observed exceeds several times that for changes at T=300 K. Note that the changes under examination qualitatively differ from the well-known photo darkening phenomena. As for the latter, it takes place at any value of irradiation power;

threshold behavior was not characteristic of them. The magnitude of photo darkening depends mainly on the amount of absorbed energy and significantly increases with temperature lowering. The relatively greater efficiency in films in comparison with bulk samples is established feature of photo darkening. In contrast, in our case, the threshold power densities for a-Se films are found to be higher than for bulk samples. According to results [53,54], discernible reversible photo darkening in a-Se at T=100 K occurs at photon energy hν ≥2.0 eV with maximum efficiency at ~2.4 eV. Probably, the exciting irradiation energy, hν=1.84 eV seems to be low to induce significant photo darkening at T=100 K. At the same time the probability of transient photo darkening effects relaxing after finishing the irradiation at T=300 K for E ≈ 3.8 J/cm^2 cannot be definitively ruled out.

With regard to As_xSe_{1-x} Raman data, principal results are the following:

1. The spectra of the As_xSe_{1-x} amorphous alloy samples before irradiation were the same as those reported in Refs [15, 31, 40, 42, 43-45];

2. The value of Eth necessary for changes in Raman spectra to be observed vary with addition of As (see Table 3.1 given below);

3. Under irradiation with $E>E_{th}$ the recorded spectra clearly show a narrowing and increase in the intensity of the 237 cm^{-1} Raman band;

4. In As_xSe_{1-x} samples with $x\leq0.05$, no additional (to that recorded for pure Se) photo induced changes in their Raman spectra are observed (see Fig. 4.15 and compare with the results for a-Se). It should be accentuated that, on introducing such a relatively large quantity of As additives, there is no appreciable influence on the photo crystallization product. It is well known that Se is likely to be photo crystallized at ~350 K [22, 50]. Reasonably, X-ray diffraction patterns of the samples have been measured. Since the illumination region is of ~3mm in radius, the pattern is noisy. However, we can clearly see four crystalline peaks located at $2\theta = 24^o$, 30^o, 41^o, and 45^o. The peaks can be indexed, respectively, as 100, 101, 110, and 111 of the trigonal (hexagonal) Se crystal [55];

5. For As content >15 at%, the main result of this study is the appearance and disappearance of new Raman bands typical for $As_{0.4}Se_{0.6}$.

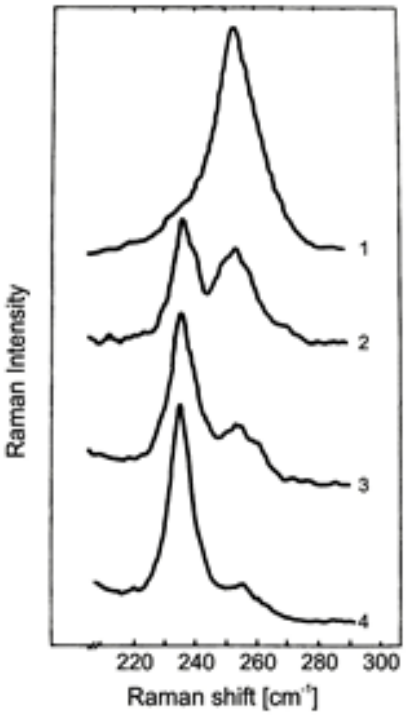

Fig. 4.15. Development of the photo crystallization effect in $As_{0.05}Se_{0.95}$ as a function of exposure: 1, reference spectrum of amorphous state; 2, 3, after exposure to 15, 20 and 25×103 J/cm^2, respectively. I = 1.3×10^2 W/cm^2.

As concentration (at.%)	E_{th}* (kJ/cm^2)
0	2±1
5	12±3
8	7±2
12	8±2
20	45±5

Table 4.1. E_{th} values as a function of As concentration in As_xSe_{1-x} alloys.

* The E_{th} values are shown for the case I = 1.3 × 10^2 kJ/cm^2

For example, Fig. 4.15 shows the appearance of an additional peak (~264 cm^{-1}) superimposed on the amorphous peak (~255 cm^{-1}). With a further increase of the irradiation energy density, crystallization starts immediately. Here we should

note an evolution qualitatively similar to that shown for pure Se and $As_{0.05}Se_{0.95}$ in the shape of spectra over the concentration range 0-20 at %. In the final stage of photo crystallization, the spectra of As_xSe_{1-x} alloys are free of key crystalline features that occur [56] in the spectra of crystalline As_2Se_3. It is of particular significance that only the 237 cm^{-1} band of trigonal selenium contributes to the spectra of photo crystallized As_xSe_{1-x} ($0<x<0.20$) films.

We define E_{th} (e.g. $E_{th}=2\times10^3$ J/cm^2 at $I=1.3\times10^2$ W/cm^2 in the case of pure Se) as the energy density for which the system is not yet perturbed structurally (on the scale of short-range order) by laser irradiation. The absence of any significant bonding changes in films is supported by the identity of the Raman spectra recorded in repetitive cycles. This result holds for both pure amorphous selenium and Se-rich As_xSe_{1-x} alloys. For energies less than E_{th} reversible photo darkening and transient transmission changes are observed. These effects are characteristic of the amorphous phase and the system remains in the amorphous phase under or even after irradiation. The lack of any noticeable variation in the transient behavior T_{rel} for samples of different substrate material and film thickness exclude the possibility of the effect being due to small changes in sample temperature during and after illumination, i.e., to photo induced heating.

We have recently reported similar dynamical photo induced changes in some photo electronic properties detected by time-of-flight and xerographic technique [18- 20, 57]. These experiments may provide the first evidence that deep defects can be altered temporarily by room-temperature irradiation. Note that there is a close correlation between the recovery of optical parameters and photo electronic characteristics in exposed samples.

Although a complete correlation of microscopic structural modifications with macroscopic photo darkening phenomena must await further experimental measurements, it is only natural that we relate the transient changes in the transmissivity with changes in deep defect states. We identify such centers as arising from native (thermodynamic) structural defects (e.g., C_3^+ and C_1^- in amorphous selenium). Band-gap light can probably initiate conversion of traps of small cross-section to those of larger cross-section [8,58].

By contrast, above E_{th}, all the observed irreversible changes may be attributed to optical constant variations and modifications in the kinetics of light-induced crystallization.

The present experimental results resolve successive stages of photo crystallization in a-Se (these were mentioned above). In such a photo crystallization process, amorphous Se undergoes a transformation to the trigonal selenium which is the most stable modification. Raman scattering studies together with X-ray diffraction data gave an unambiguous indication of trigonal selenium.

On the basis of the present Raman data, we conclude that the features of the photo crystallization effects in As_xSe_{1-x} alloys with $x<0.15$ are qualitatively the same as those in amorphous selenium. Some deviation in pre-crystallization behavior of $As_{0.2}Se_{0.8}$, namely the appearance and disappearance of the weak quasi-crystalline peak at 264 cm^{-1}, probably indicates As_2Se_3-like cluster creation and annihilation. The latter could be clusters with a more ordered structure with respect to that existing in amorphous phase. At the same time, they are not yet micro crystallites with inherent Raman peaks. It seems to be reasonable that the environment of the clusters prevents their growth and transformation into micro crystallites. Other Se clusters reach the critical size required for micro crystallite formation. After that, sample exposure to $E>E_{th}$ crystallized selenium, while the As-containing clusters remained in amorphous phase. The above explanation is in agreement with the results of the study of laser-induced structural transformations in glassy As_2Se_3 [58] and also with the mechanism proposed by Phillips [59].

It is known [50] that As is an effective additive to decrease the tendency to crystallization. Our experimental results, namely the greater value of E_{th} for a-As_xSe_{1-x} films, indicate that the addition of As effects the suppression of the crystal nucleation and growth in amorphous selenium. The long Se chains in amorphous selenium branch at the site of As atoms. The length of Se chains becomes short [45, 60] and the amorphous Se cannot easily crystallize with increase of As concentration.

Although a complete correlation of microscopic structural modifications with macroscopic photo darkening phenomena must await further experimental

measurements, it is only natural that we relate the transient changes in the transmissivity with changes in deep defect states. We identify such centers as arising from native (thermodynamic) structural defects (e.g., C_3^+ and C_1^- in amorphous selenium). Band-gap light can probably initiate conversion of traps of small cross-section to those of larger cross-section [8,58].

By contrast, above E_{th}, all the observed irreversible changes may be attributed to optical constant variations and modifications in the kinetics of light-induced crystallization.

The present experimental results resolve successive stages of photo crystallization in a-Se (these were mentioned above). In such a photo crystallization process, amorphous Se undergoes a transformation to the trigonal selenium which is the most stable modification. Raman scattering studies together with X-ray diffraction data gave an unambiguous indication of trigonal selenium.

On the basis of the present Raman data, we conclude that the features of the photo crystallization effects in As_xSe_{1-x} alloys with $x<0.15$ are qualitatively the same as those in amorphous selenium. Some deviation in pre-crystallization behavior of $As_{0.2}Se_{0.8}$, namely the appearance and disappearance of the weak quasi-crystalline peak at 264 cm^{-1}, probably indicates As_2Se_3-like cluster creation and annihilation. The latter could be clusters with a more ordered structure with respect to that existing in amorphous phase. At the same time, they are not yet micro crystallites with inherent Raman peaks. It seems to be reasonable that the environment of the clusters prevents their growth and transformation into micro crystallites. Other Se clusters reach the critical size required for micro crystallite formation. After that, sample exposure to $E>E_{th}$ crystallized selenium, while the As-containing clusters remained in amorphous phase. The above explanation is in agreement with the results of the study of laser-induced structural transformations in glassy As_2Se_3 [58] and also with the mechanism proposed by Phillips [59].

It is known [50] that As is an effective additive to decrease the tendency to crystallization. Our experimental results, namely the greater value of E_{th} for a-As_xSe_{1-x} films, indicate that the addition of As effects the suppression of the crystal nucleation and growth in amorphous selenium. The long Se chains in amorphous

selenium branch at the site of As atoms. The length of Se chains becomes short [45, 60] and the amorphous Se cannot easily crystallize with increase of As concentration.

At the same time, it is necessary to note that the changes in optical transmissivity and diffraction efficiency that occur are not monotonic with increasing As content. It seems to be reasonable to connect such a behavior with some discontinuity of atomic arrangement with increasing As content. Our recent study of composition dependence of Raman bands in amorphous As_xSe_{1-x} supports this suggestion.

4.5. Raman scattering in pure and alloyed amorphous selenium: low-frequency spectral region

It has become evident that traditional techniques of structural investigation are inefficient for study of disordered materials. They give information on the structure of a short-range order only and are slightly sensitive to more long-range correlations in arrangement of atoms. The existence of the medium-range order is admitted: periodical atomic arrangement inherent in crystals remains within several coordination spheres and then is violated. It is assumed that the character of the violation may depend on preparation and chemical composition of the sample [28, 61]. A number of experimental procedures were proposed, for measurement of a size ordered micro regions, or structural correlation range R_c. One of these methods permits to determine R_c by the position of a low-frequency boson peak in Raman spectra [62]. It has been shown [61-63] that the Raman intensity can be described by

$$I/\varpi(n(\varpi)+1) = \sum_b C_b(\varpi) g_b(\varpi)/\varpi^2$$

where g_b is the density of states and C_b is the matrix element of the coupling of the vibration mode b to the light, $n(\varpi)$ is the boson occupation number. In the low-frequency region $I/\varpi(n(\varpi)+1) \sim \varpi^2$ increases and then reaches a maximum

at certain value $E = E_{max}$ (Fig. 4.16(a)), which depends on chemical composition and thermal prehistory of the sample [63, 64]. This peak was called in literature as a boson peak. It accounts for 30 to 90% of integrated intensity of Raman spectrum in glasses.

Authors [61] have compared spectral form of the low-frequency band in various samples. For the sake of simplicity all the spectra are given in the same energy scale $E_n = E / E_{max}$ (Fig. 4.16 (b)). A unique property of the boson peak was found: in a broad frequency range the spectral form of the peak is independent of chemical composition of the sample. Additional analysis of results (Fig. 4.16 (b)) indicates that the boson peak has a universal nature, which is due to the most general features of vitreous structure and is not associated with the concrete chemical composition of glass or with the structure of corresponding crystal. One of these features is the medium-range order. Universal form of the boson peak is assumed to be due to this general character of vitreous solids.

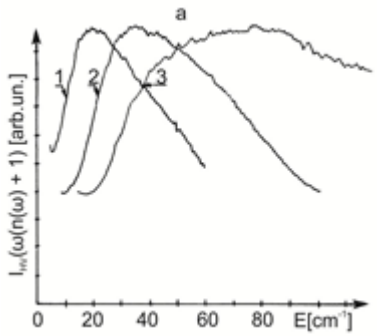

Fig. 16. (a) Low-frequency Raman spectra of As_2S_3 – 1, $Bi_4Si_3O_{12}$ – 2, $La_2S_3Ga_2S_3$ – 3 glasses [61].

The low frequency region $0 < \omega < 100$ cm^{-1}, in which the boson peak appears in a-Se, is of special interest. It has been found that the spectral form of the boson peak is nearly the same for a wide series of oxides, chalcogenides, and low-weight molecular organic glasses. The universal form of the low frequency peak is due to universality of glassy material in the scale of medium-range order L $L \sim \upsilon / \varpi_{max}$ = 1 to 2 nm (υ is the sound velocity). For the case of a-Se, it is observed (Fig. 4.17) that the spectral form of the boson peak essentially differs from that

characteristic of the majority of inorganic glasses. The spectral form of the boson peak in a-Se seems to be intermediate between that in polymeric and low-molecular glasses.

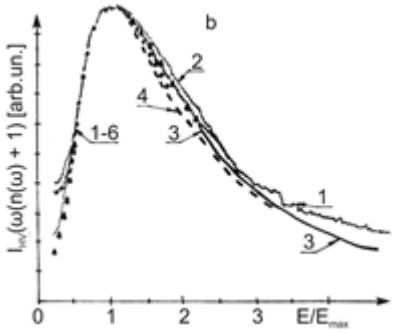

Fig.4.16. (b) Raman spectra of different glasses in a scale $E_n = E / E_{\max}$: 1 – As_2S_3 ($E_{\max}$ = 26 cm^{-1}), 2 – $Bi_4Si_3O_{12}$ (34 cm^{-1}), 3 – SiO_2 (52 cm^{-1}). In addition it is shown spectrum: 4 – B_2O_3 (28 cm^{-1}), 5 – B_2O_3 (45 cm^{-1}), 6 – GeS_2 (22 cm^{-1}) and 7 – Li_2O (88 cm^{-1}) [61].

Normalized Raman spectra $I_n = I / \varpi(n(\varpi)+1)$ for a-Se and series of other composition samples are given in the same energy scale $\varpi_n = \varpi / \varpi_{\max}$, where $n(\varpi)+1 = 1/\exp(h\varpi / kT)-1)+1$ is the boson factor for the Stokes component.

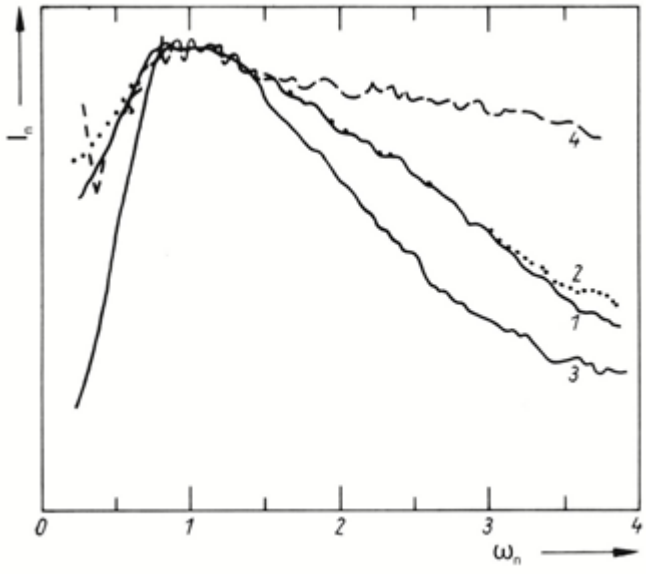

Fig. 4.17. Low-frequency Raman spectra of different glasses in a scale $\varpi_n = \varpi / \varpi_{\max}$. (1) Se ($\varpi_{\max}$ = 17 cm^{-1} at T=100 K), (2) Se ($\varpi_{\max}$ = 17 cm^{-1} at T=300 K), (3) As_2S_3 ($\varpi_{\max}$ = 26 cm^{-1}, T = 300 K), (4) polymethylmetacrylate (PMMA) ($\varpi_{\max}$ =17 cm^{-1}).

This result can be explained by a preferentially chain-like structure of a-Se. The latter may form a structure similar to the structure of linear polymers PMMA. In other words, with regard to its structure on the scale of medium-range order, a-Se may be placed between 3-dimensional network glasses and polymeric ones. Examples of mediate-range order in elemental and compound materials, including a-Se, have been extensively discussed in [65-70].

There exists another possible explanation. Selenium has its glass transition temperature near room temperature; therefore it is in a well annealed state. It is known [61] that the intensity of the boson peak relative to the main bond modes in the Raman spectrum significantly decreases as the structural order of the sample increases (e.g. in "equilibrated" or annealed samples). This decrease in turn may lead, respectively, to an increased contribution from other modes to the high-frequency side $\varpi > \varpi_{max}$ of the boson peak. This is clearly seen if we compare the shape of corresponding peaks in a-Se and As_2S_3 (Fig. 4.17).

4.6. Finite size microcrystalls in glasses

Relatively great number of studies has been performed to understand the structure of non-crystalline solids from light scattering investigations. The majority have concentrated on spectral features in the optical mode region of the Raman scattering spectra. Recent interest has developed in the low-frequency or acoustic Raman modes region. This interest is a manifestation of theoretical works on the properties of light scattering from acoustic modes in disordered solids [71,72]. A direct explanation for the universal presence of low-frequency modes in non-crystalline modes was given by Shuker and Gammon [1] and Martin and Brenig [72] (the later authors exemplified it for the case of oxide glasses). Studies appeared on other aspects of Raman scattering as a sensitive probe for the structure of glasses. To the author's best knowledge, Duval [73] was the first who established that Raman spectroscopy is a powerful and sensitive technique to determine the size of the microcrystal's in a glass. It has been shown that, in the case of microcrystals included in a glassy phase, only the lowest energy vibration

eigenmodes (surface modes) are active in the acoustic Raman scattering region [74-76]. Interestingly, the frequency of these surface vibration modes (modes with large amplitudes at the particle surface) are related to the diameter of the microcrystals.

The low-frequency Raman spectra of glasses with microcrystals have been investigated in this paragraph. It is shown that the spectra permit to determine conditions at the boundaries, sizes and concentrations of structural microinhomogeneities in disordered materials.

Model glasses ($K_2O \cdot Al_2O_3 \cdot 6GeO_2$, Photochromic glasses, chalcogenide glasses) were chosen as samples for these studies for several reasons. These materials can be prepared as well characterized high optical quality bulk glasses. Optical quality is important to minimize the spectral component due to elastically scattered light which masks low frequency Raman spectral features. In addition, both glasses can be easily prepared and crystallized. Fortuitously, one can study properties aroused from differences in structure (caused by thermal treatment) in detail.

Right angle Raman spectra were performed in the usual VV and HV polarizations.

Fig. 4.18 shows Raman spectra for the not-annealed and annealed photochromic glass samples. A low-frequency (the so-called boson peak, typical of the spectra of any vitreous material) is observed at the frequency $\omega \approx 60$ cm^{-1}.

Annealing of samples caused a change of the spectra in the frequency range $\omega <$ 20 cm^{-1}; the peak with $\omega_{max} \sim 10$ cm^{-1}appears (Fig. 4.19). The latter corresponds to vibrational spectrum of microcrystals which grow during annealing.

Clearly, the amplitude of the low-frequency peak increases while decreases with annealing temperature.

In general, the annealed samples contain inhomogeneities of two types. The first corresponds to inhomogeneities of matrix itself. The second is associated with microcrystals.

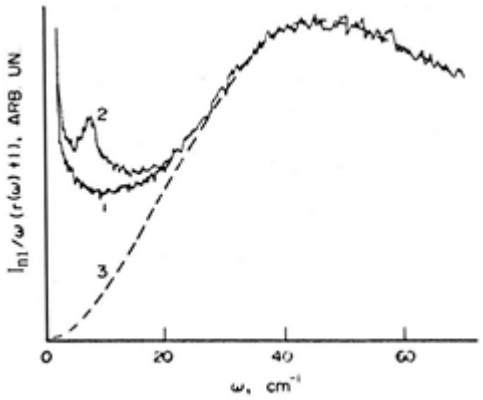

Fig. 4.18. The low-frequency Raman spectra of the not-annealed (1) and annealed (2) samples; (3) – the calculated spectrum [77] for the contribution from acoustic vibrational excitation.

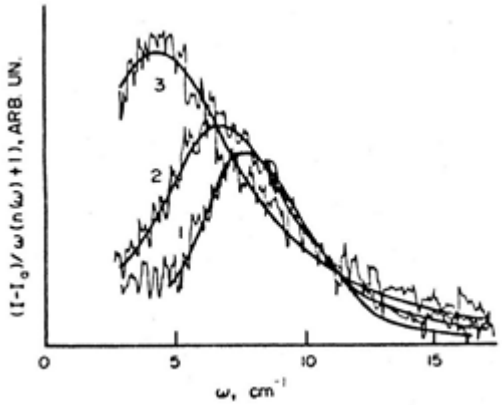

Fig. 4.19. The difference between spectrum of not-annealed sample and spectra of samples: annealed during 2 h at: 550^o C (1), 573^o C (2) and 600^o C (3).

The results obtained can be interpreted in terms of phenomenological model. Let us consider homogeneous medium. The density-of-states, $g(\omega)$, is described by the Debye's law

$$g_0(\omega) = 3\omega^2 2\upsilon^3\pi^2 \quad , \qquad (1)$$

where $\upsilon = (\upsilon_t^{-1}2/3 + \upsilon_l^{-1}/3)^{-1}$, with υ_t and υ_l being transverse and longitude sound velocities, respectively. The presence of microcrystals in glassy matrix changes the Debye density-of-states. There appear additional low-frequency modes due to surface vibrations of microcrystals. These modes are localized at ω

$\approx \upsilon / D$. To describe their contribution to the density-of-states, a simple phenomenological model is used.

The form of the microcrystals is assumed to be close to spherical ones of D_0 in diameter. The density of vibrational states, with account of the contribution from low-frequency modes of a sphere vibrations ω , can be written in the form:

$$g(\omega) = g_0(\omega) + N\delta(\omega - \omega_0) \quad . \qquad (2)$$

Both the finite lifetime and the scatter in sizes and shapes of microcrystals results in the broadening of vibrational modes. We can express the Lorentz distribution of width Γ in the form:

$$g(\omega) = 3\omega^2 / 2\upsilon^3\pi^2 + N\Gamma((\omega - \omega_0)^2 + \Gamma^2)^{-1} / \pi \quad . \qquad (3)$$

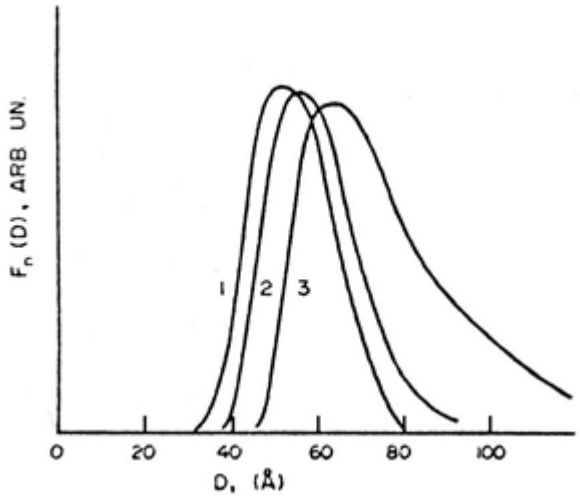

Fig. 4.20. Distribution functions of microcrystal's size in the samples. Numeration of the curves is the same as in Fig. 4.19.

As evident from Eq. (3), there is the resonant peak at $\omega = \omega_0$, superimposed on the smooth Debay density of states.

In disordered materials, the Raman intensity is proportional to the density of vibrational states $g(\omega)$ [71]

$$I_0(\omega) \sim C_{ij}(\omega)g(\omega)(n(\omega)+1)/\omega \quad , \qquad (4)$$

where C_{ij} is the square of matrix element of light interaction with vibrational excitation, $n(\omega)+1$ is the bose-factor.

In the low-frequency range, for the acoustic vibrations

$$C(\omega) \sim \omega^2, \qquad (5)$$

and the factor of proportionality depends on elasto-optic constants P_{ij} of the material [78]. Assuming Eq. (5) for simplicity, we have

$$I / \omega(n(\omega)+1) \sim g(\omega) . \qquad (6)$$

The frequency of a spherical mode, $I = 0$, is related to the sphere diameter D_0 as follows:

$$\omega_0 \cong 0.7\upsilon_c / cD_0 , \qquad (7)$$

where c is the light velocity. Spherical and torsional modes have the frequency

$$\omega^l = \omega^t \cong 0.85\upsilon_t / cD_0 . \qquad (8)$$

Therefore, the Raman intensity is of the form:

$$I(\omega_0) / \omega_0(n(\omega_0)+1) \approx (P_{ij}{}^g)^2 3\omega_0{}^2 / 2\upsilon^3\pi^2 + P_{ij}{}^m N / \pi\Gamma . \qquad (9)$$

Here $P_{ij}{}^g$ and $P_{ij}{}^m$ are elasto-optic constants of the glass and microcrystal, respectively. In Eq. (9), the first term corresponds to the scattering on acoustic phonons of the glass I^{ac}, while the second is the contribution of vibrations localized on microcrystals I^{loc} . Therefore, one can estimate: a) microcrystal sizes using the position of the localized mode in Raman spectrum ω_0 ; b) the microcrystal concentration for Γ and I^{loc} / I^{ac} given

$$N \cong (I^{loc} / I^{ac})(P_{ij}{}^g / P_{ij}{}^m)^2 3\omega_0{}^2\Gamma / 2\upsilon^3\pi . \qquad (10)$$

The model predicts the lowest surface modes to be localized at $\omega_{\max} = \beta / D_0$, where $\beta \approx 10^{-6}$.

It seemed that the appearance of spherical or torsional modes is determined by interaction between the microcrystal surface and the surrounding glassy matrix: spherical modes if the glass matrix is softer than the microcrystal; torsional for the case of weak coupling between the microcrystal surface and the environment.

In addition to D_0 , the Raman spectrum allows to estimate the microcrystal concentration for I^{loc} / I^{ac} given. It is well-known [79] that a central peak make considerable contribution to the intensity of light scattered at room temperature in the range ω < 20 cm-1. Contribution from acoustic vibrations can be separated via approximation of the boson peak. Taking all factors into account, one obtains $N \approx 10^{17}$ cm^{-3}.

Finally, the low-frequency Raman scattering appears to be a sensitive method for the investigation of the initial stage of nucleation in multi- and mono-component systems [79]. In the case of the mono-component systems, when the crystalline nuclei do not have an acoustic mismatch as compared to the amorphous matrix, we cannot observe their surface vibrations, but we can make use of the fact that in nucleation there is a jump in a structure correlation length. This results in a sharp decrease in contribution to the density of the acoustic vibration states because of decreasing the concentration of structural correlations on which acoustic phonons are localized. In addition, low-frequency Raman spectroscopy may be useful in the research into the phase transformation in materials for phase-change memories. From the fact that the 17 cm-1 band is the only observed in a-Se, does not contain microcrystalline-related features which shift in frequency or increase in intensity with thermal treatment, it may be deduced that all our Raman spectra correspond to the advanced stages of crystallization. That means Raman spectra do not show the formation of the very small microcrystal's or nuclei but only reflect the more advanced crystal growth process.

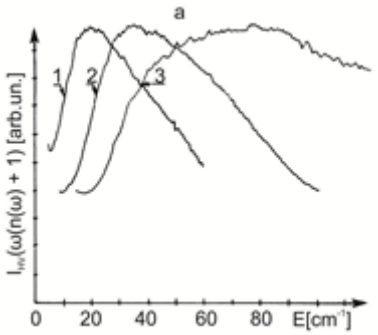

Fig. 4.21(a). Low-frequency Raman spectra of As_2S_3 – 1, $Bi_4Si_3O_{12}$ – 2, $La_2S_3Ga_2S_3$ – 3 glasses [61].

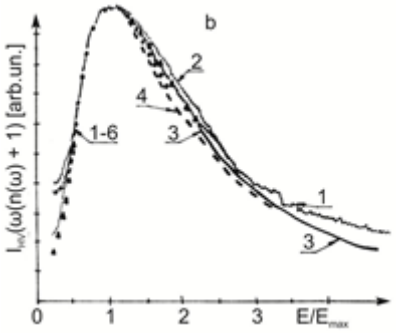

Fig. 4.21(b) Raman spectra of different glasses in a scale : 1 – As_2S_3 (= 26 cm-1), 2 – $Bi_4Si_3O_{12}$ (34 cm^{-1}), 3 – SiO_2 (52 cm^{-1}). In addition it is shown spectrum: 4 – B_2O_3 (28 cm^{-1}), 5 – B_2O_3 (45 cm^{-1}), 6 – GeS_2 (22 cm^{-1}) and 7 – Li_2O (88 cm^{-1}) [61].

The low frequency region $0 < \omega < 100$ cm^{-1}, in which the boson peak appears in a-Se, is of special interest. It has been found that the spectral form of the boson peak is nearly the same for a wide series of oxides, chalcogenides, and low-weight molecular organic glasses. The universal form of the low frequency peak is due to universality of glassy material in the scale of medium-range order L ~ = 1 to 2 nm (is the sound velocity). For the case of a-Se, it is observed (Fig. 4.22) that the spectral form of the boson peak essentially differs from that characteristic of the majority of inorganic glasses. The spectral form of the boson peak in a-Se seems to be intermediate between that in polymeric and low-molecular glasses.

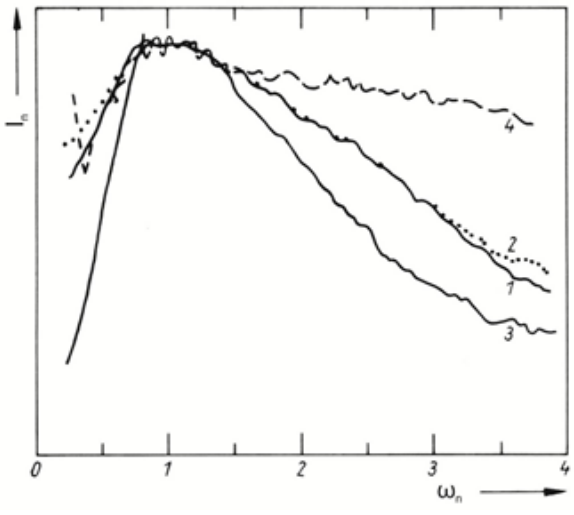

Fig. 4.22. Low-frequency Raman spectra of different glasses in a scale. $\varpi_n = \varpi / \varpi_{max}$ (1) Se (ϖ_{max} = 17 cm^{-1} at T=100 K), (2) Se (ϖ_{max} = 17 cm^{-1} at T=300 K), (3) As_2S_3 (ϖ_{max} = 26 cm^{-1}, T = 300 K), (4) polymethylmetacrylate (PMMA) (ϖ_{max} =17 cm^{-1}).

Normalized Raman spectra for a-Se and series of other composition samples are given in the same energy scale $I_n = I/\varpi(n(\varpi)+1)$, where $n(\varpi)+1 = 1/\exp(h\varpi/kT)-1)+1$ is the boson factor for the Stokes component.

Q This result can be explained by a preferentially chain-like structure of a-Se. The latter may form a structure similar to the structure of linear polymers PMMA. In other words, with regard to its structure on the scale of medium-range order, $\varpi_n = \varpi/\varpi_{\max}$ a-Se may be placed between 3-dimensional network glasses and polymeric ones. Examples of mediate-range order in elemental and compound materials, including a-Se, have been extensively discussed in [65-70].

There exists another possible explanation. Se has its glass transition temperature near room temperature; therefore it is in a well annealed state. It is known [61] that the intensity of the boson peak relative to the main bond modes in the Raman spectrum significantly decreases as the structural order of the sample increases (e.g. in “equilibrated” or annealed samples). This decrease in turn may lead, respectively, to an increased contribution from other modes to the high-frequency side > of the boson peak. This is clearly seen if we compare the shape of corresponding peaks in a-Se and As2S3 (Fig. 4.22).

4.7. On the origin of Boson Peak

The boson peak is a broad peak found in the low-frequency region of Raman scattering spectra in a wide range of many solid state materials, including amorphous films, inorganic glasses, liquids/melts, polymers/ bio-polymers, and partially crystalline materials. The peak is recognized as a universal feature of very different amorphous materials. Here, we give a state of the art of the low-frequency (Boson) peak.

Light scattering can be used to obtain information about the static structure and the dynamics of gases, crystals, liquids, amorphous solids, glasses and polymers.

It is well-known that all glasses and polymers and even some disordered crystals exhibit excess vibrations in the terahertz frequency range. The density of vibrational states at these frequencies far exceeds the expectation of the Debye model. The latter is based on a simple assumption of homogeneous isotropic elastic continuum. Despite the long history of studies, the microscopic nature of these low-frequency vibrations remains a subject of active discussions [88-103]. In fact, these discussions started already some 50 years ago with the observation of a low-frequency Raman band that usually is not present in crystalline Raman spectra and which has been called “boson peak”.

Among general features inherent to disordered solids the so-called Boson peak (BP) is the most intriguing. It is observed in the inelastic photon (Raman & X-ray) and neutron scattering spectrum in a THz frequency range and is recognized as a universal feature of quite different amorphous materials such as, e.g., glasses, polymers, super-cooled liquids or even amorphous ice.

Another important topic that is ultimately connected to the nature of the excess vibrations is the attenuation of the sound-like waves at the frequencies of the boson peak In particular, the connection between the damping of the vibrational modes, the plateau in the low temperature thermal conductivity, and the boson peak itself, is still highly debated. A new interest to these topics has been inspired by recent developments in experimental techniques and theoretical approaches. Also, the observed correlations between the terahertz dynamics and the peculiarities of the glass transition fragility call for additional attention to the microscopic mechanisms controlling the fast dynamics.

Vitreous materials like silica, boric oxide and soda-lime-silica glass are the classic materials from which both the physics of the amorphous state and the modern concepts of atomic structure of glass originated

In an amorphous solid, Shuker and Gammon [86] showed that the first order Raman scattered Stokes intensity could be written as

$$I(\boldsymbol{\omega}) \approx [C(\boldsymbol{\omega})g(\boldsymbol{\omega})/\boldsymbol{\omega}](n(\boldsymbol{\omega})+1)$$

where $C(\boldsymbol{\omega})$ is the coupling coefficient, $g(\boldsymbol{\omega})$ is the density of states and $n(\boldsymbol{\omega})$ is the Bose-Einstein thermal population factor.

The Boson peak can be defined as an excess contribution to the usual Debye density of states (DOS). The name is give because the temperature dependence of the intensity of the peak follows that of a harmonic oscillator characterized by the Bose factor. It can be observed with a variety of optical, neutron and thermal measurements, including Raman spectroscopy.

Krishnan observed in 1953 the boson peak with Raman scattering [94]. He found for v-SiO_2 a broad band in the vicinity of 30-120 cm^{-1} (note that 1THz=33.35 cm^{--1}) which markedly differs from the behavior of crystals.

Because the Raman light scattering is an electronically driven process, not all the vibrations will be able to interact with the incoming light. The intensity of Raman scattered light depends not only on the vibrational density of states, but also on the coupling between photons and vibrations.

Disordered solids, especially glasses, are compelling materials to study from a fundamental point of view as they pose challenging and yet unsolved problems in the field of condensed matter physics. Ranging from silicates to halides and chalcogenides, inorganic glasses have found amazingly widespread use in our lives that ranges from windshields, flat-panel displays and electric bulbs all the way to optical fibers and amplifiers in modern day telecommunication networks. Vitreous materials like silica, boric oxide and soda-lime-silica glass are the classic materials from which both the physics of the amorphous state and the modern concepts of atomic structure of glass originated. From a historical standpoint silicate glasses are the most ancient materials known to mankind. They also occur naturally, predominantly amongst volcanic rocks, and indeed offer important insight into the physic-chemical conditions in the interior of our planet. At the other extreme, chalcogenide and halide glasses represent some of the most recent functional materials to be discovered.

In the last decades our understanding of the static atomic structure of amorphous solids has advanced substantially. These advancements have been due

primarily to huge improvements in experimental methods like Raman spectroscopy and elastic and inelastic neutron scattering.

All of these experimental advances reveal a wealth of order, both at the local level of individual structural entity as well as in the intermediate range governed by the connectivity's between adjacent units. The discovery of sources of more distant or longer-range order in inorganic glass systems is an additional exciting development.

Fundamental physical properties of amorphous solids differ strongly from those of crystals. An interesting feature of their vibrational dynamics is a broad band observed in Raman scattering spectra in the low-frequency region. This band is identified as the boson peak. The origin of this boson peak, as mentioned above, is still under debate.

Vibrational properties of disordered materials are one of the currently lively topics of modern condensed matter physics. Features of the disordered vibrational spectrum, such as the boson peak, the quasi-elastic scattering and the vibrational localization or propagation are being investigated. In fact, the physical nature of the modes responsible for the boson peak is still unclear and represents a problem of current interest. In the last years the boson peak properties have been studied as a function of temperature, near and far from the glass transition, and as a function of pressure in strong and fragile glasses, in porous systems, by means of several experiments as Raman and neutron scattering measurements.

Inelastic light scattering experiments in the low frequency domain (Boson peak) are interpreted as being due to inhomogeneities in the structure of the glass but these models are still a matter of discussion. Besides, elastic scattering (Rayleigh scattering) in elemental and a simple component glass is well interpreted as due to density fluctuations. The role of thermal treatment on the energy of the Boson peak was demonstrated in [83-85,95].

In this Paragraph, we will make an attempt to separate the different contributions of Rayleigh, Brillouin, and Raman processes. We propose further to follow their evolution with the fictive temperature to correlate these observations with the structure of the glass.

The Boson peak can be defined as an excess contribution to the usual Debye density of states (DOS). The name is give because the temperature dependence of the intensity of the peak follows that of a harmonic oscillator characterized by the Bose factor. It can be observed with a variety of optical, neutron and thermal measurements, including Raman spectroscopy.

Because the Raman light scattering is an electronically driven process, not all the vibrations will be able to interact with the incoming light. The intensity of Raman scattered light depends not only on the vibrational density of states, but also on the coupling between photons and vibrations.

4.7.1. Theoretical models for Boson peak

There are essentially three different scenarios that have been proposed for the origin of the boson peak in glasses [88-10] One assumes that vibrational modes additional to sound waves exist, another ascribes the boson peak to localized vibrational modes, perhaps associated with inhomogeneities in the glass structure, while the third ascribes the non-Debye excess of modes to the effect of disorder (strong scattering) on sound wave excitation. None of these theories has yet fully described every aspect of the physical origin of the BP.

Model 1: Soft Potential Model

In the first model, the localized modes in the very low frequency (<1GHz), which is called tunneling modes, are postulated to extends to the Boson peak region and gives rise to the Boson peak. This model is called soft potential model, in which both the relaxational and vibrational modes are explained in same physics. The Boson peak is attributed to the existence of anharmonic localized potential wells (and double wells). Simulations have been performed successfully for vitreous silica, suggesting the Boson peak of which arises from coupled rotations and bodily translations of SiO4 tetrahedrons.

The tunneling model postulates the existence in glasses of localized modes, whose character is still disputed, that are responsible for low-temperature

anomalies in thermal properties. Such modes are believed to exist at frequencies below 1GHz.

In the so-called soft potential model, it is postulated that such localized modes persist up to much higher frequencies, crossing over to vibrational modes in soft harmonic potential wells at frequencies in the boson peak region. This approach, naturally accounts for both relaxational and vibrational modes. Quasi-localized modes have been identified in simulations of vitreous SiO_2. Such modes comprise coupled rotations and bodily translations of SiO_4 tetrahedra.

Model 2: Localized Vibration Model

This model assumes that the structure of glasses is inhomogeneous, consisting of an aggregated blobs with different density from the matrix. The boson peak is assumed to be due to vibrational modes spatially localized in such blobs. However, there is no evidence, from computer simulation, that the sort of density fluctuations envisaged exist in the structure of glass network. There is no evidence that true localization of modes exists at low frequencies of the order of 1THz. Also, Vibrational localization should occur only at the edges of the acoustic and optic bands in the VDOS at much higher frequencies.

The second model ascribes the Boson peak to localized vibrational modes. It assumes that the structure of the glasses is inhomogeneous, consisting of an aggregate of “blobs” with a different density or elastic constants from the matrix. The Boson peak is assumed to be due to vibrational modes spatially localized in such blobs. No computer simulations, however, have proved such density fluctuations neither exist, nor are there any evidence that localized mode can occur at such low frequency.

Model 3: Medium Range Disorder Model

The third model attributes the extra, non-Debye-like modes in the boson peak region to the result of strong scattering of sound waves by the disorder (in force constants or atomic positions) characteristic of the amorphous states. W. Schirmacher et. al [23] presented compelling evidence that a strongly disordered

three-dimensional system of coupled harmonic oscillators with a continuous force constant distribution exhibits an excess low-frequency DOS (Boson Peak) as a generic feature. This was achieved by comparing the results of a CPA (coherent-potential approximation) calculation with those of a numerical diagonalization[55]. The extra states in the boson peak region are supposed to be the high k acoustic or low k optics modes pushed down in frequency by disorder and mixed with the low k acoustic modes.

The medium range disorder will induce the broadening of the vibration lines in the high frequency range, some vibration states will extend to the low frequency range, which gives rise to the excess of density of states in the low frequency range as compared with what is predicted by the Debye's model.

When the disorder increases, more broadening will cause the vibrational peaks in the high frequency region to broaden more, thus more excess of density of states will extend to the low frequency region, giving rise to a higher Boson peak intensity; while on the other side, more broadening will cause the peaks extend to lower frequency, which means the Boson peak energy will decrease [4-6,9-12]. According to the theoretical prediction of this model, Boson peak energy decreases and its intensity increases with increasing disorder.

To obtain a better understanding of the density of states in the Boson peak regime more spectral information is needed. This is hard to get merely from Raman spectroscopy because of the coupling coefficient is frequency dependent. In the case of inelastic neutron scattering, the VDOS is obtained more directly, with no strongly frequency-dependent coupling coefficient being involved. In the third model, it was proposed the Boson peak originates from the medium range disorder of the system.

The previous two models are actually the utilization of the model that was used to describe the higher and lower frequency regions. We will base our analysis on the third model, which in its simple yet convincing way gives a clear explanation for the Boson peak.

In a simplified language, this model basically states that the disorder leads to a local repulsion of vibrational states, which includes a downward shift of low frequency states as compared to the Debye prediction.

In this model, it is proposed that the more disordered the system is, the higher the Boson peak is.

Chalcogenide glasses are often called covalent network glasses which can be categorized between fragile (e.g., polymer and molecular glasses) and strong (e.g., silica and other oxides) glasses, and therefore significantly different from silica and polymer/molecular glasses in structural/glassy properties and hence in the origin of the Boson peak. The Boson peak of typical chalcogenide glasses, is observed as an excess peak at about 3 meV in the vibrational density of states. Several models [1-4] have been proposed to explain the origin of the Boson peak in chalcogenide glasses. Features and the origin of Boson peak were often discussed in relation to microscopic and/or intermediate range structure, and sometimes explained together with the origin of the first sharp diffraction peak (FSDP) which is characteristic for the glasses. However, the proposed ideas seem to be still controversial. Besides localized or propagating vibrational modes, the low-energy excitations of glasses can be involved also with relaxation and/or deformational motions of restricted structures. This fact has made the exploration of the low-energy modes (including the Boson peak) of glasses difficult and complicated.

Experimental results indicate that the BP intensity decreases when a glass is compressed or when the fictive temperature decreases with the important exception of hyper quenched vitreous silica from very high temperatures. This exception, however, can be explained if the anomaly of the density of silica at high temperature is taken into account.

When considered from the viewpoint of vibrational dynamics, crystalline and non-crystalline (glasses and amorphous solids) materials exhibit noticeable differences at energies that are material dependent, but that always lie around 1 THz. These differences, that have their origin at the lack of long–range periodicity, can all be traced back to the universal presence in glasses of low–energy

excitations in excess of the parent crystals. The term low–energy excitations has been coined to account for properties concerning:

(i) the specific heat excess (bump in the plot) at temperatures around 5-10 K;

(ii) (ii) the plateau in thermal conductivity at about the same temperature;

(iii) (iii) the strong attenuation of sound waves;

(iv) (iv) the presence of scattering intensity– absent from the parent crystal – in Raman and inelastic incoherent neutron scattering (INS) spectra.

The last issue, low energy scattering intensity excess, has recently resurfaced in view of new theoretical and experimental approaches [4-15]. In particular, crystalline solids obey rather accurately the predictions of the Debye model for an elastic continuum, according to which the vibrational density of states is a quadratic function of the frequency. On the contrary, non-crystalline phases ubiquitously exhibit some extra low-energy vibrational modes in excess.

The inherent difficulty in the formulation of successful theories for glasses has led to the suggestion of numerous empirical correlations among different glass properties. Such correlations usually relate a spectral characteristic of the Boson peak (intensity, peak position etc.) with a specific property of the glass.

An efficient way to obtain information on Boson peak is to study its spectral changes by changing the glass composition and/or the magnitude of certain external parameters.

Rayleigh scattering is 5-10 orders higher in intensity comparing with the Raman scattering. The Rayleigh scattering can thus obscure most of the Raman scattering signals and must be rejected using appropriate method.

In these Tellurium oxide glasses, the very high Boson peak indicates high disorder. Since the Boson peak is caused by the broadening of the high frequency vibrational peaks, the high Boson peak in the low frequency range comes as no surprise because these Tellurium oxide glasses do have high Raman scattering intensity in the high frequency region. Especially, the very high vibrational peak in

the low frequency region, just above the Boson peak region, e.g. >100cm-1, might has been a major contribution.

A systematic analytical study of the relationship between Boson peak and the composition or structure, however, requires a glass family with gradual systematic structural change. A binary glass family with one component percentage increases gradually and the other component decreases gradually would be a good glass system for this study. This leads to the making of the binary phosphate glasses and the study of relationship between Boson peak and medium range disorder.

4.7.2. Depolarization ratio curves in the Boson Peak Region

For the same material, the Boson peak shape of polarized and depolarized Raman spectra are almost the same. As a result, the depolarization ratio, the ratio of intensities of depolarized Raman spectra over polarized Raman spectra, should be a constant. The depolarization ratio is supposed to be at its minimum when the vibrations are symmetric, because when the vibration is symmetric, the scattering tends to be symmetric and the possibility for the incoming light to change polarization is very small. So the depolarization curves further confirmed the accuracy of the assignments of the two peaks.

It was found that the vh and vv spectra have the same reduced Raman intensity profile in the Boson peak region (30-100cm^{-1}) which tells us that the depolarization ratio should be a constant in the Boson peak region.

As stated in this Chapter, from Raman spectra alone, it is not possible to obtain directly the density of states, because the expression of the Raman intensity, IR, contains a frequency dependent unknown function.

Raman spectroscopy basically reveals the density of states information, but not all density of states are Raman active, only a certain portion of all the density of states are coupled into Raman scattering. There is a factor to quantify this coupling which is called the coupling coefficient.

Some evidence is provided that the boson peak and floppy modes share a common origin. In the particular case of periodic systems, we show how a boson peak occurs as a consequence of a reduction of constraints in an over-constrained lattice, in contrast to floppy modes, which occur for a reduction of constraints in a flexible or isostatic lattice. In fact, the present approach allows us to follow the transformation of the boson peak into a floppy mode when a system goes from rigid to flexible.

For over-constrained lattices, it was found that the boson peak frequency depends on the square root of the coordination of the lattice, and is at most 0.3 of the Debye frequency, a value close to the observed experimental ratio of 0.1.

From the above we can conclude the following.

The molecular structure of amorphous selenium differs from that of the majority of inorganic glasses on a scale of medium-range order. Apparently, Se chains form a structure similar to the structure of linear polymers on the scale ~1 nm.

Depending on the irradiation energy density, two qualitatively different regions are observed. Below the energy density threshold, Eth, only small changes in the local structure of the system can be detected. Above Eth, the changes were attributed to crystallization transformation. In addition, we have detected the successive phases in such a transition which is a threshold phenomenon.

It has been shown that Raman scattering spectra of amorphous AsxSe1-x alloys change non-monotonically with composition in the region of bond stretching modes. Certain extrema in various physical properties exist at composition range 6-12 at % As. The presence of this topological threshold is established by direct evidence, such as peculiarities in the compositional dependence of the Raman vibration modes of glasses. These peculiarities are caused by the transition from a chain-ring-like structure to chain-like structure with increasing degree of cross-linking.

Based on Raman scattering studies, we have shown how the structure transforms chronologically in amorphous AsxSe1-x recording media. Laser-

induced changes at room temperature involve two phenomena essentially different in their origin: transient reversible changes (photo darkening) and irreversible changes (photo crystallization) with gross structural reorganization. For high values of energy density, the Raman spectrum has pronounced crystallization-related changes.

Our explanation are based on the assumption that the radiation pumps the material from an amorphous state towards the crystalline state through the formation of small clusters, which coalesce to form large clusters attaining micro-crystallite size at high energy density levels.

In our opinion, the very low-frequency region of the Raman scattering could be an important source of information on the structure of disordered solids on the scale ~ 10-100 Å. It should be stressed on that the above method is efficient in distinguishing of micro-inhomogeneities.

References

1. S. O. Kasap, J. B. Frey, G. Belev, O. Tousignant, H. Mani, L. Laperriere, A. Reznik, J. A. Rowlands, Phys. Status Solidi B 246, 1794 (2009).

2. M. Popescu, J. Non-Cryst. Solids 352, 887 (2006).

3. A. Madan, M. P. Shaw, The Physics and Applications of Amorphous Semiconductors, Academic Press, Boston, MA, 1988.

4.;A. Feltz, Amorphous Inorganic Materials and Glasses, VCH, Weinheim, Germany, 1993.

5. V. I. Mikla, V. V. Mikla, J. Mater. Sci.:Mater. Electron 20, 1095 (2009).

6. V. I. Mikla, V. V. Mikla, J. Optoelectron. Adv. Mater. 10(1), 131 (2008).

7. V. I. Mikla, V. V. Mikla, Optoelectron. Adv. Mater. – Rapid Comm. 1(6), 272 (2007).

8. S. O. Kasap, in Handbook of Imaging Materials, edited by A. S. Diamond and D. S. Weiss, Marcel Dekker, Inc., New York, Second Edition, and references therein, p. 329, 2002.

9. K.Tanaka, in Encyclopedia of Materials, Elsevier Science Ltd., p. 1123,

2001.
10. K. Shimakawa, Advances in Physics 44, 474 (1995).
11. S. O. Kasap, J. A. Rowlands, J. Mater. Sci. Mater. Electron. 11, 179 (2000).
12. Z. Borisova, Glassy Semiconductors, Plenum Press, New York, 1981.
13. N. F. Mott, E. A. Davis, Electronic Processes in Non-Crystalline Materials, Oxford University Press, Oxford, Second Edition, 1979.
14. K. Hulls, P. W. Mc Millan, J. Non-Cryst. Solids 15, 357 (1974).
15. J. Schottmiller, M. Tabak, G. Lucovsky, A. Ward, J. Non-Cryst. Solids 4, 80 (1970).
16. A. E. Owen, A. P. Firth, P. J. S. Ewen, Philos. Mag. B 52, 347 (1985).
17. A. E. Owen, W. E. Spear, Phys. Chem. Glasses 17, 174 (1976).
18. V. I. Mikla, D. G. Semak, A. V. Mateleshko, A. R. Levkulich, Sov. Phys. Semicond. 21, 266 (1987).
19. V. I. Mikla, D. G. Semak, A. V. Mateleshko, A. R. Levkulich, Sov. Phys. Semicond. 23, 80 (1989).
20. V. I. Mikla, J. Phys.: Condens. Matter 9, 9209 (1997).
21. K. Tanaka, Rev. Solid State Sci. 2-3, 644 (1990).
22. J. Dresner, G. B.Strinfellow, J. Phys. Chem. Solids 29, 303 (1968).
23. J. P. De Neufville, in Optical Properties of Solids – New Developments, edited by D. O. Seraphin, North-Holand, Amsterdam, p. 437, 1975.
24. H. Fritzsche, in Insulating and Semiconducting Glasses edited by P. Boolchand, World Scientific, Singapore, Ch. 10, 2000.
25. V. I. Mikla, I. P. Mikhalko, J. Non-Crystall. Solids 180, 236 (1995).
26. M. Chomat, D. Lezal, J. Gregore, I. Srb, J. Non-Crystall. Solids 20, 427 (1976).
27. V. I. Mikla, J. Phys.: Condens. Matter 9, 9209 (1997).
28. V. P. Zakharov, V. S. Gerasimenko, Structural Peculiarities of Semiconductors in Amorphous State, Naukova Dumka, Kiev, 1984.
29. F. L. Galeneer, J. Non-Crystall. Solids 123, 182 (1990).
30. M. Cardona, Light Scattering in Solids, Springer-Verlag, Berlin, 1975.

31. R. J. Nemanich, G. A. Connell, T. M. Hayes, R. A. Street, Phys. Rev. B 18, 6900 (1978).
32. O. V. Luksha, V. I. Mikla, V. P. Ivanitsky, A. V.Mateleshko, D. G. Semak, J. Non-Crystall. Solids 144, 253 (1992).
33. L. Cervinka, Czech. J. Phys. B 25, 1193 (1985).
34. S. R. Elliott, J. Non-Crystall. Solids 106, 26 (1988).
35. J. S. Lannin, Phys. Today 41, 28 (1988).
36. A. J. Leadbetter, A. J. Apling, 21, 47 (1976).
37. A. C. Wright, R. N. Sinclair, A. J. Leadbetter, J. Non-Crystall. Solids 71, 295 (1985).
38. M. F. Daniel, A. J. Leadbetter, A. C. Wright, R. N. Sinclair, J. Non-Crystall. Solids 23, 271 (1979).
39. A. A. Baganich, V. I. Mikla, D. G. Semak, A. P. Sokolov, Phys. Stat. Sol. (b) 166, 297 (1991).
40. M. Gorman, S. A. Solin, Solid State Commun. 18, 1401 (1976).
41. M. H. Brodsky, M. Cardona, J. Non-Crystall. Solids 31, 81 (1978).
42. P. J. Carroll, J. S. Lannin, Solid State Commun. 40, 81 (1981).
43. P. J. Carroll, J. S. Lannin, J. Non-Crystall. Solids 35-36, 1277 (1980).
44. T. Mori, S. Onari, T. Arai, J. Appl. Phys. 19, 1027 (1980).
45. S. Onari, K. Matsuishi, T. Arai, J. Non-Crystall. Solids 74, 57 (1985).
46. J. C. Phillips, J. Non-Crystall. Solids 43, 37 (1981).
47. M. F. Thorpe, J. Non-Crystall. Solids 57, 355 (1983).
48. K. Tanaka, Phys.Rev. B 39, 1270 (1989).
49. T. Wagner, S. O. Kasap, Phil.Mag. B 74, 667 (1996).
50. Z. Borisova, Glassy Semiconductors, Plenum Press, New York, 1981.
51. P. Boolchand, M. Jin, D. I. Novita, S. Chakravarty, J. Raman Spectroscopy 38, 660 (2007).
52. E. Ahn, G. A. Williams, P. C. Taylor, Phys.Rev. B 74, 174206 (2006).
53. K. Tanaka, N. Odajima, Solid State Commun. 43, 961 (1982).
54. R. T. Phillips, J. Non-Crystall. Solids 70, 359 (1985).
55. Powder Diffraction File, ASTM card, ed. L. G. Berry, Joint Committie

on Powder Diffraction Standard, Philadelphia, 1974.
56.] R. Zallen, M. L. Slade, A. T. Ward, Phys. Rev. B3, 4257 (1971).
57. M. Abkowitz, R. C. Enck, Phys. Rev. B27, 7402 (1983).
58. V. I. Mikla, Dr.Sci. Thesis, Institute of Solid State Physics, Academy of Sciences, Kiev, 1998.
59. J. C. Phillips, Solid State Phys. 10, 165 (1982).
60. V. I. Mikla, D. G. Semak, A. V. Mateleshko, A. A. Baganich, Phys. Stat. Solidi (a) 117, 241 (1990).
61. V. K. Malinovsky, V. P. Sokolov, Solid State Commun. 57, 757 (1986).
62. A. J. Martin, W. Brenig, Phys. Status Solidi B 63, 163 (1974).
63. R. J. Nemanich, Phys. Rev. B 16, 1977.
64. H. Kawamura, F. Fukumasu, Y. Hamada, Solid State Commun. 43, 229 (1982).
65. G. Lucovsky, F. L. Galeneer, J. Non-Crystall. Solids 35-36, 1209 (1980).
66. J. Jakle, in: Amorphous Solids: Low-Temperature Properties, Ed. W. A. Phillips, (Springer-Verlag, Berlin, p. 135, 1981.
67. V. K. Malinovsky, V. N. Novikov, V. P. Sokolov, Phys. I Khim. Stekla, 15, 331 (1989).
68. G. Lucovsky, J. Non-Crystall. Solids 97-98, 155 (1987).
69. H. Richter, Z. P. Wang, L. Ley, Solid State Commun. 39, 625 (1981).
70. V. A. Bagrynskii, V. K. Malinovsky, V. N. Novikov, L. M. Puschaeva, A. P. Sokolov, Fiz. Tverd. Tela 30, 2360 (1988).
71. R. Shuker, R.Gammon, Phys. Rev. Lett. 25, 222 (1975).
72. A. J. Martin, W. Brenig, Phys. Status Solidi (b) 64, 163 (1974).
73. E. Duval, A. Boukenter, B. Champagnon, Phys. Rev. Lett. 56, 56 (1986).
74. H. Lamb, Proc. London Mat. Soc. 13, 187 (1982).
75. A. Tamura, K. Higeta, T. Ichinokawa, J. Phys. C 15, 4957 (1982).
76. A. Tamura, T. Ichinokawa, J. Phys. C 16, 4779 (1983).
77. V. K. Malinovsky, V. N. Novikov, A. P. Sokolov, Solid State Commun. 67, 725 (1988).
78. J. Jackle, Amorphous Solids: Low-Temperature Properties, Springer,

New York, 1981.

79. K. E. Lipinska-Kalita, G. Mariotto, J. Non-Crystalline Solids 128, 285 (1991).

80. R.J. Nemanich, Phys. Rev. B 16 (1977) 1655.

81. H. Kawamura, K. Fukumasu, Y. Hamada, Solid State Commun. 43(1982) 229.

82. A. Boukenter, E. Duval, T. Achibat, J. Condens. Matter 2 (1990) 10227.

83. V.K. Malinovsky, A.P. Sokolov, Solid State Commun. 57 (1986) 757.

84.V.K. Malinovsky, V.N. Novikov, P.P. Parshin, A.P. Sokolov, M.G.Zemlyanov, Europhys. Lett. 11 (1990) 43.

85.A. Boukenter, B. Champagnon, E. Duval, J.L. Rousset, H.M. Rosenberg, Philos. Mag. B – Phys. Condens. Matter Statist. Mech.Electron. Opt. Magn. Prop. 59 (1989) 125.

86. R.Shuker, R.Gammon. Phys. Rev. Lett. 25 (1970) 222.

87. A,J.Martin, W.Brenig. Phys.Seatus Solidi B 64 163 (1974)

88. A.P.Sokolov, U.Buchenau, W.Steffen. Phys.Rev. B 52 (1995) R9815.

80. A.P.Sokolov, A.Kisliuk, D.Quttmann, E.Duval. Phys.Rev. B 48 (1993) 7692.

91. I.Hong, B.Begen, A.Kisliuk, C.Simioneco,, V.Novikov, A.P.Sokolov. Phys.Rev. B 78 (2008) 134201.

92. I.Hong, B.Begen, A.Kisliuk, V.Novikov, A.P.Sokolov.Phys.Rev. B81 (2010) 104207.

93. I.Hong, B.Begen, A.Kisliuk, S.Pawlus, M.Paluch, A.P.Sokolov. Phys.Rev.Lett. 102 (2009) 145502.

94. R.S.Krishnan. Proc. Indian Acad. Sci. A 37 (1953) 3778.

95. N.Yannapoulos, K.S.Andrikopoulos. Journal of Chemical Physics 121 (2004) 4747.

96. K.S.Andrikopoulos, D.Kristofilos, S,N.Yonnapoulos. J. Non-Cryst. Solids 352 (2006) 4594.

97. Reiner Zorn. Physics 4 (2011) 44.

98. A.I.Chumaov et all. Phys.Rev.Lett. 106 (2011) 225501.

99. V.I.Mikla. J. Phys.:Cond. Matter. 8 (1996) 429.

100. V.I.Mikla, V.V.Mikla. J. Mater. Sci.: Mater. in Electr.20 (2009) 1095.

101. A.A.Baganich, V.I.Mikla, D.G.Semak, A.P.Sokolov. Physica Status Solidi (b) 166 1991) 297.

102. V.I.Mikla, A.A.Baganich, A.P.Sokolov, A.P.Shebanin. Physica Status Solidi (b) 175 (1993) 1029.

103. W.Schirmacher. J.Phys.: Condens Matter 25 (2013) 495.

CHAPTER 5. Raman spectroscopy in medicine

In recent decade there has been a remarkable increase in the application of Raman spectroscopy to the field of medicine. This has come out of awareness that Raman, like IR spectroscopy, is a vibrational spectroscopic technique capable of providing details on the chemical composition, molecular structure, and molecular interactions in cells and tissues. Raman spectroscopy has recently been applied *ex vivo* and *in vivo* to address various biomedical issues such as the early detection of cancers, monitoring of the effect of various agents on the skin, determination of atherosclerotic plaque composition, and rapid identification of pathogenic microorganisms. As disease leads to changes in the molecular composition of affected tissues, these changes should be reflected in the spectra. Clearly, if the spectral changes are specific (inherent) for a particular disease state, they can be used as phenotypic markers or signs of the disease. Numerous studies presented in the literature demonstrate that differences can be observed between *ex vivo* Raman spectra of healthy and diseased tissues. The clear message of the majority of these studies (which are preferentially exploratory in nature) is that clinical diagnostic tools can be successfully developed from the Raman spectroscopic fingerprints of tissues.

Nowadays Raman spectroscopy becomes a potentially important clinical tool for real-time diagnosis of disease and *in situ* evaluation of living tissue. The purpose of this Chapter is to review the biological and physical basis of Raman spectroscopy of tissue, to assess the current status of the field and to explore future directions. The principles of Raman spectroscopy and the information it provides on molecular level are briefly explained. The authors try to present an overview of the evolution of Raman spectroscopic techniques in biology and medicine, from early investigations using visible laser excitation to present-day technology based on near-infrared laser excitation and charge-coupled device array detection. State-of-the-art Raman spectrometer systems both for research laboratory and clinical settings are described. Modern methods of multifunctional spectral analysis for

extracting diagnostic, chemical and morphological information are reviewed. Several in-depth applications are presented to illustrate the methods of collecting, processing and analyzing data. Various clinical applications of Raman spectroscopy, as well as some directions for future are discussed.

5.1. Introduction

Successive advances in biomedical technology have been driven by the need to provide objective, and quantitative diagnostic information. Novel biomedical applications of optical spectroscopy, such as fluorescence, reflectance and Raman scattering, can provide information about the composition of tissue at the molecular level. Among these techniques, Raman spectroscopy can provide the most detailed information about the chemical composition of the tissue under study. The progression of disease is accompanied by certain chemical change. In this context Raman spectroscopy can provide the physician with valuable information for diagnosing disease. Since light can be delivered and collected rapidly *via* optical fibers (these can be incorporated into catheters, endoscopes, cannulas and needles, to say about few), Raman spectroscopy can be performed *in vivo* in real time.

Diagnostic applications of Raman spectroscopy currently under investigation are widespread [1]. For example, Raman spectroscopy may be used to monitor blood analyzes noninvasively. Further, it may be used to perform minimally invasive, real-time, tissue diagnosis *in vivo*, in cases where biopsy cannot be performed readily, such as coronary artery disease and Alzheimer's disease, or where a high incidence of false positive screening tests leads to unnecessary biopsy procedures, as in a case of breast cancer. The purpose of this Chapter is to discuss the potential of Raman spectroscopy to provide real-time, objective, and at the same time quantitative diagnostic information *in vivo*.

There is no doubt that the early detection of cancers, monitoring of the effect of various agents on the skin, determination of atherosclerotic plaque composition, and rapid identification of pathogenic microorganisms is vitally important.

Taken from the viewpoint of clinicians and medical analysts, the potential of Raman spectroscopic techniques as new tools for biomedical applications is discussed here and a path for the clinical implementation of these techniques is proposed.

The Raman scattered light can be collected by a spectrometer and displayed as a "spectrum", i.e. intensity *versus* frequency change. Since each molecular species has its own unique set of molecular vibrations, the Raman spectrum of a particular species will consist of a series of peaks or "bands", each shifted by one of the vibrational frequencies characteristic of that molecule.

As an example, the Raman spectrum of cholesterol, a representative biological molecule, is shown in Fig. 5.1 [2]. The spectrum is a plot of the scattered light intensity *versus* its change in frequency, relative to that of the incident light. Raman frequency shifts are conventionally measured in wave numbers ([cm^{-1}]), a unit convenient for relating the change in vibrational energy of the scattering molecule to the change in frequency of the scattered light. One cm^{-1}equals 30 000 MHz; this is typically 10 000 times smaller than the frequency of the light itself. Each band of scattered light in the cholesterol Raman spectrum is characteristic of molecular vibrational motions, which, taken all together, are unique for cholesterol.

If a sample of biological tissue contains cholesterol, characteristic peaks (e.g., peak at 1440 cm^{-1} is due to the CH_2 and CH_3 deformation vibrations, and the peak at 1670 cm^{-1} is due to C=C stretching vibrations) will be present in its Raman spectrum. In other words, the molecular structure and composition of a material under study is encoded as a set of frequency shifts in the Raman scattered light. Thus, the Raman spectrum can provide a 'fingerprint' of a substance from which the molecular composition can be determined.

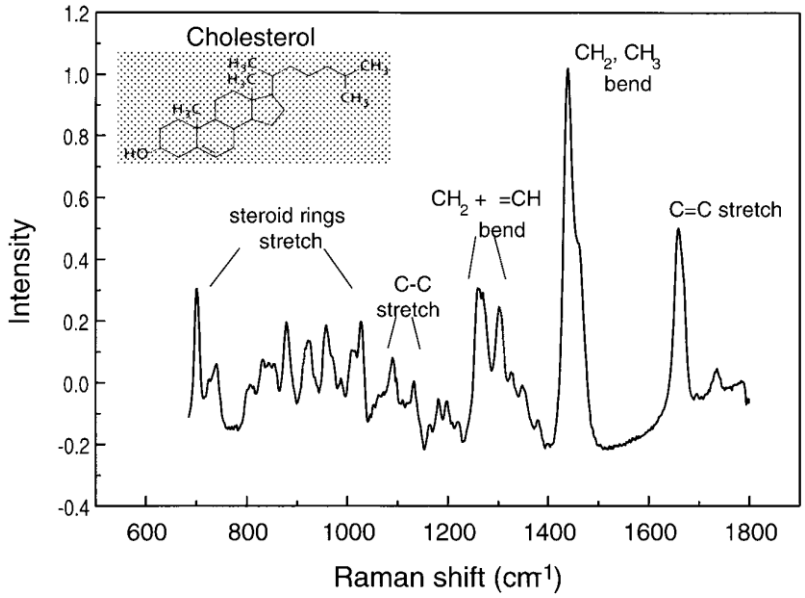

Fig. 5.1. Near-IR Raman spectrum of cholesterol. Shown are typical vibrational bands. The background has been removed by subtracting [2].

In Raman spectroscopy the incident light is often referred to as ‘excitation’ light, because it excites the molecules into vibrational motion. Ultraviolet, visible and infrared light can each be used for Raman excitation.

In general, Raman spectra of tissue consist of relatively narrow bands, typically 10–20 cm^{-1} in width, which exhibit the presence of many biochemical. The relative contributions of these biochemicals to the whole Raman spectrum are proportional to their relative abundance in the tissue. This is the basis for the quantitative nature of the information Raman spectroscopy can provide for diagnosis. The quantitative nature of Raman spectra, combined with the ability to provide unique “signs” of the biochemical present in tissue, demonstrate the potential of Raman spectroscopy to provide objective, quantitative diagnostic information for tissue analysis.

Raman spectroscopy had been widely used for chemical and molecular analysis for many years [3]. At the same time, its application to biomedical problems is relatively recent. Raman studies of biological tissue have been facilitated over the past 20 years by advanced technology, particularly in the areas of lasers and detectors. However, the true success of these studies in providing insight into the molecular basis of disease and showing the potential for medical

diagnostic applications has relied on advanced methods of analyzing tissue Raman spectra. In order to exploit the full potential of Raman spectroscopy, methods of analysis that employ the full information content of the Raman spectrum (not the prominent peaks only) must be used. The problem of extracting the full, diagnostically useful information that tissue Raman spectra contain, can be divided on three distinct levels: statistical, chemical and morphological:

(a) *Statistical analysis:* Up to now, much of the work in this field has relied largely on empirical methods of analysis, such as correlating tissue type with prominent spectral bands. However, mathematical methods such as principal component analysis can be used to characterize the full range of spectral variations. The principal components can then be fitted to the observed Raman spectral contours. Correlating the fit coefficients with tissue type can be used to classify tissue by diagnostic category. Additionally, features of the principal components can be used as a guide in identifying key biochemical or morphological constituents of the tissue or disease under study;

(b) *Chemical analysis:* Raman spectroscopy can provide information about the chemical composition of tissue. A Raman spectrum can be modeled as a superposition of the spectra of its chemical constituents, thereby providing quantitative chemical information. Chemical information is of importance: the onset of disease is accompanied by biochemical changes, and Raman spectroscopy can be an excellent method for detecting biochemical changes (even if they are vanishingly small) that may occur in either the cellular or extracellular compartments of tissue. At present, few techniques are capable of providing detailed *in vivo* biochemical analysis of tissues. Such techniques have an enormous potential, both in diagnosing disease and in understanding its origins and evolution;

(c) *Morphological analysis:* Quantitative methods to extract information regarding microscopic constituents present in a tissue sample, i.e. the morphological structures, are also possible. Pathologists make a tissue diagnosis by assessing the presence, absence or relative abundance of such constituents, which

include various types of cells, fibers, mineral deposits etc. Raman spectroscopy has the potential to provide such morphological information without tissue removal, in real time and in a quantitative and objective manner. Further development of this interesting area needed.

5.2. Clinical applications of Raman spectroscopy

5.2.1. Clinical Raman system

Laboratory Raman system for blood analytes (Fig. 5.2) has been designed to study how best to optimize delivery and collection geometries in liquid samples of varying turbidity - whole blood, blood serum, interstitial fluids and saline solution [3]. For this, the delivery and collection geometries can be precisely varied. When used with multivariate techniques, physiological concentrations of analytes (e.g. glucose) at sub-millimolar levels can be measured. Noting that water is 55 molar, this represents a Raman concentration measurement sensitivity of 10 ppm, illustrating the potential sensitivity of Raman spectroscopy for precise, quantitative measurements. The system uses a tunable diode laser operating at 830 nm and 500 mW power, a holographic imaging spectrograph, liquid nitrogen-cooled deep depletion CCD detector, and special collection optics.

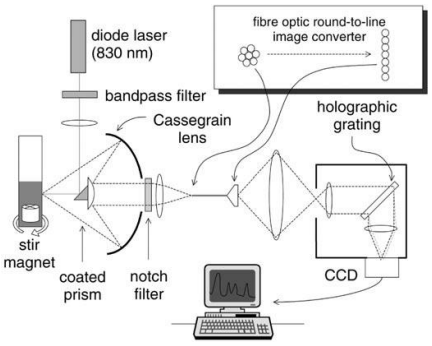

Fig.5.2. Schematic diagram of Raman spectroscopic system for the analysis of blood analytes. The reflective objective has high collection efficiency. Inset: The collection efficiency and high throughput are maintained, while preserving resolution, by configuring the *f* -number matched fiber bundle into a linear array at the spectrograph entrance. This linear array of fibers forms the spectroscopic slit that determines resolution [3].

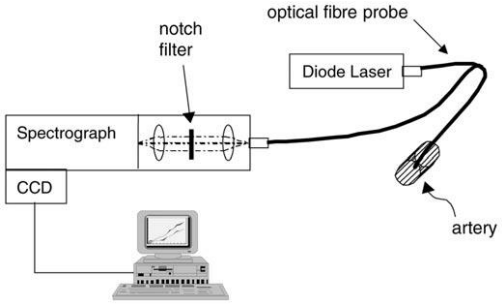

Fig. 5.3. Clinical Raman system designed for rapid data acquisition, portability, and safety in a hospital environment [3].

5.2.2. Atherosclerotic Plaques, Breast Cancer, Lung Cancer, and Skin Cancer

The characterization of atherosclerotic plaques is an example of an application in which the feasibility of Raman spectroscopy to obtain certain information about tissue composition has been demonstrated [1,2,4]. Information extracted from Raman data essentially improves correct clinical decision.

A detailed *ex vivo* analysis of the molecular composition of a plaque can be obtained by Raman spectroscopy [1,5]. For example, it is not certain whether the chemical composition of a plaque has an affect on the occurrence of re-stenosis after interventions such as (balloon) angioplasty or stenting and if a particular drug regime can be particularized to find and promote therapeutic efficiency. Hence, knowledge of the plaque chemical composition might play a role in the choice of a certain therapy.

Further, in recent years much of the debate about the occurrence of heart attacks has revolved around the questions of whether all plaques are putting a patient at risk and whether a distinction should be made between different types of

plaques. For example, “vulnerable” plaques (composed of lipid pools separated from the bloodstream by a fibrous cap) are responsible for most, often fatal, heart attacks.

The rupturing of the fibrous cap exposes the blood to the highly thrombogenic contents of the lipid pool, resulting in a blood clot that occludes the artery. At the other end of the spectrum are the “stable” plaques that may be highly calcified and often occlude a significant percentage of the blood. These latter plaques cause fatal heart attacks less frequently because they give distinct signs in the form of symptoms such as chest pain during physical exercise and they do not cause formation of blood clots that can suddenly occlude a blood vessel.

Figs. 5.4–5.8 illustrate the potential of Raman spectroscopy in diagnosis of cancer in breast, lung, and skin tissues.

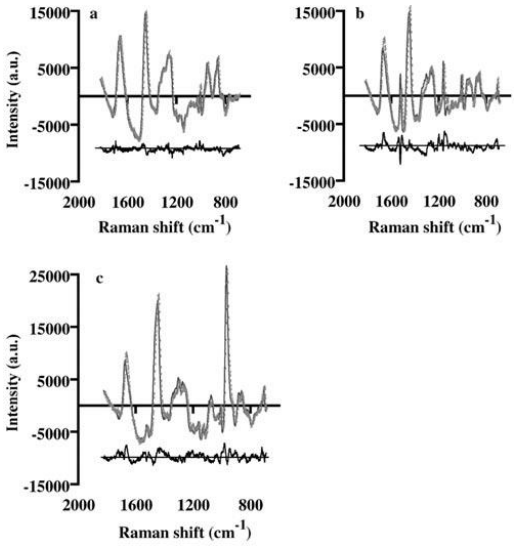

Fig. 5.4. Chemical model fits (curve) and spectral data (dots) for coronary arteries in various stages of atherosclerosis: (*a*) non-atherosclerotic tissue, (*b*) non-calcified atheromatous plaque and (*c*) calcified plaque. The residuals are plotted below the fits [5].

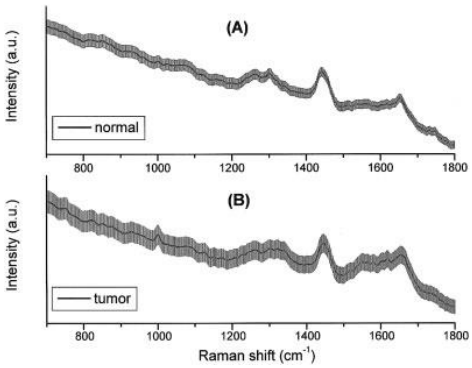

Fig. 5.5. Mean Raman spectra (solid line) 1 SEM (gray area) were obtained from single representative samples of normal tissue *(a)* and tumor *(b)* (SCC) by performing multiple measurements (n = 10) for each sample at different tissue orientations (epithelial and stromal sides of the tissue). All spectra were acquired in 5 sec with 785 nm excitation and corrected for the spectral response of the system [5].

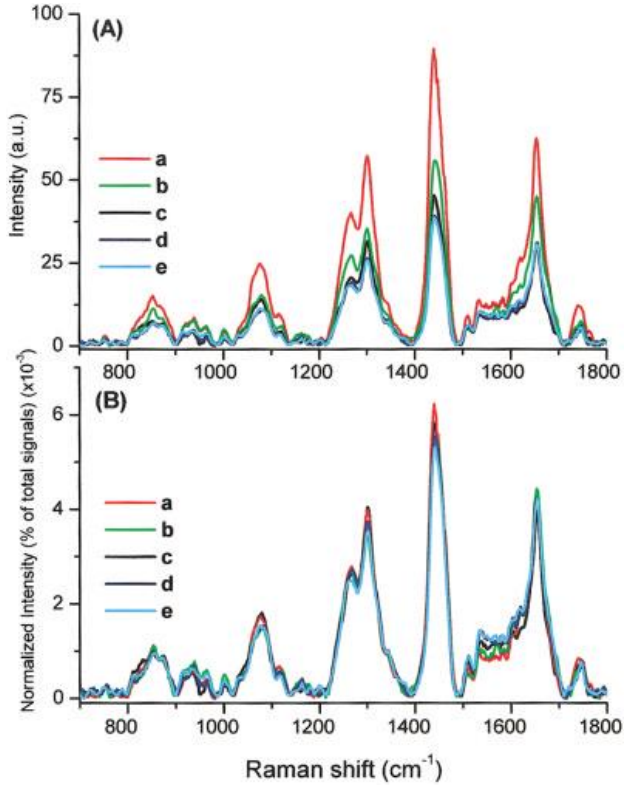

Fig. 5.6. Effect of specimen sizes on Raman spectra of bronchial tissues. Before normalization for sample sizes: a) 8 × 8 × 1.5 mm; b) 5 × 5 × 1.5 mm; c) 4 × 4 × 1.5 mm; d) 3 × 3 × 1.5 mm; e) 1 × 1 × 1.5 mm. The larger specimen has a stronger Raman signal. *(b)* After normalization, all Raman spectra for different specimen sizes display almost identical patterns with intensity variations of 10–20% for major Raman peaks [5].

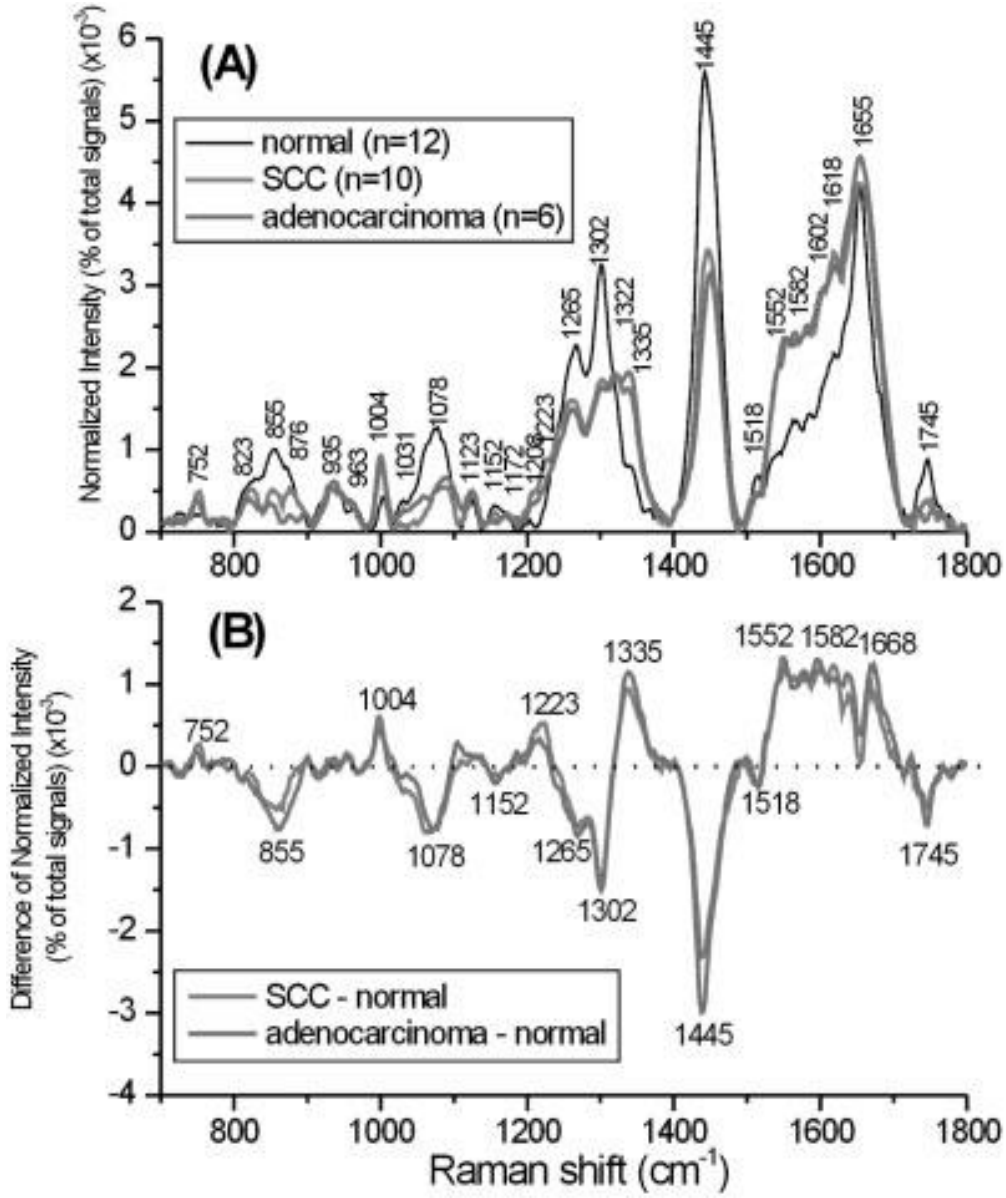

Fig. 5.7. The mean Raman spectra of normal bronchial tissue (*n* = 12) and malignant adenocarcinoma (*n* = 6) and SCC (*n* = 10) bronchial tissue samples. Each spectrum was normalized to the integrated area under the curve to correct for variations in absolute spectral intensity. *(b)* Difference spectra were calculated from the mean spectra: SCC minus normal and adenocarcinoma minus normal [6].

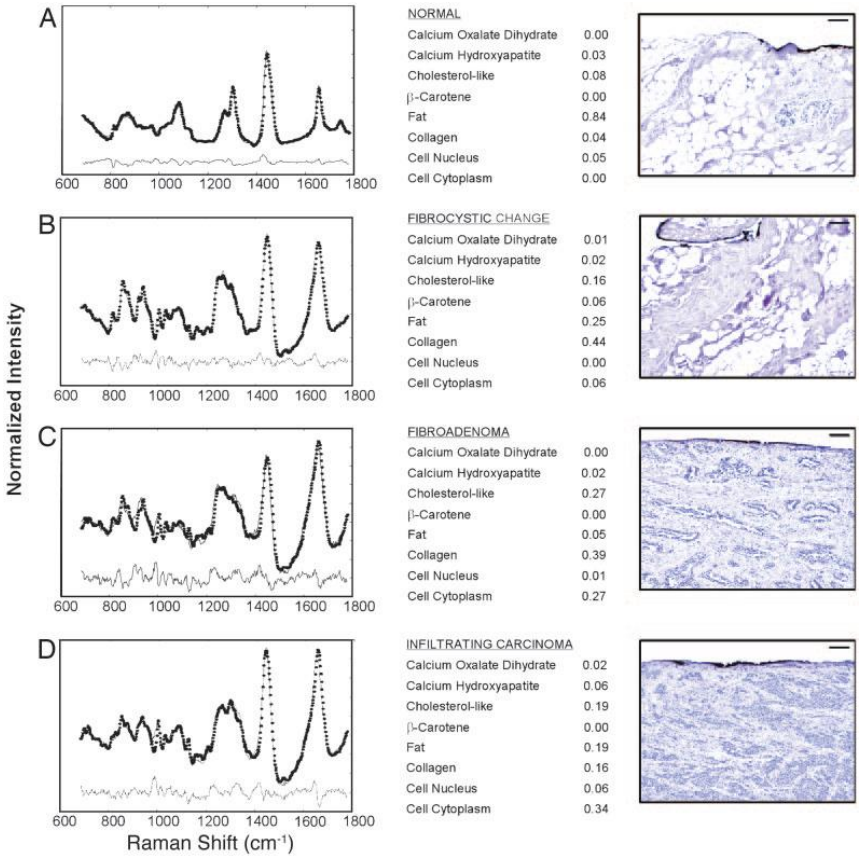

Fig. 5.8. Raman spectra: (A) normal breast tissue, (B) fibrocystic change, (C) fibroadenoma, and (D) infiltrating carcinoma [6].

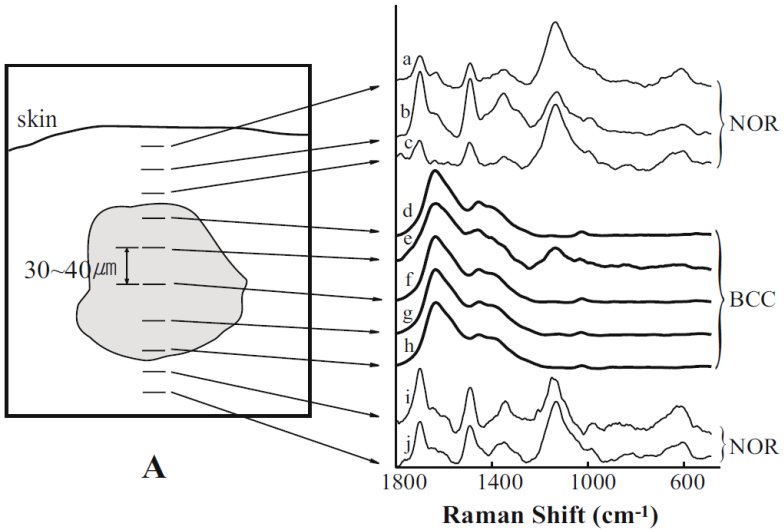

Fig. 5.9. Confocal Raman profiles of skin tissue with an interval of 30–40 μm [6].

References

1. International Reviews in Physical Chemistry 7 (1988).
2. E.B.Hanlon et al, Phys. Med. Biol. **45** (2000) R1–R59.
3. Annika M.K. Enejder, et al. Optics Letters 27, iss.22 (2002) 4.
4. Z.Huang et al, Int. J. Cancer: **107,** 1047–1052 (2003).
5. A.Downs, Sensors, 10, (**2010)** 1871-1889.
6. L.P.Choo-Smith et al. Biopolymers (Biospectroscopy) 67 (2002) 1.

CHAPTER 6. Some Novel Results of Physical Aging Studies in Glassy Selenium

6.1. Introduction

The physical aging of glass was first documented by J.P. Joule as early as 1884 [1]. To date, the kinetics of changes in the physicochemical properties of many silicate glasses has been well studied on timescales from several hours to several decades [2]. At the same time, little is known about the physical aging kinetics of chalcogenide glasses (ChGs), which became the subject of intense studies only after the discovery in the 1950s of their semiconducting behavior [3]. There are still contradictory data on both the possibility of aging of ChGs and the timescale of this process [4].

Selenium is a nutritiously essential element. People used selenium for healthy joints, heart, and eyes [5]. It plays a crucial role in DNA system, the immune system and the reproductive system [5]. It also helps fights cancer and other diseases [5]. Over than internal human uses selenium it also used in manufacturing. It is used to color and decolorized glasses. Glassy selenium is one of the potential productive materials of the materials science [6]. Recently, Selenium has been found useful for rechargeable batteries and solar cell applications too [7, 8]. Glass is often made starting from the liquid phase when the liquid could be cooled sufficiently quickly (quenched) so that crystallization could be bypassed, then the disordered structure characteristic of a liquid could be frozen-in, and a glassy solid which is spatially homogeneous, but without any long-range lattice order (amorphous) would result. Hence a glass can be defined as a solid, brittle material that has an amorphous, liquid-like structure without obvious fluidity. The short-range order for the glassy state of a material is often very similar to that of the crystalline state, that is, it has a similar average nearest-neighbor distance and coordination number but, unlike the crystal, the glass has no long-range order. Chalcogenide glassy semiconductors (ChGs) belong to the non-crystalline materials with the sophisticated structure which is not structurally in equilibrium state [9, 10]. The processes of structural relaxation lead to a change

(sometimes significant) in physical properties, including mechanicaland dielectric. Selenium, the simplest representative of amorphous chalcogenides is known to consist of a chain and ring fragments [11]. Aging of pure Se glass is intrinsically tied to the flexibility of the chain network.

Physical aging (PhA) of soft materials is still an important problem in different research areas of science for the thorough study [12-14]. The results of PhA effects are still highly disputable even for such canonical glass-former as floppy selenium and glassy alloys of high selenium content [11, 15-18]. It represents the changes in physical-chemical properties of the material (during natural storage) caused by its tending towards more thermodynamically equilibrium state.

Physical aging, in general, is understood as the overall tendency towards thermodynamic equilibrium. It depends on two factors:

(i) glass composition (types and content of chemical elements, glass-forming units and groups, etc.);

(ii) (ii) the glass pre-history (cooling rate; additional thermal treatment near a glass transition; the duration, temperature, moisture and other environment conditions of time exposure from as-prepared state; etc).

Glasses covered a wide spectrum of materials which range from those with simple structures such as the metallic and chalcogenide glasses to more structurally complex organic materials and polymers. A class of these materials is the chalcogenide glasses which include selenium, tellurium, and sulfur and their compounds or alloys.

Result of physical aging causes the time-instability in the exploitation of glass-based devices like optical and electrical memory systems; telecommunication and energy transfer; the industrial sensors; optical waveguide sensing and thermal imaging. Thus, the studies of PhA effects are significant from both scientific and application points of view [12-14]. The key objective of the current work is to depict the influence of the physical aging in aged and

asquenched glassy selenium in terms of the structural changes caused by aging. For this purpose, we have used ten years old g-Se sample.

When a glass having non-equilibrium state evolves towards the equilibrium, the change in its structure causes the enhancement in the medium-range ordering with time. However, when a fresh sample of non-crystalline chalcogenide glass is kept at a temperature below the glass transition, it is unclear whether noteworthy and measurable changes can occur on experimentally accessible time scales. Under such situations of aging, the structural relaxations on the level of entire long polymeric Se chains are not expected. Rather, a local motion at the level of chain segments is feasible. This raises the question, whether such segmental relaxations have an impact on the kinetic properties of glassy Se observed at a macroscopic level, for example, the enhancement in the rate of crystallization or the reduction in thermal stability. In addition, the long-term stability (slow aging behaviour) may be enhanced through the identification and implementation of long-lived meta-stable non-equilibrium structures. Thus, such studies are very important for increasing the durability of the solid state devices made from such materials.

6.2. Experimental techniques and theoretical basis

Glassy selenium was obtained by conventional melt-quenching technology. The details of this technique may be found in [15]. Ten years "aged" specimen of g-Se was chosen to study the aging effect with respect to a fresh sample of g-Se. For the present studies, different techniques [like Differential Scanning Calorimetry (DSC), X-Ray Diffraction (XRD), Scanning Electron Microscopy (SEM), Transmission Electron Microscopy (TEM), Raman spectroscopy] have been employed.

PhA changes in physical-chemical properties of the material (during natural storage) caused by its tending towards more thermodynamically equilibrium state. Glass is genetically always in the meta-stable state owing to its origin. Physical aging, in general, is understood as the overall tendency towards thermodynamic equilibrium. It depends on two factors:

(i) glass composition (types and content of chemical elements, glass-forming units and groups, etc.);

(ii) (ii) the glass pre-history (cooling rate; additional thermal treatment near a glass transition; the duration, temperature, moisture and other environment conditions of time exposure from asprepared state; etc).

The concept of PhA as a permanent feature of glass is shown in Fig. 6.1 which is the plot of enthalpy versus temperature for a typical ChG.

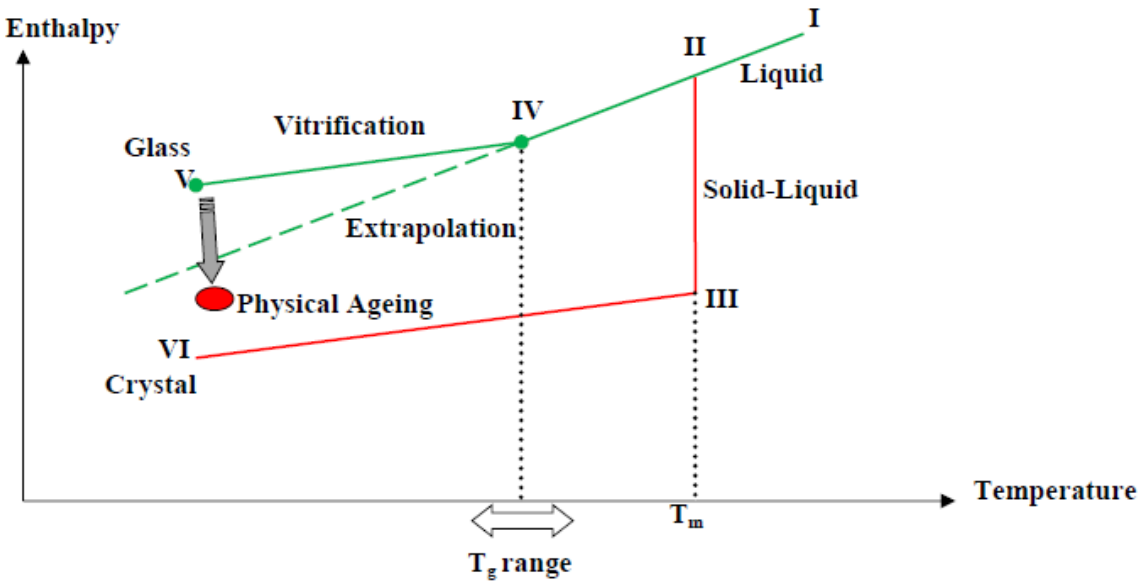

Fig. 6.1. Physical aging as a permanent feature of glass.

6.3. Results and discussion

There are various methodological aspects of PhA in glasses that can be studied by employing either Differential scanning calorimetric (DSC) or Differential Thermal Analysis (DTA) technique [19-21].

Result of the structural relaxation is revealed by DSC on the as-quenched sample and the sample aged for more than ten years of glassy selenium. The structural relaxation phenomenon is clearly visible as well-defined endothermic peaks are observed in DSC scans of both samples (see Fig 6.2).

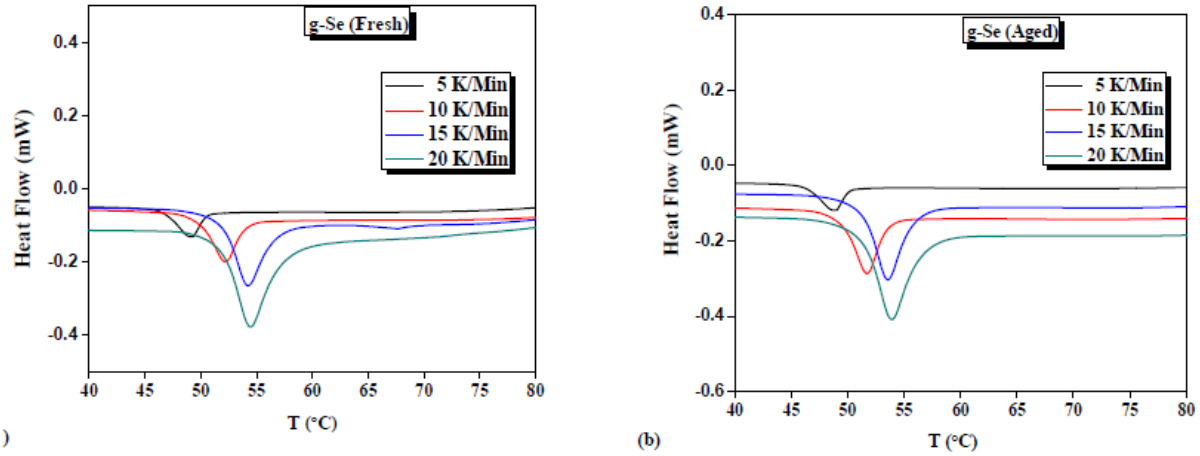

Fig. 6.2. DSC scans of (a) fresh g-Se glass and (b) aged g-Se at different heating rates.

To understand the effect of aging on the structural relaxation of glassy Se, we have determined the glass transition temperature *Tg* using the DSC scans at four different heating rates (β = 5, 10, 15, 20 K /min). The values of glass transition temperature *Tg* are given in Table 1 for both aged and as-quenched samples of Se glass. This table clearly reveals that the glass transition temperature is decreased slightly in the aged sample; thereby indicating that the thermally activated structural relaxation starts at slightly less glass transition temperature in aged g-Se as compared to fresh g-Se.

The XRD patterns confirm the amorphous origin of aged and as-quenched samples (see Fig. 6.3). From the comparison of both XRD patterns, one can see that the only one significant peak appeares in as-quenched Se glass. This peak in fresh glass may appears as the consequence of medium-range ordering at some sites in the glass network of as-quenched Selenium [22-25]. On the other hand, several noticeable peaks are observed in the XRD pattern of the aged sample.

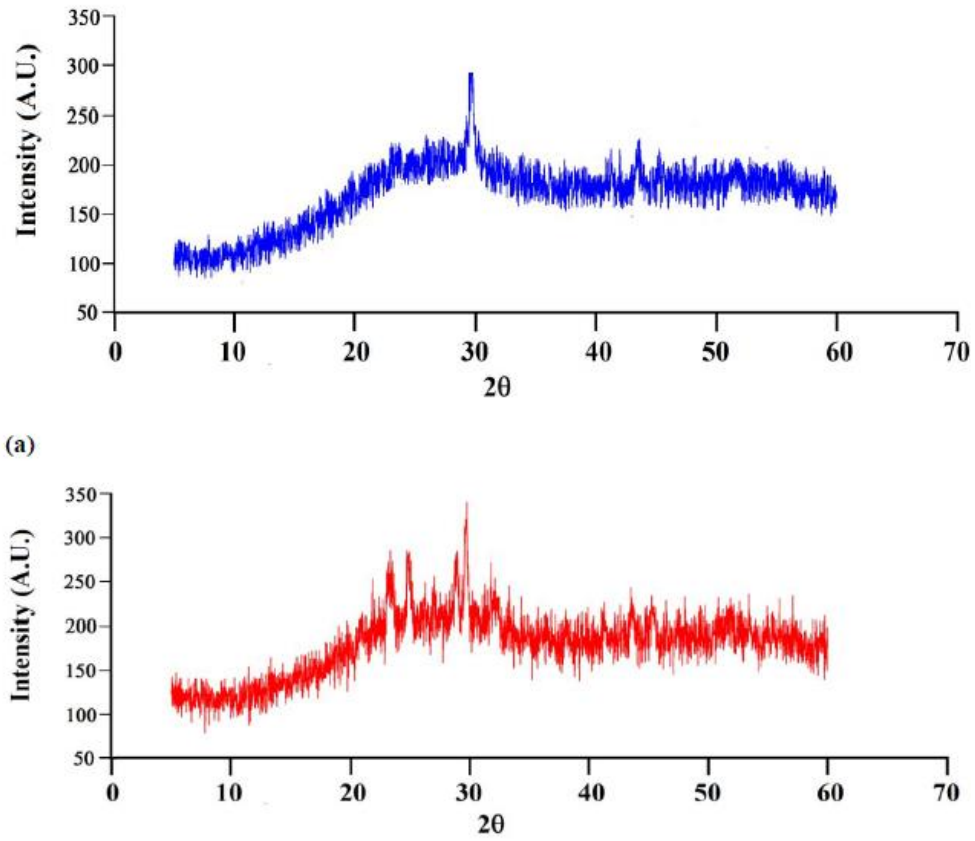

Fig. 6.3. XRD patterns of (a) as-quenched sample and (b) aged sample.

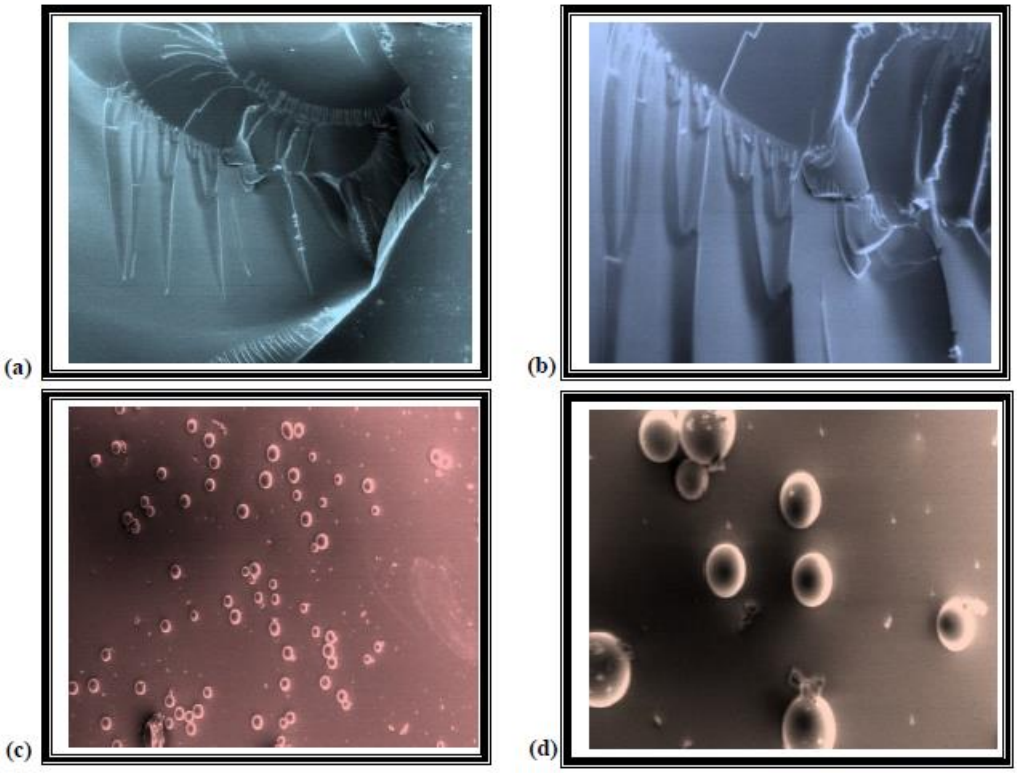

Fig.6.4.Micro-fracture patterns of (a), (b) as-quenched g-Se and (c), (d) aged g-Se.

Fig. 6.4 shows the images of the micro-fracture pattern of aged and as-quenched g-selenium that were obtained by an optical microscope. The images of as-quenched in Fig. 6.4(a) and 6.4(b) clearly shows that there is no signature of any kind of crystal growth. However, the appearance of crystallites having spherical geometry can be easily noticed in the images of the aged sample in Fig 6.4(c) and 4(d). Thus, the results of micrographs shown in Fig. 6.4 also support the observations of XRD results.

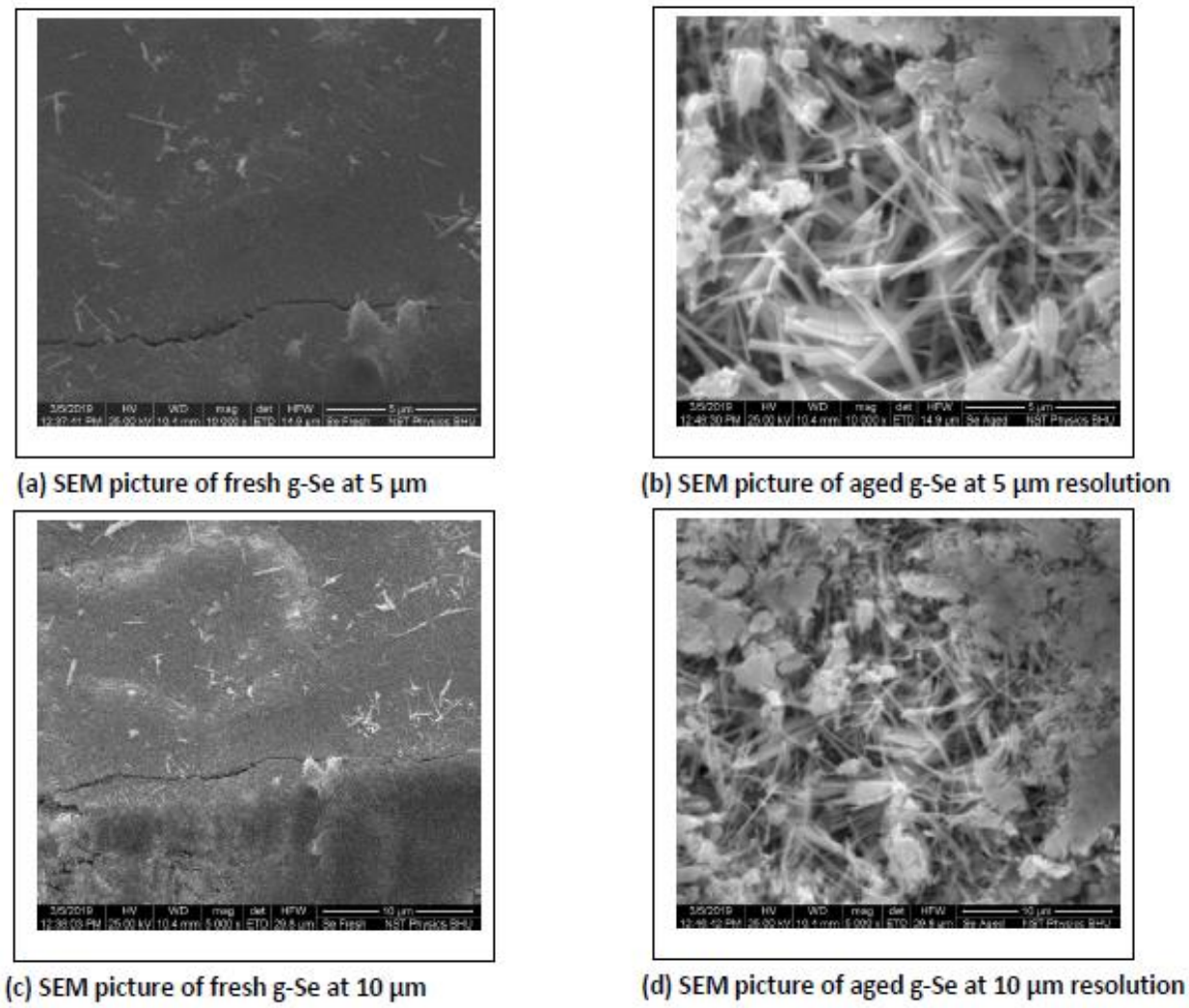

Fig. 6.5. SEM images of as-quenched g-Se and aged g-Se.

Fig. 6.5 shows the SEM images of aged and as-quenched g-Se. The images shown in Fig. 6.5(a) and 6.5(c) reveal that the almost a dark and the smooth region

is observed in the as-quenched sample which is again a sign of glass-matrix. On the other hand, the appearance of nanowires embedded in glass matrix is observed in the aged sample as a signature of its nano-structuring [see the image shown in Fig. 6.5(b) and 6.5(d). The TEM images shown in Fig. 6.6(a) and 6.6(c) also indicate the absence of any distinguishable or perceptible structure in fresh g-Se, while an impression of crystalline at nano-scale is observed in the TEM images shown in Fig. 6.6(b) and 6.6(d) for aged g-Se. Similarly, the electron diffraction patterns of as-quenched g-Se possess the indistinct rings, while clearly noticeable reflections are observed in aged g-Se (see Fig. 6.7).

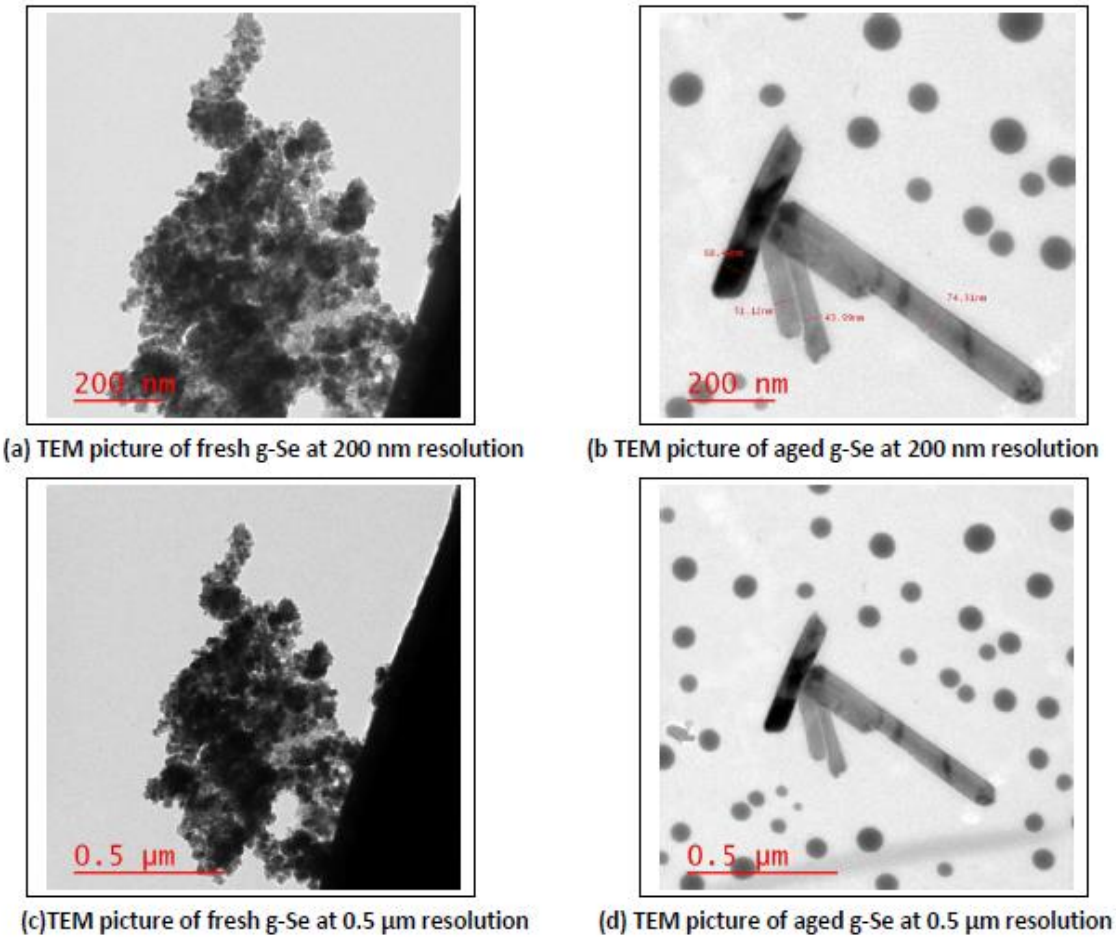

(a) TEM picture of fresh g-Se at 200 nm resolution

(b TEM picture of aged g-Se at 200 nm resolution

(c)TEM picture of fresh g-Se at 0.5 µm resolution

(d) TEM picture of aged g-Se at 0.5 µm resolution

Fig. 6.6. TEM images of as-quenched g-Se and aged g-Se.

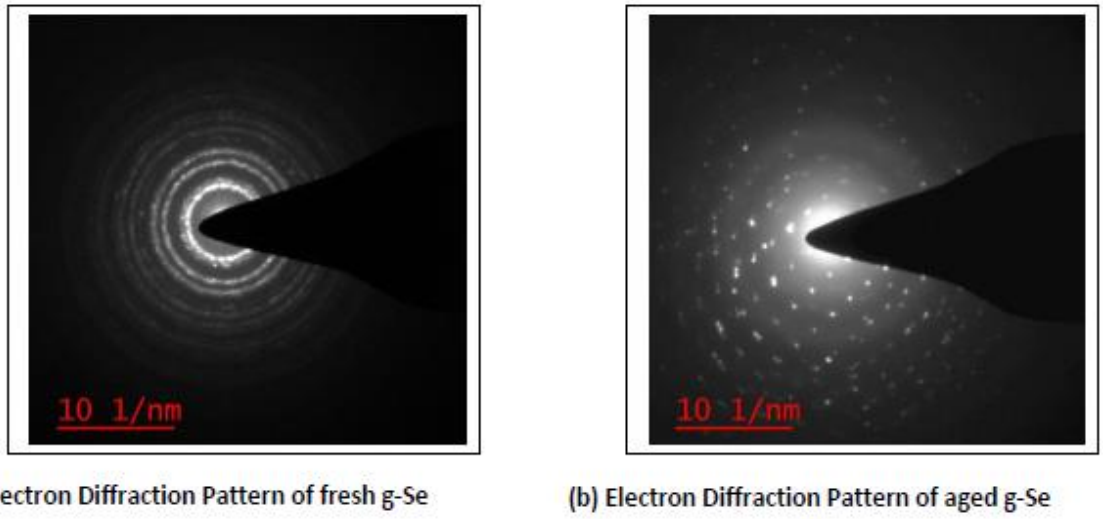

Fig. 6.7. Electron diffraction patterns of as-quenched g-Se and aged g-Se.

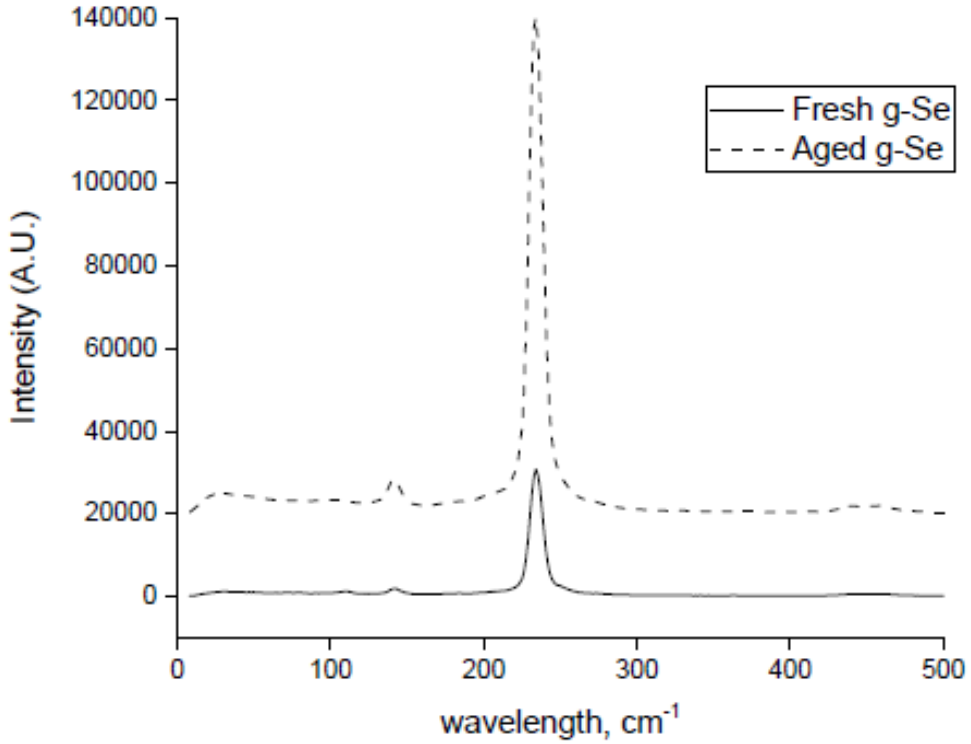

Fig. 6.8. Raman spectra of as-quenched g-Se and aged g-Se.

Fig. 6.8 shows the Raman spectra of aged and as-quenched g-Se. Detailed Raman Mode analysis of g-Se in fresh and aged samples show the A1 mode of Sen chains (near 250 cm-1) to narrow by 26% and a concomitant decrease in its

scattering strength as the modes of correlated chains (near 235 cm-1) and A1 mode of Se8 rings (near 264 cm-1) steadily grow. These findings are viewed to come from the "molecular" chains of Sen predominant in the fresh glass reconstructing with each other, and leading to a compaction of the network due to an "aginginduced growth of inter-chain correlations".

The observed PhA effects can be understood in terms of Chains Crossing Model (CCM)'. Since the natural physical aging effect has been assumed to be associated with the existence in the glass structure of elementary –Se–Se–Se– segments [26, 27], we consider only the inner Se atoms within Sen chains. This model suggests that only fragments (……–Se–Se–Se–……) with Se central atom long polymeric chains of Se are expected in the structure of pure glassy Selenium [25].

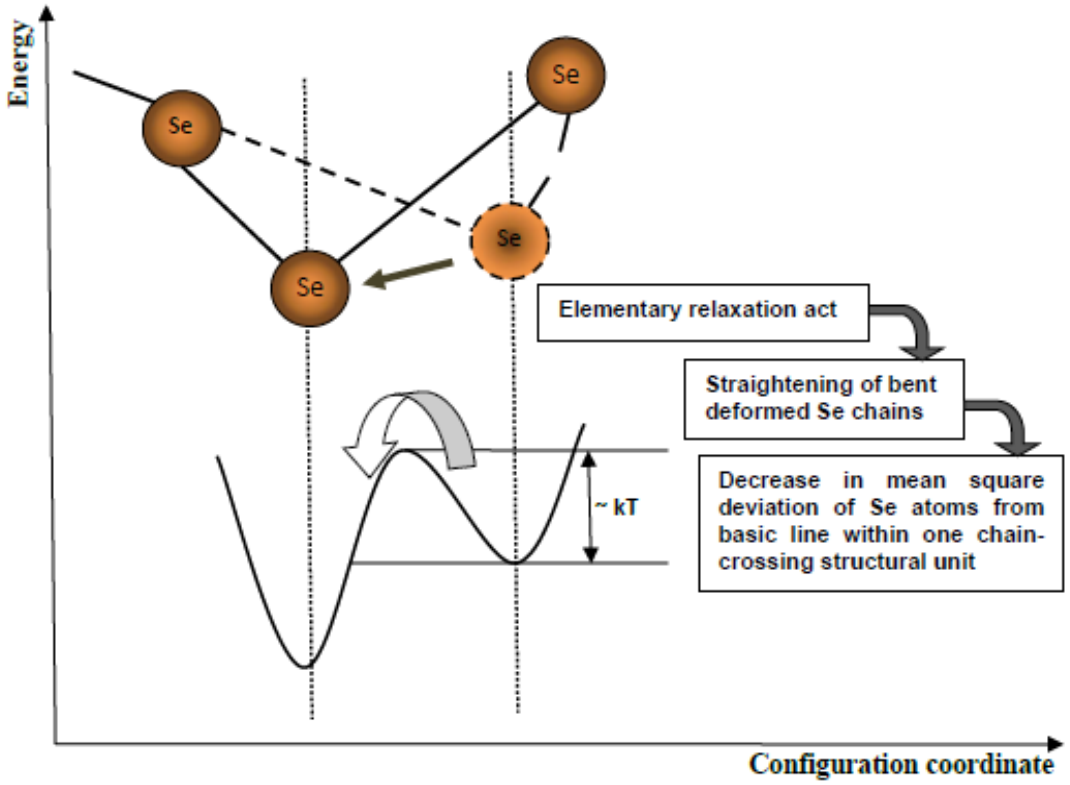

Fig. 6.9. Boundary dislodgments of Se atoms along – Se–Se–Se– chain towards a further equilibrium thermodynamic state within local DWP.

A model of double-well potential (DWP) having a barrier height of energy ~ kT is shown in Fig. 6.9 for the characterization of soft and flexible configurations formed by Se atoms [28-30]. This model depicts that no considerable perturbations in energy take place when Se atoms of the Sen chains reside in either cis or trans configuration inside the polymeric chains. This condition is followed by inner atoms only because of the recognized flexibility of arrays of Se atoms and it is not found suitable in bulk chalcogens glasses for $n < 3$. A noteworthy number of Se atoms are probably not occupied the favorable and highly energetic positions within the glass network because glass structure is so far from the thermodynamic equilibrium after synthesis in the asquenched state according to the classical definition of glass [31]. Consequently, their conversion into favorable positions of comparatively more energetic states (shown by arrows in Fig. 6.9) may play the role in the PhA through an elementary low-energy action. These processes of the elementary relaxation process begin in the diverse regions of the sample. Further, they attain a cooperative environment by opening similar processes within the same and/or neighboring Se depending on their steric constraints) on account of inter- and intra-chain interactions. Fig. 6.9 also reveals that the straightening bent deformations of chains happen by means of the boundary displacements of bridge chalcogen atoms within DWP as the basic relaxation acts. The straightening of –Se–(Se)n–Se– chains and shrinkage of glass matrix are probably responsible for the decrease in the deviations of Se bond lengths and angles leading at the microstructural level [26]. Such circumstances cause the reduction in the common connectivity strength of the glass backbone (due to elastic strains and partitioning of the system into loosely and more densely packed regions, in the first approximation). Ingram et al. established this fact to some extent experimentally by employing concurrent measurements of positron annihilation lifetime spectroscopy (PALS) and differential scanning calorimetric (DSC) techniques [32].

Fig. 6.10 describes the schematic illustration showing subsequent stages of “straightening” and “shrinkage” effects in Se-enriched covalent-bonded glass backbone caused by interim physical aging. It is realistic to believe that such a

cooperative process is linked with the straightening of Se-based structural fragments and their better space utilization (see Fig. 6.10), because straightening/alignment of Se chains allow them to reside in the configurations having less geometrical volume as compared to that of the bent ring-like configurations. The occupied volume is cross-hatched in Fig. 6.10. Thus, they can be regarded as energetically more favorable. This hypothesis is supported by the molecular dynamics simulations of amorphous selenium showing that Se chains, which contain ring-like fragments (Se atoms in the cis configuration), are energetically unsteady and tend to be excluded from samples [33]. The straightened fragments (Se atoms in the trans configuration) cause a decrease in the total ChG volume (and, consequently, a corresponding increase in the value of *Tg*) because of the shrinkage effect.

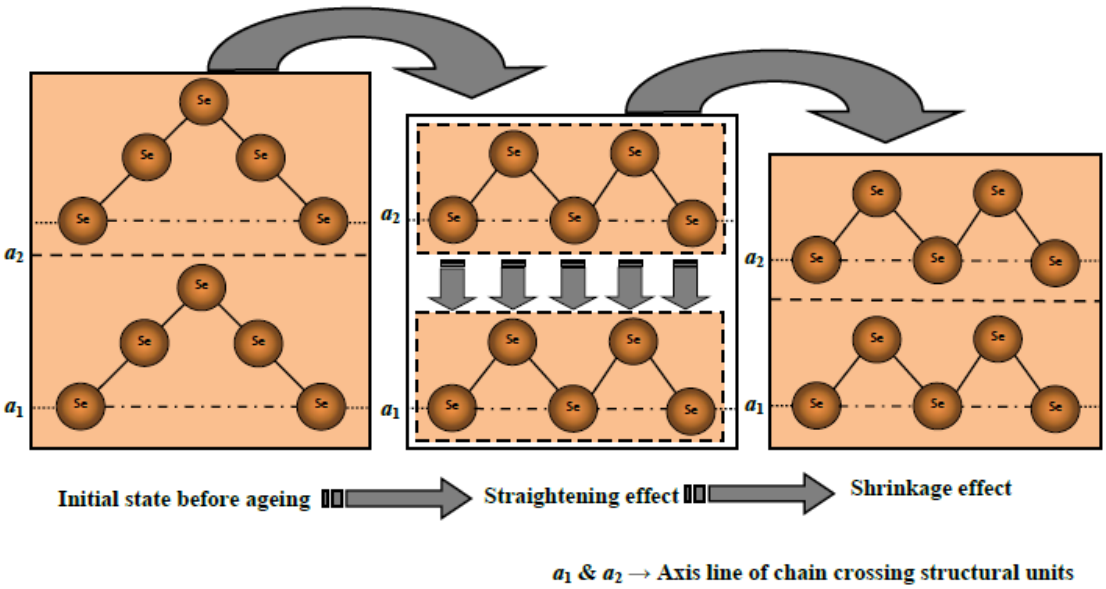

Fig. 6.10. Diagram showing the idea about the consequent stages of straightening/shrinkage effects in Selenium glass consisting of long-polymeric chains of covalent-bonded Se atoms.

6.4. Conclusions

The effect of PhA on glassy selenium studied by DSC, Optical microscopy, XRD, SEM, TEM, and Raman Spectroscopy techniques. The results indicate the possibility of the medium-range ordering in some local sites of the glass matrix of as-prepared i.e., fresh g-Se. We have observed the different structural behavior of aged and as-quenched samples of glassy selenium due to the noticeable presence of crystalline phase nuclei (formation of crystalline phases of Se from nanoscale to micro-scale) in aged g-Se as compared to fresh g-Se. The noticeable reduction in the parameters GFA and TS for aged samples of Se glass also confirm the aging effect. All the techniques employed in present work to study the structural properties of glassy selenium evince a significant aging behavior.

References

1. J. Joule, *The Scientific Papers of J.P. Joule*, London: Physical Soc., 1884, **1**, 558.

2. S.V. Nemilov, *Glass Phys. Chem.*, 2000, **26**, 511.

3. B.T. Kolomiets and N.A. Goryunova, *Zh. Tekh. Fiz.*, 1955, **25**, 2069–2078.

4. R. Golovchak, H. Jain, O. Shpotyuk A. Kozdras, A. Saiter, and J.-M. Saiter, *Phys. Rev. B*, 2008, **78**, 014202.

5. F. A. Devillanova and W.-W. du Mont, *Handbook of Chalcogen Chemistry 2nd Edition, Volume 1*, RSC Publishing 2013.

6. S. Choudhary, A. Umar and S. K. Mehta, *Prog. Mater. Sci.*, 2016, **83**, 270–329.

7. J. Li, X. Zhao, Z. Zhang and Y. Lai, *J. Alloys Comp.*, 2015, **619**, 794-799.

8. M. Panahi-Kalamuei, M. Salavati-Niasari and S. M. Hosseinpour-Mashkani, *J. Alloys Comp.*, 2014, **617**, 627-632.

9. L. Tichy and H. Ticha, *Mater. Lett.*, 1994, **21**, 313-319.

10. L. Tichy and H. Ticha, *J. Non-Cryst. Solids*, 1995, **189**, 141-146.

11. V. I. Mikla, J. M. Turovci, V. V. Mikla and N. Mehta, *Prog. Sol. Stat. Chem.,* 2018, **49**, 1-15.

12. S. Napolitano, *Non-equilibrium Phenomena in Confined Soft Matter,* Springer International Publishing Switzerland 2015.

13. A. Y.-H. Liu and J. Rottler,*Soft Matter,* 2010, **6**, 4858-4862.

14. R. Angelini, L. Zulian, A. Fluerasu, A. Madsen, G. Ruocco and B. Ruzicka,*Soft Matter,* 2013, **9**, 10955-10959.

15. J. M. Saiter, and J. Otoelectron. *Adv. Mater.,* 2001, **3**, 685 – 694.

16. R. Ya. Golovchak, S. A. Kozyukhin, A. Kozdras, O. I. Shpotyuk, and V. M. Novotortsev, *Inorganic Mater.,* 2010, **46,** 911–913.

17. M. K. Vanitha, M.V. H. Rao, S. Asokan and K. Ramesh, *J. Phys. Chem. Sol.,* 2013, **74**, 804–810.

18. M.M.A. Imran, O. Lafi, N. Mehta, A.F. Alshwabkeh, A. Shaheen and A. Al-bqoor *Chalcogenide Lett.,* 2017, **14,** 203-209.

19. H. Y. Zhao, Y. P. Koh, M. Pyda, S. Sen and S. L. Simon, *J. Non-Cryst. Solids,* 2013, **368**, 63-70.

20. K. Chen and S. Vyazovkin, *J. Phys. Chem. B,* 2009, **113**, 4631-4635. Soft Matter Page 10 of 21

21. V. M. Boucher, D. Cangialosi, A. Alegría, J. Colmenero, I. Pastoriza-Santos and Luis M. Liz-Marzan, *Soft Matter,* 2011, **7,** 3607-3620.

22. M. A. Popescu, A. Andriesh and M. Bertolotti (eds) *Medium range order in chalcogenide glasses,* NATO ASI Series, Springer, Dordrecht, 1997.

23. M. A. Popescu, *J. Ovonic Res.,* 2005, **1**, 7-19.

24. M. A. Popescu and H. Bradaczek, *J. Optoelectron. Adv. Mater.,* 2001, **3**, 249-254.

25. B. Bureau, J. Troles, M. Le Floch, F. Smektala and J. Lucas, *J. Non-Cryst. Solids,* 2003, **326–327,** 58–63.

26. R. Golovchak, Cz. Gorecki, A. Kozdras and O. Shpotyuk, *Sol. State Commun.,* 2006, **137,** 67–69.

27. J.M. Saiter, M. Arnoult and J. Grenet, *Physica B* 2005, **355**, 370.

28. M. Misawa and K. Suzuki, *J. Phys. Soc. Jpn.* 1978, **44**, 16125.

29. Y.M. Galperin, V.G. Karpov and V.I. Kozub, *Adv. Phys.*, 1989, **38**, 669.
30. L. Tichy, H. Ticha and P. Nagels et al., *J. Optoelectron. Adv. Mater.*, 2002, **4**, 785.
31. L.C.E. Struik, *Physical Ageing in Amorphous Polymers and Other Materials*, Elsevier, New York, 1978.
32. A. Ingram, A. Kozdras, O. Shpotyuk and R. Golovchak, *Phys. Status Solidi B*, 2012, **249**, 1017–1019.
33. K. Nakamura and A. Ikawa, *Phys. Rev. B*, 2003, **67**, 104203.